

# Sea Ice Decay for Marine Navigation

## *Final Report*

David G. Barber, John J. Yackel and John M. Hanesiak  
Centre for Earth Observation Science (CEOS)  
Department of Geography, The University of Manitoba  
Winnipeg, MB, Canada; R3T 2N2.

**CEOSTEC-10-1-99**

## **Preamble**

Transport Canada through the Marine Safety division (AMNS) has the responsibility to administer marine navigation in the coastal waters of Canada; the Canadian Ice Service (CIS; Environment Canada) provides operational support in the form of ice information for navigation in ice covered waters. The Centre for Earth Observation Science (CEOS; Department of Geography, University of Manitoba) specializes in the study of geophysical, thermodynamic, electrical, and microwave scattering properties of snow covered sea ice.

Transport Canada has a requirement to understand the navigational implications of sea ice within the framework of the Arctic Ice Regime Shipping System (AIRSS) standards, as part of the Arctic Shipping Pollution Prevention Regulations (ASPPR). Of particular relevance to this work is the characterization of the sea ice ablation process from the perspective of marine vessel navigation.

Within the research community we understand the primary thermodynamic mechanism responsible for sea ice ablation and we can categorize these into discrete stages of accretion and ablation. We have a fairly complete understanding of the mechanical properties which are associated with the ablation process and we have a rudimentary understanding of the associated dielectrical properties which result from various ablation states. We have recently made significant advances in being able to determine various thermodynamic states using satellite based synthetic aperture radars (SARs) such as RADARSAT and we are in the process of understanding the spatial and temporal dynamics which are associated with sea ice ablation.

This report represents the combined results of a multiyear research project which addressed the issues of sea ice information currently being utilized within the framework of the AIRSS structure. Phases 1 through 3 of this project were designed to develop a theoretical framework for the detection of sea ice decay; to examine particular issues which are poorly understood; and then to apply this knowledge in the generation of ice decay information within CIS ice information products.

## **Executive Summary**

Sea ice occurs when ocean water reaches a temperature of approximately -1.8 °C. Arctic sea ice is a dynamic component of the earth's cryosphere over all spatial and temporal scales. The areal extent and subsequent ablation rate of sea ice undergoes tremendous seasonal variation in response to the surface radiation receipt and the timing of the import or advection of energy from lower latitudes. Because the average thickness of Arctic sea ice is only about three meters, small changes in the energy absorbed will significantly effect its spatial extent due to the relatively small thermal capacity of sea ice.

Arctic sea ice coverage has a dynamic seasonal extent from  $15 \times 10^6 \text{ km}^2$  in winter to  $8 \times 10^6 \text{ km}^2$  in the summer. The aerial difference is approximately  $7 \times 10^6 \text{ km}^2$ , or equivalent to the landmass of all the Canadian provinces combined. Recent research results show that the average annual extent of sea ice has been reducing at a rate of  $34,300 \text{ km}^2$  per year over the past 18 years (Parkinson et al. 1999). We feel that this reduction is the first evidence of global climate change. The alternating presence/absence of sea ice significantly affects marine vessel navigation and operations in Arctic marine waters. Radiative and energy balances are intimately linked with ice cover, as is the development and sustenance of ecosystems, both marine and terrestrial.

In this report we review the theoretical framework required to understand sea ice as a physical material and how we can use electromagnetic energy interactions to improve our understanding of the physical, electrical and mechanical properties of sea ice. We show how the thermodynamics of the snow/sea ice volume drive the physical, electrical and mechanical properties

of the ice over the annual cycle (Section 1). We then review our current understanding of the extraction of physical, mechanical and energy balance information using a variety of electromagnetic frequencies, at various spatial and temporal resolutions (Section 2). From this theoretical base we then focus on the requirements of the AIRSS structure pertaining to: i) ice type information; and ii) the thermodynamic state of a particular ice type. We suggest new approaches to obtaining ice type information and its thermodynamic state using information obtained from EM interactions at different frequencies, incidence angles and times (Section 3). We conclude with a brief description of the salient components of sections 1 through 3 and provide some evidence on how RadarSAT products can be used operationally to meet the objectives of the AIRSS structure (Section 4).

## **Acknowledgment of Co-Authors**

This report represents a single synthesis of ten years of sea ice field research spanning the disciplines of Geography, Geophysics, Climatology, Engineering, and Remote Sensing. We have benefited from the direct input of various students currently associated with the Centre for Earth Observation Science: Mr. A. Thomas, Mr. S. Drobot, Mr. C.J. Mundy, Ms. T. Nichols and Mr. J. Iacozza. We have also had the pleasure of collaborating with several Canadian Scientists through our involvement with the Seasonal Sea Ice Monitoring the Modelling Site (SIMMS; LeDrew and Barber, 1994) and its follow-on program, the Collaborative Interdisciplinary Cryosphere Experiment (C-ICE). In particular we would like to acknowledge the contributions of Dr. E. LeDrew, Dr. T. Papakyriakou, Dr. R. De Abreu, and Dr. J. Piwowar all most recently associated with the University of Waterloo; Dr. M. Shokr (AES), Dr. N. Sinha (NRC), and Dr. M. Williams (NRC); Mr. M. Manore and Dr. C. Livingstone (CCRS). Thanks also to Dr. B Goodison (AES), PI of the CRYSYS project for support contributing to this research programme. From an International perspective, we have benefited from the collaborations of: Dr.'s Grenfell, Winebrenner, Onstott, Nghiem, Gogineni, Jezek, Ding, Golden, Perovich, Gow and Tucker (collaborators on the US Navy funded ARI). Input by Dr.'s Drinkwater, Holt, Kwok and Carsey (Jet Propulsion laboratory, Pasadena, CA) are also acknowledged. My long-term relationship with the Canadian Ice Services through Mr. J. Falkingham, Mr. B. Ramsay, Mr. K. Asmus and most recently Mr. W. Lumsden have been both challenging and enjoyable. This project was initiated and funded by Transport Canada (Mr. R. Wolfe) and by the Canadian Ice Services (Mr. W. Lumsden).

# Table of Contents

Preamble .....	3
Executive Summary .....	5
Table of Contents .....	8
 Section 1 - The Physical, Electrical, Thermodynamic and Mechanical Properties of Sea Ice throughout the Annual Cycle .....	14
Background.....	15
Physical Properties of Sea Ice .....	17
Freeze-up .....	19
Winter .....	21
Ablation State 1 .....	24
Ablation State 2 .....	28
Ablation State 3 .....	30
Ablation State 4 .....	31
Ablation State 5 .....	36
Ablation State 6 .....	37
Electrical Properties of Sea Ice .....	45
Freeze-up .....	53
Winter .....	56
Ablation State 1 and 2 .....	61
Ablation State 3 .....	64
Ablation State 4 .....	66
Mechanical Properties of Sea Ice .....	68
 Section 2 - Sea Ice Information Products from Remote Sensing .....	83
Background.....	84



Remote Sensing of Sea Ice through the Annual Cycle .....	88
Role of Radarsat in the detection and monitoring of sea ice ablation. ....	110
Section 3 - Ship Navigation, Sea Ice Ablation, and Remote Sensing .....	114
Introduction .....	115
The AIRSS system.....	116
Evolution of $\sigma^{\circ}$ .....	117
Extracting Sea Ice Information.....	123
Section 4 - Summary and Conclusions .....	132
Summary of Section 1 .....	133
Summary of Section 2 .....	138
Summary of Section 3 .....	141
Conclusions .....	142
Literature Cited .....	143



## **Project Objectives**

In this report we address five objectives which taken as a whole, provide a review of the physical, electrical and mechanical properties of sea ice throughout its annual cycle. This is the final report of a multiyear project which addresses the general information requirements of the Arctic Ice Regime Shipping System (AIRSS) as they pertain to marine vessel navigation over an annual cycle. Our objectives in this work were to conduct a detailed literature study of issues pertaining to sea ice accretion/ablation and then to examine the detection of these thermodynamic states with remote sensing and/or numerical models. For purposes of clarity we present this material within the framework of five objectives:

**Objective 1:** to describe the sea ice ablation process using the perspective of the annual cycle of both first-year and multiyear sea ice, and to evaluate our current knowledge of these processes using the following perspectives:

- i) geophysical characteristics at the mm to cm scale
- ii) electrical properties at the mm to cm scale
- iii) mechanical characteristics at the mm to km scale

**Objective 2:** to evaluate the current sources available for ice information relative to the annual cycle of sea ice.

This step involves an evaluation of current research results in sea ice information processing relative to the operational requirements of the AIRSS

framework. The following questions serve to illustrate the range and focus of this objective:

- i) Can SAR be used to identify sea ice ridging?
- ii) What is a reasonable coding descriptor for ice ridging (e.g., density of ridging, magnitude, etc.)?
- iii) Do the 'adjustment factors' used in AIRSS represent reasonable coefficients given our understanding of the physical and mechanical properties of sea ice?
- iv) Are there areas where new research results can be integrated into ice chart products (e.g., ice pressure fields, crack/lead density, snow thickness distributions, etc.)?

**Objective 3:** to describe the operational implications of the sea ice ablation process from the perspective of marine navigation.

This step involves rationalizing the results of objectives 1 and 2 with the operational realities of marine navigation. The following questions serve to illustrate the range and focus of this objective:

- i) What is the spatial/temporal variability in the sea ice ablation process?
- ii) Is the strength of sea ice 'thickness' and 'ice type' dependent?
- iii) Can we predict the 'rate' and/or 'state' of the ablation process from modeled or observed data (e.g., SAR, SSM/I, NOAA, or temperature records)?

- iv) What are the interrelationships amongst microwave scattering, sea ice ablation, and mechanical properties of the sea ice?

**Objective 4:** to develop a research project which will focus on the validation/verification of issues identified in objectives 1 to 3.

To address this objective we partition the detailed responses from objectives 1 to 3 into those areas that are sufficiently well understood to be considered operational, and those which require further development.

**Objective 5:** to report on the findings of the research project described in Objective 4 from the perspective of operational detection of ablation states in landfast first-year sea ice

In this work we relate the theoretical relationship between microwave scattering, thermodynamics and mechanical properties of sea ice. The focus here is on using Radarsat ScanSAR data as an operational tool for estimating the ablation state of snow covered landfast sea ice.

# **Section 1**

**The Physical, Electrical, Thermodynamic and Mechanical Properties of  
Sea Ice throughout the Annual Cycle**

## **Background**

The ocean-sea ice-atmosphere interface operates as a highly coupled, complex system, which has processes operating over a full range of spatial and temporal scales. The physical properties of the snow/sea ice system are affected by both oceanic and atmospheric forcing in response to local, regional and global scale processes. The physical properties of the snow and ice are fundamental variables affecting the electrical and mechanical properties of the volume. The sea ice thermodynamic properties drive the seasonal and temporal evolution of each of the physical, electrical and mechanical characteristics and as such are the fundamental focus of this report.

Physical properties of the system include snow and sea ice microstructure (grain structures and inclusion morphology), mesostructure (density, bulk salinity, and thickness) and macrostructure (ice type, surface roughness, kinematics and spatial distribution). Engineering properties include the thermal, electrical (complex dielectric constant) and mechanical (ice strength, elasticity and friction) characteristics of the snow and ice. The dielectric properties define the electrical conductivity of the snow and ice relative to the wavelength and polarization of incident electromagnetic energy. Microwave scattering from a synthetic aperture radar (SAR) is strongly linked to the dielectric properties of the material (Ulaby et al., 1986). Brine volume is a function of ice temperature and salinity, and strongly dictates the dielectric properties and various mechanical strength characteristics of sea ice.

Research has evolved to a point where we can now consider the development of an 'Electro-Thermophysical'<sup>1</sup> model of snow covered sea ice. Development of such a model would link the physical, electrical, thermodynamic and EM scattering characteristics of the seasonally evolving sea ice cover (hereafter referred to as an icescape (LeDrew and Barber, 1995)). A significant opportunity from such a modeling framework would be the estimation of sea ice strength based on the remote measurement of EM interactions with a seasonally evolving icescape. In what follows we review our current understanding of the theory relating to the development of each of the components of this proposed 'Electro-Thermophysical' model.

---

<sup>1</sup>I was first introduced to the nomenclature of this model by M. Drinkwater (personal communication). I have adapted his terminology (electro-thermodynamical) to more suitably address the objectives of this report and have settled upon a slightly different term of 'electro-thermophysical' within which to represent the cogent theory.



## Physical Properties of Sea Ice

Sea ice is an important component of the Earth's Cryosphere and is more appropriately considered as a multiphase alloy rather than a single phase purer ice form such as snow or lake ice. Once ice has formed, the relationships between ice, liquid brine, and solid salts are governed by the thermodynamic structure within the snow and sea ice volume. This relationship is fundamental to the creation of our conceptual model of an 'Electro-Thermophysical' relationship and is characterized by the phase diagram developed by Weeks and Ackley, 1986 (Figure 1.1).

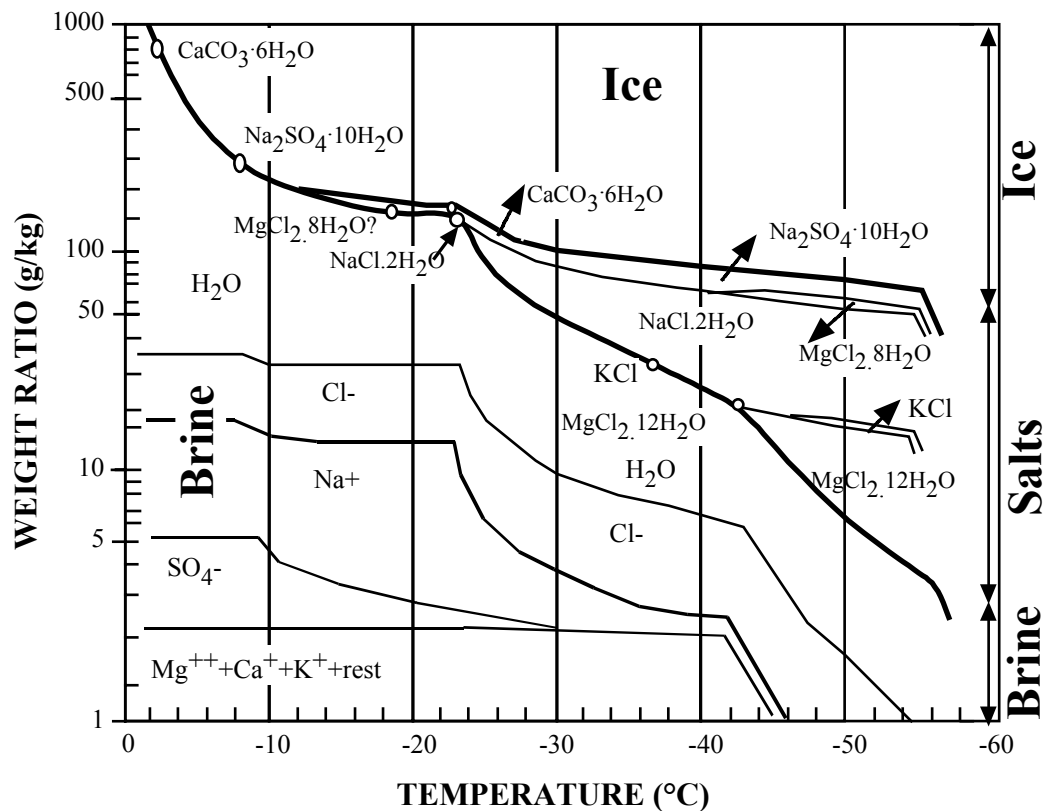


Figure 1.1. Phase diagram of sea ice showing the relationships between ice in solid phase, brine, and solid salts as a function of temperature.

The interpretation of these phase relationships relative to the thermodynamics of the icescape is a continuous function of the atmospheric temperature<sup>2</sup>. For simplicity we have adopted a categorical structure within which to compartmentalize the salient theory. If we consider average conditions of the snow thermodynamic properties we can identify several regimes based on the principal processes operating within the snow/sea ice system. Although the thermodynamic evolution of the system is inherently continuous we partition the system into a series of discrete ablation states: freeze-up, winter; ablation 1 (very early melt); ablation 2 (sustained snow melt); ablation 3 (saturated snow); ablation 4 (melt pond formation); ablation 5 (drainage of ponds) and ablation 6 (rotten ice). This process is variable in both space and time and thus requires measurement by direct observation or through remote sensing with a calibrated synthetic aperture radar (SAR). This single fact is cited as a primary motivator for determining remote sensing estimates of the thermodynamic state of the sea ice rather than relying on climatologies of these conditions. It is also a strong motivator for development of the Arctic Ice Regime Shipping System (AIRSS) structure rather than using the more static Zone/Date system.

In what follows we provide a detailed overview of the physical properties of the snow and sea ice over a range spanning the mm to km scale within the framework of the thermodynamic regimes described in Figure 1.2.

---

<sup>2</sup>For simplicity we consider the ocean temperature to be a constant -1.8°C. This is a reasonable simplification for most icescape conditions of interest in this report but the reader is cautioned that notable exceptions occur (such as in sensible heat polynyas).





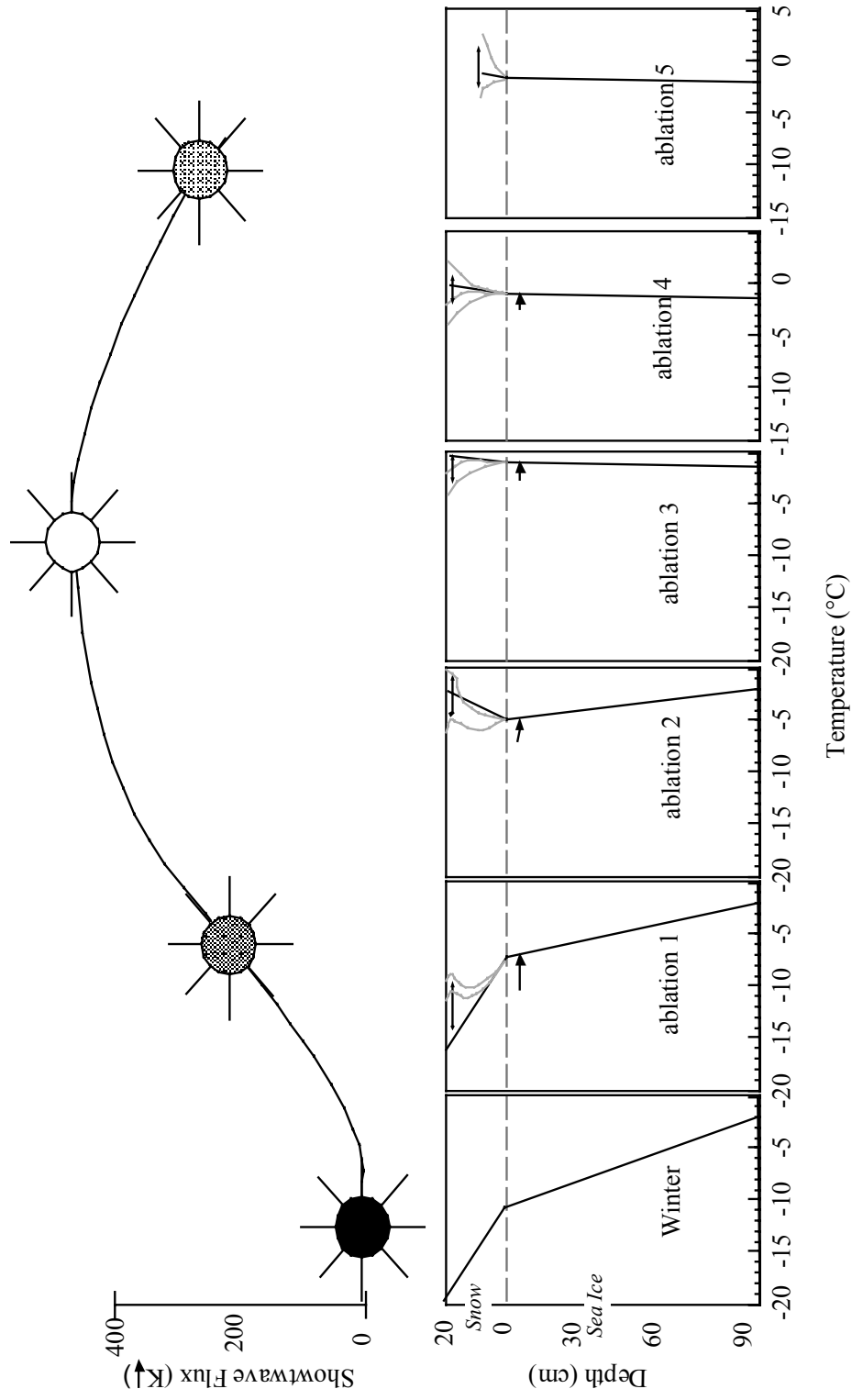


Figure 1.2. Categorical structures of the general thermodynamic regimes representing the transition from Freeze-up, winter and into the proposed ablation states 1-6 for landfast first-year sea ice in the Canadian Arctic. Temperature profiles are summarized from 10 years of measured in situ temperature profiles. The available shortwave energy is denoted in summary above the thermodynamic profiles.

## **Freeze-up**

During the freeze-up period new ice formation begins with the appearance of frazil, slush or columnar ice crystals within the water column. Frazil ice typically occurs under conditions when the ocean surface is roughened by wind. The frazil platelets form within the top few cm of the surface and float to the surface. These particles aggregate to form shuga or grease ice. Further cooling of this slushy layer results in consolidation of the surface into a dark thin ice type called nilas. This primary ice layer (frozen frazil) is characterized by platelet-shaped crystals in the millimeter size range. Columnar crystals are typical of calm growth conditions and slush ice is a mixture of snow (blown in from surrounding surfaces) and sea water.

As the number of freezing degree days increases the ice starts to consolidate into the water column. This is termed secondary ice growth which results in ice crystals that have columnar shaped grains. As the surface continues to cool, brine pockets within the frazil layer are extruded to the surface resulting in frost flowers (Hollinger et al., 1984; Drinkwater and Crocker, 1988, Martin, 1979). The salinities of this layer can be considerably higher (45-100 ppt; Drinkwater and Crocker, 1988, Martin, 1979) than the bulk salinities of the ice. These frost flowers consist of delicate crystalline shapes which typically grow to heights of 2-4 cm above the ice surface (Martin, 1979). Brine is also expelled either into the ocean beneath or into brine pockets within the young ice mass as it grows. Salinity of this ice drops rapidly after the initial freeze-up. After about a week (0.4 m thickness) the desalination stabilizes to a gentler (linear) desalination as the ice sheet thickens. Throughout the growth process, surface and bottom salinities are

higher than those in the center. Bulk salinities range from 5 to 15 ppt (Vant et al., 1978).

Thermodynamically, the ice volume separates the atmosphere from a potentially strong oceanic heat flux. Modelling work has shown that the first 30 cm of ice growth is the most critical to the overall heat flux from the ocean to the atmosphere (Maykut, 1978). At early stages of ice growth brine is expelled through the constriction of brine pockets captured within the early phase changes of the ice grains. This brine is highly concentrated and can be manifested as 'salt' or 'frost' flowers on the surface of young growing ice. These frost flowers have salinity concentrations between 80 and 140 ppt and can create a significant effect on EM interactions with this young ice form. Brine expelled downwards creates a convective overturning in the ocean water beneath sea ice. This is termed thermohaline circulation. Current theory suggests that this process is fundamental to both regional and global scale circulation of the world's oceans. Regionally this ice formation process creates deep water along the marginal zones<sup>3</sup> of the Arctic and Antarctic. Globally this process manifests itself as the 'oceanic conveyor belt' which is thought to be the primary exchange mechanism for deep nutrient rich waters of the poles to be exchanged with warmer surface waters of the equatorial regions of the planet.

A significant feature of new ice formation is that it allows for a platform upon which snow can be deposited. This significantly alters the thermodynamic profile within this young ice form thereby altering all of the thermal, physical and electrical properties. Vagaries of the role of solid phase precipitate remains a significant unknown in the modeling of the

---

<sup>3</sup>Polynyas are thought to be a small scale feature which can create a globally significant amount of this



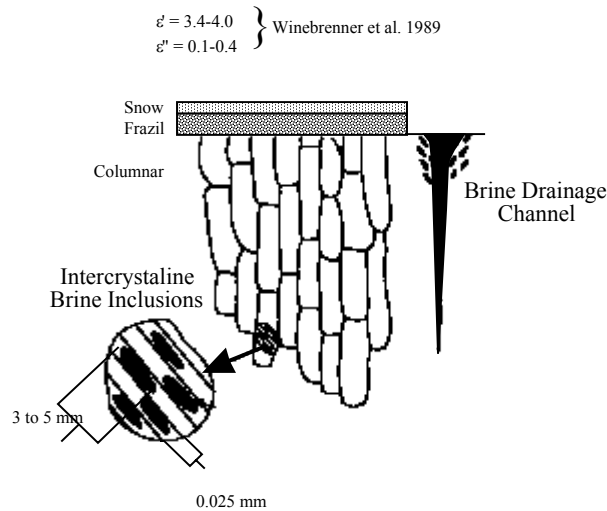
impacts of climate variability and change within the sea icescape. The freeze-up period is considered to end when a significant fraction of the young ice has grown to first-year ice thickness ( $>30$  cm).

## **Winter**

Winter is the dominant season, lasting from December to April at a minimum. During this season first-year ice types cover a range of thickness conditions from  $>30$  to  $<200$  cm. Younger ice forms such as nilas, shuga and frazil are rare (Maykut, 1978). Typically, first-year ice (Figure 1.3) consists of a snow layer covering a primary layer of frazil ice overlaying columnar grains. Total snow cover increases throughout the winter season reaching accumulations from 5 cm to over 1.0 m. The frazil layer consists of randomly oriented crystals while the columnar grains are more vertically oriented. The vertical profile of ice salinity is usually characterized as a 'C' shape (5-16 parts per thousand [ppt] at the surface; 4-5 ppt in the center; and near 30 ppt at the ice-ocean interface). Ice density is relatively uniform at  $0.91$  to  $0.92 \text{ gm}\cdot\text{cm}^{-3}$  (Weeks and Lee, 1958). Liquid brine is interspersed throughout the ice as intercrystalline brine inclusions and brine drainage channels (Figure 1.3). The brine inclusions are generally formed in the orientation of growth (vertical) or directed according to the predominant ocean current (Vant et al., 1978). The brine drainage channels are distributed heterogeneously across the ice surface and provide a primary mechanism for brine drainage in the spring (Wakatsuchi and Kawamura, 1987).

---

deepwater because of the latent heat export associated with these phenomena.

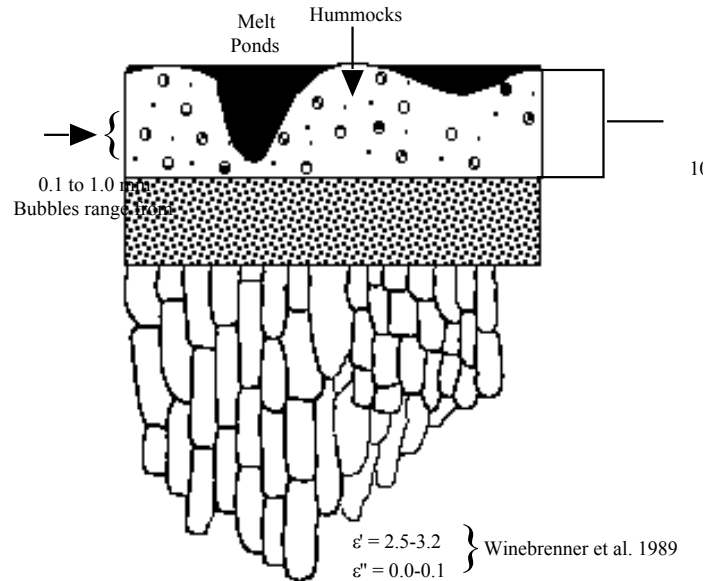


Adapted from Vant et al.,(1978)

Figure 1.3. First-year ice schematic showing the frazil and columnar grain positions relative to intercrystalline brine pockets and more macroscale brine drainage channel networks.

Multiyear ice (Figure 1.4) typically consists of a surface which has undergone an extensive process of recrystallization during the summer melt period. The surface consists of an array of preferential melt areas (melt ponds) and desalinated low porous hummocks surrounding the melt ponds. The upper layer of recrystallized ice (in the hummocks) has widely varying densities, typically around  $0.7 \text{ g}\cdot\text{cm}^{-3}$ . This layer merges into an intermediate layer of slightly higher density which in turn merges into a more solid layer with densities in the range  $0.8$  to  $0.9 \text{ g}\cdot\text{cm}^{-3}$ . The salinity of both hummocks and melt ponds is considerably lower than first-year ice because of brine drainage during the summer. The snow cover is typically

deep over frozen melt ponds and shallow over hummocks since the former create natural entrapments for blowing snow.



Adapted from Vant et al.,(1978)

Figure 1.4. Multiyear ice schematic.

During the winter period atmospheric forcing results in a strong temperature gradient in the snow and a slightly lower gradient in the sea ice (Figure 1.2). The higher gradient is a direct result of the different thermal conductivity ( $\kappa_s$ ) of snow ( $\kappa_s \cong 0.40 \text{ W}\cdot\text{m}^{-1}\cdot\text{C}^{-1}$ ) versus that of sea ( $\kappa_i \cong 2.1 \text{ W}\cdot\text{m}^{-1}\cdot\text{C}^{-1}$ ). The lower thermal conductivity results from the higher percentage of air as a fractional volume in snow relative to sea ice. Models have been produced which realistically recreate the thermodynamic states of both the sea ice and snow when the system is in the winter regime. Under winter conditions we can consider the snow to be insulating the sea ice from the atmosphere. This process limits the growth of sea ice to within a 1 to 2 m thickness range (depending of course on the surface temperature and snow thickness). Grain

growth within the snow cover is dominated by temperature gradient processes, particularly in the basal layer of the snow cover (i.e. initial formation of the basal layer kinetic growth grain structure).

### **Ablation State 1**

Ablation state 1 is a transitional period where water in liquid phase occurs within the snow cover for a portion of the diurnal cycle. This period coincides with large snow grain growth within the snow cover. Metamorphic processes include kinetic energy (wind induced metamorphosis) and radiant energy. Radiant energy provides for development of ice lenses and ice layers within the snow pack (Miller, 1981). Kinetic processes cause metamorphosis from a faceted hexagonal snowflake with inter crystal pore spaces consisting primarily of air, to a more rounded grain state (Colbeck, 1982). This can cause density changes from light newly fallen snow ( $\sim 0.05 \text{ g}\cdot\text{cm}^{-3}$ ) to very dense crustal snow layers ( $\sim 0.5 \text{ g}\cdot\text{cm}^{-3}$ ).

Coinciding with the return of solar irradiance, as a significant component of the surface energy balance, there is an increased forcing from the atmosphere onto the snow surface. Although the downwelling part of the shortwave flux can be very high early in this seasonal regime ( $\sim 300 \text{ W}\cdot\text{m}^{-2}$ ) the surface albedo is also high ( $>85\%$ ) resulting in a fairly small diurnal surplus of heat at the surface. The earth-sun geometry creates a diurnal pattern in the shortwave flux which sets up a diurnal temperature wave within the snow volume (Figure 1.2). Variability in the thermodynamics

within this regime can also be caused under atmospheric forcing events illustrating both high longwave fluxes (presence of low-level thick stratus cloud cover) and the advection of warm air masses over the snow/ice system.

The shortwave flux is transmitted across the snow/air interface and is absorbed within the first few cm of the snow surface. This penetration creates a subsurface maximum in the temperature profile due to the fact that the radiative exchanges dominate over the conductive exchanges within the surface layer of the snow volume. Increasing atmospheric temperatures during the day cause an increase in the surface most portion of the snow layer with reduced amplitudes at greater depth. This process is termed the thermal diffusivity of the snow and is defined as the rate at which the surface induced temperature wave can travel within the snow volume. Mathematically, the thermal diffusivity is related to the thermal conductivity and the heat capacity of the snow according to [1].

$$\kappa_{Hs} = \kappa_s / C_s \quad [1]$$

Where  $\kappa_{Hs}$  is the thermal diffusivity ( $m^2s^{-1} \cdot 10^{-6}$ );  $\kappa_s$  is the thermal conductivity and  $C_s$  is the heat capacity of the snow. Note that the thermal diffusivity is directly proportional to the thermal conductivity (i.e., as the snow becomes more conductive to thermal energy the thermal diffusivity increases). Typically, new snow has a thermal diffusivity of about 0.1 (low thermal conductivity and a good insulator). Old snow with larger snow grains has a higher thermal conductivity (0.42) and as a result a higher thermal diffusivity (0.40). The heat capacity of the snow is defined as the ability of the ice/snow mixtures (bulk snow properties) to retain heat and is

expressed as the amount of heat gained or lost for a particular change in temperature. The heat capacity of the snow layer on sea ice can be calculated by modeling the partial fractions of ice, air, water, and brine as constituent components of the snow volume. Researchers have explicit definitions for heat capacity computations for ice, air and water but little is known about the structural distribution of brine within the basal layer of the snow volume and consequently this parameter is poorly defined in thermodynamic snow layer models.

The most significant aspects of the early melt period to snow thermodynamics is the rapid changes to the geophysics of the snow volume. Because of the oscillations in the temperature profile (Figure 1.2), ablation state 1 represents a rapid growth period for snow grains throughout the snow layer. Under strong negative temperature gradients (like the winter regime or cold atmospheric temperatures in ablation state 1) a process of kinetic growth dominates the snow metamorphism. Sublimation of snow grains next to the ice surface (basal layer of the snow volume) occurs and the resulting vapour travels along the vapour pressure gradient (i.e. along the temperature gradient) upwards toward the snow/air interface. The vapour travels through pore spaces within the interstices of the snow grains and is deposited onto the top parts of grains creating an isotropically aligned layer of large grains (Figure 1.5). The process of temperature gradient metamorphism occurs throughout this period and can create substantial increases in kinetic growth grains (sizes up to several cm in length).

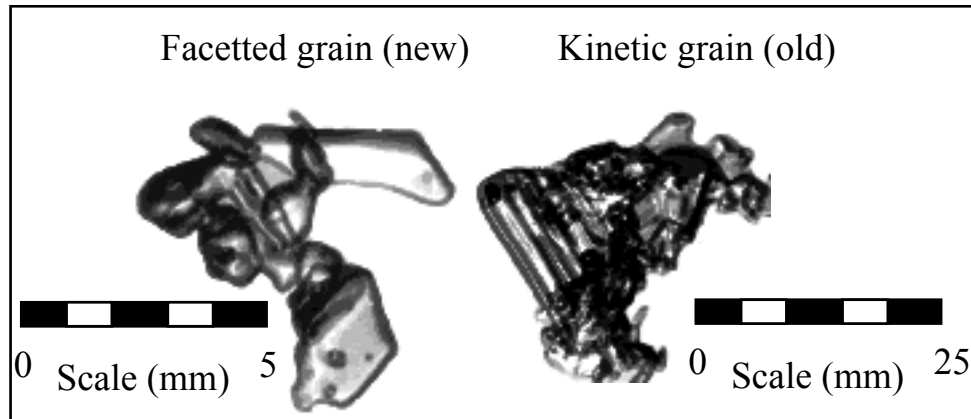


Figure 1.5 Typical new (Faceted) and old (Kinetic) snow grains which result from the metamorphic processes described in the text.

There is a feedback mechanism operating within this system at the time of the ablation state 1 regime. As basal layer grains enlarge (primarily as a result of kinetic growth processes) and as the mid-pack grains grow under equitemperature regimes there are corresponding changes in the thermal diffusivity, heat capacity and thermal conductivity of the snow layer. Although this feedback mechanism has not been extensively studied there is sufficient information to piece together the primary components of the process:

- Grains enlarge thereby reducing the amount of air in the volume. Less air means that the thermal conductivity will increase from a very low value of 0.1 towards that of very dense snow (0.42).
- Since the thermal conductivity is directly proportional to the thermal diffusivity we can expect the temperature waves to penetrate faster and further into the snow volume.

- This increase in thermal diffusivity tends to enhance the metamorphic processes - both those of equitemperature (warming during the day) and temperature gradient (cooling at night) thereby enhancing the overall rate of grain growth.

During this state there is a slight increase in the brine volumes of the sea ice because of the increased temperature within the volume. The magnitude of the increase in the ice volume temperature is controlled by the atmospheric temperature and thicknesses of the snow cover and sea ice. Brine pockets within the sea ice begin to grow but in general remain discrete thus making the sea ice mechanically strong. Visually this ice type appears as cold (winter period) snow covered sea ice.

## **Ablation State 2**

Once water in liquid phase occurs throughout the diurnal cycle (usually at bulk percentages of about 2 percent water by volume) and the ice surface becomes damp at the snow-ice interface, we categorize the period as Ablation State 2. In this state water is held within the interstices of adjacent snow grains (termed the Pendular Regime). Polycrystalline aggregates form locally at the snow base and superimposed ice layers sometimes form on first-year ice (Holt and Digby, 1985).

Once the surface temperature increases and the thermodynamic regime begins to oscillate (Figure 1.2) there is a tendency for snow metamorphism



to be dominated by equitemperature processes. Equitemperature metamorphosis occurs when the temperature gradient is relatively equal over the given volume of snow. Under this process smaller grains connect together and there is a tendency for small faceted grains to grow together into a state which minimizes the surface tension of the snow grain. In nature this minimum is found as a sphere or circle thus resulting in a tendency for rounded grains to occur under this metamorphic process. In dry snow, grain growth occurs slowly, but with the addition of small amounts of water (2-5 percent water by volume) grain growth increases markedly (Colbeck, 1982).

During this state there is a continued increase in the brine volumes of the sea ice because of the increased temperature within the volume. In general the rate of sea ice brine volume expansion increases over this period (relative to Ablation State 1) due to the reduced albedo of the snow volume. Much of the energy gained in the snow layer is lost due to phase changes deeper into the sea ice volume. This leads to formation of freshwater ice layers within both the snow layer and in the upper surface of the sea ice. Brine pockets enlarge to such a size that some may begin to interconnect. This significantly reduces the mechanical strength of the sea ice. It is possible for the system to revert to winter thermodynamic and geophysical conditions any time during the period up to and including Ablation State 2. This is usually caused by advection of cold air into the region or increase in the shortwave albedo of the surface due to new snow deposition.

### Ablation State 3

When sufficient water by volume is accumulated within the snow cover the poor spaces will become filled with water (this is termed the funicular regime, Colbeck, 1982). This transition occurs at approximately 7 percent water by volume (note – you can make a snow ball at about 5 percent by volume). During this period liquid is drained from the saturated snow resulting in a gradient of water volume with a surface minimum and basal maximum. Tightly packed grain clusters occur after the liquid has drained. Colbeck (1982) reports that grain clusters under these conditions are typically two to four crystal arrangements (Figure 1.6). These multi-crystal forms can also form aggregates of several hundred crystals, often called polycrystalline aggregates.

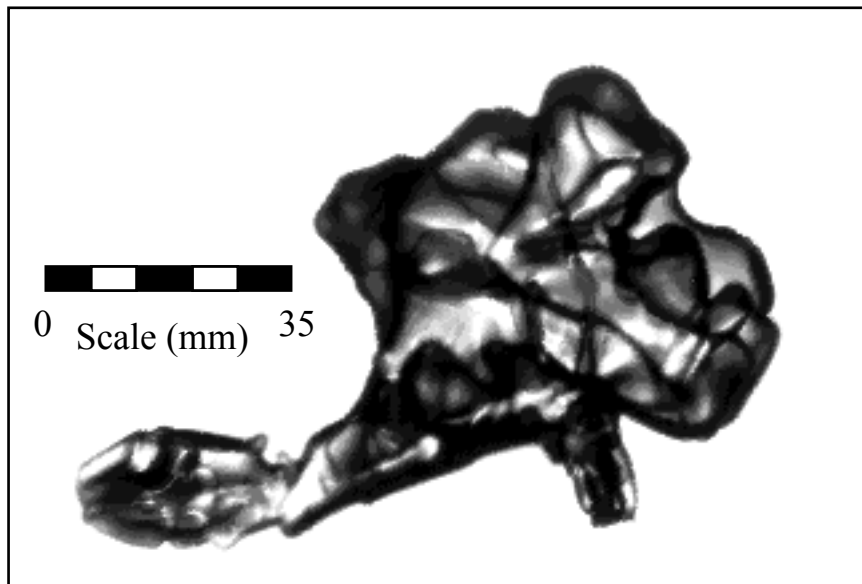


Figure 1.6. Example of a polymorphic grain structure typical of late season snow covers on sea ice.

During this state, the brine volume within the sea ice volume continues to increase, due to the increased shortwave penetration into the snow cover (reduced snow albedo). The brine volume relationships are well understood and can be modeled using heat conduction equations. Over this period salinities at the sea ice surface decrease rapidly as freshwater infiltrates into the rapidly growing brine drainage channels within the sea ice. The spatial distribution of these surface salinities is heterogeneous, probably due to the non-uniform distribution of brine drainage channels (Wakatsuchi. and Kawamura, 1987). The average surface temperature is near freezing and, generally, we consider that the system cannot return to its winter state. The reason for this is that the grains are sufficiently large that advection of cold air into the region will create a transitory phase change to solid then a rapid return to these ablation conditions whenever sufficient solar illumination occurs (due to the sufficiently low surface albedo).

#### **Ablation State 4**

From Ablation State 3 there is a preferential snow melt process whereby shallower interdrift patches melt first. This is because the shallower snow cover generally results in larger snow grains, created during cold season temperature gradient metamorphosis (i.e., thinner snow cover results in a stronger temperature gradient and more kinetic grain growth). The drifts themselves are preserved longer to eventually become the snow patches evident on melt ponded sea ice surfaces (Figure 1.7 and 1.8).

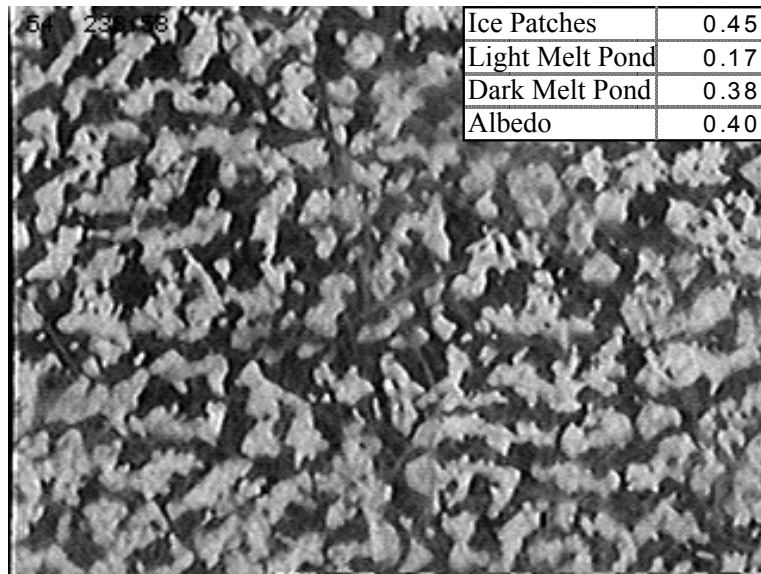


Figure 1.7. Typical melt ponded first-year sea ice surface measured with aerial video then digitized into a microcomputer for morphological measurements of pond sizes and structure (adapted from Barber and Yackel, 1999).

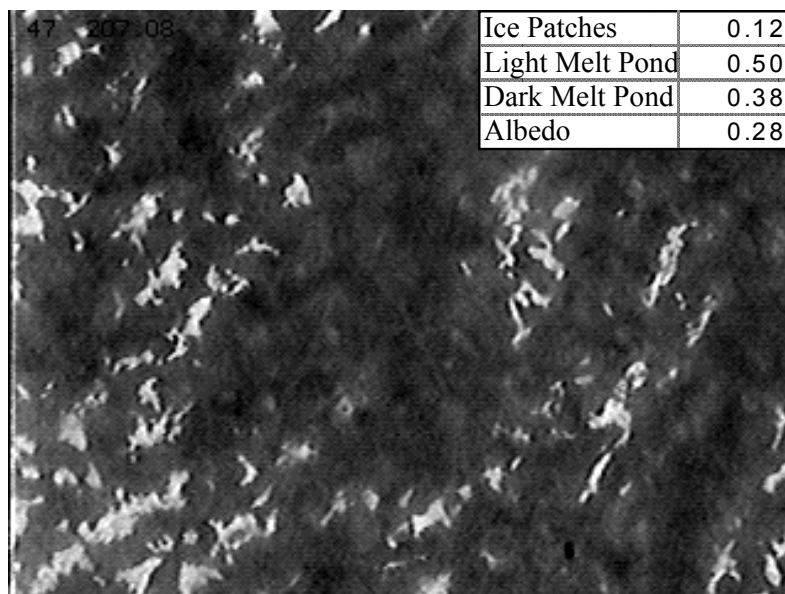


Figure 1.8. High concentration of flooded first-year sea ice measured with aerial video then digitized into a microcomputer for morphological

measurements of pond sizes and structure (adapted from Barber and Yackel, 1999).

The development of drainage networks begins primarily through seal holes (Figure 1.9), cracks, and leads (Figure 1.10). Statistical characteristics of these features are highly variable in both space and time. Results show that the size and percent cover of both ponded surfaces and residual snow patches vary according to: the type of sea ice; the timing of consolidation; and the pattern of snow distribution prior to melt (Barber and Yackel, 1999).

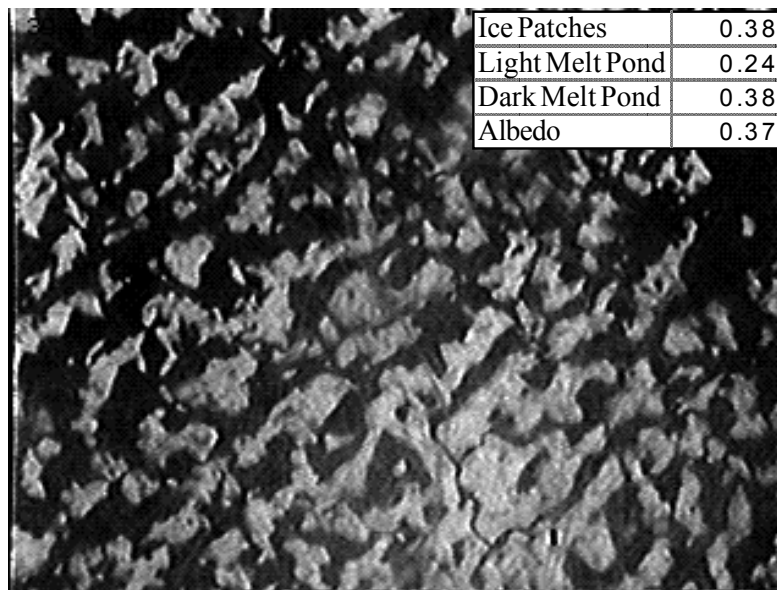


Figure 1.9. Typical example of a sea hole drainage feature and its effect (increased snow patch concentrations) on the local area drainage of first-year sea ice (adapted from Barber and Yackel, 1999).

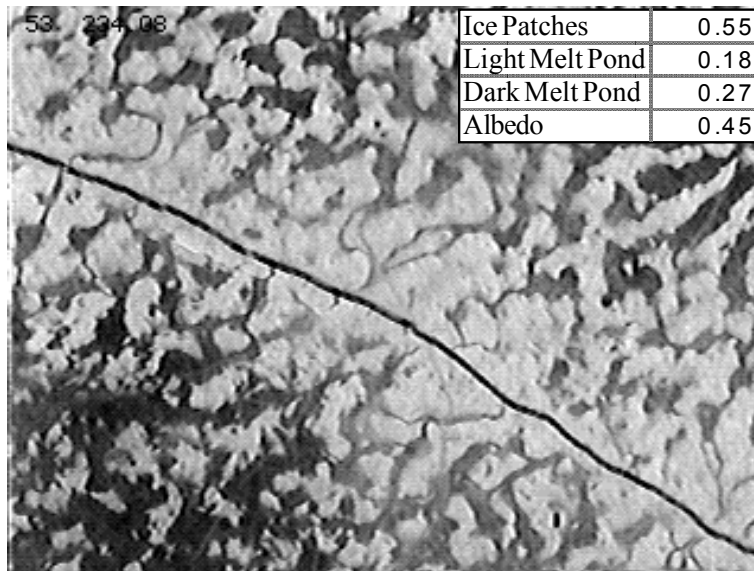
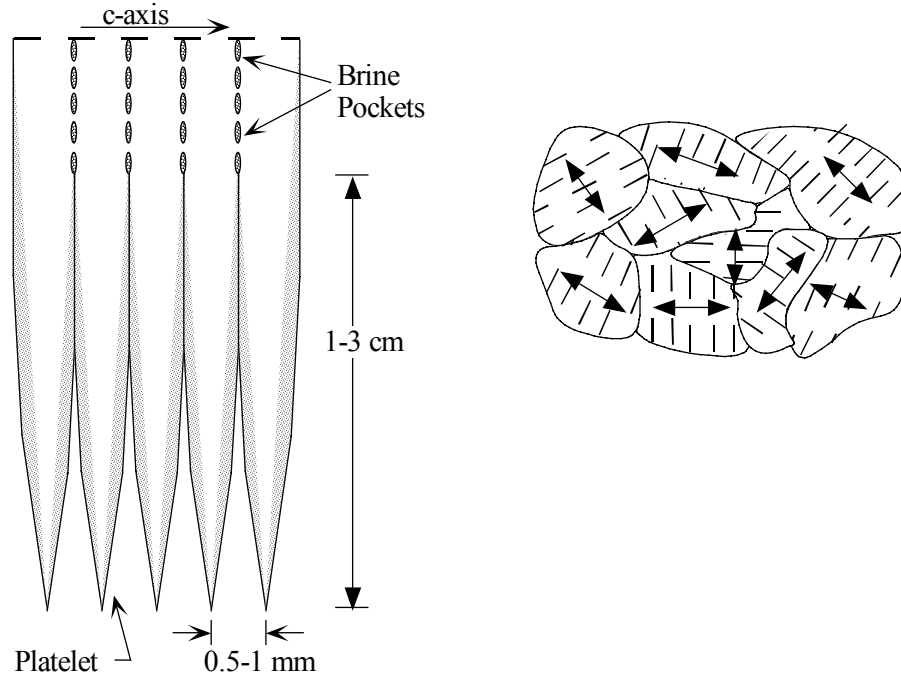


Figure 1.10. Typical example of a crack drainage feature causing pond water drainage (increased snow patch concentrations) for first-year sea ice (adapted from Barber and Yackel, 1999).

The bulk salinity of the sea ice and the basal layer of snow on first-year sea ice, both decrease within ablation state 4. The processes which lead to this rapid desalination are however poorly understood. We do know that brine is held within the interstices of the ice grains in both frazil and columnar sea ice grains. At cold temperatures these brine pockets are 'pinched' off by increasing the size of the ice grains (Figure 1.11).



Adapted from Ackley, (1996)

Figure 1.11. Schematic of the brine constriction in growing sea ice

As the temperature increases in Ablation State 4 the brine pockets enlarge as a function of the phase relationships within sea ice (Figure 1.1). Practically speaking this means that once the ice reaches a temperature above  $-7^{\circ}\text{C}$  there is a rapid increase in the brine volume within sea ice. It has been estimated (from a variety of sources) that the increase in brine volume accomplishes little in the desalination until brine volumes exceed 5 percent by volume. After this point the brine pockets align linearly (generally along the boundaries of adjacent columnar grains). These brine pockets form tubes which join to larger features to create brine drainage channels. Once brine channels are re-established then brine drainage occurs rapidly. Fresh melt water from the melting snow pack can enhance this brine drainage mechanism thereby increasing the desalination process over both first-year

and multiyear forms of sea ice. Desalination is highly variable spatially and temporally with average conditions showing a curvilinear decrease with time (Figure 1.12).

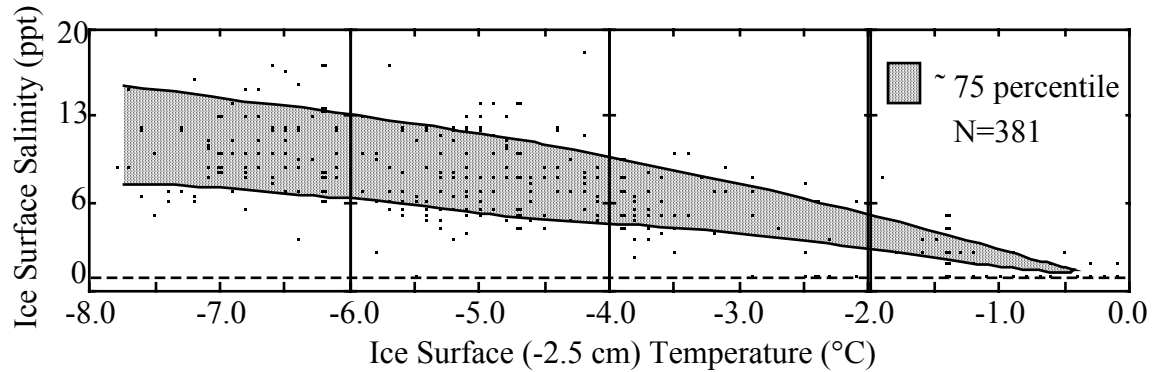


Figure 1.12. Sea ice surface salinities (-2.5 cm) relative to ice surface temperatures (-2.5 cm) obtained from the snow pit sampling conducted during field projects in 1990 and 1991 in the Canadian Archipelago. The approximate 75th percentile ranges of the variables within a particular temperature range are shaded.

## Ablation State 5

This state is typified by the drainage of the melt ponds through the opening of the brine drainage channels within the sea ice. Shortwave energy is found to be a significant factor in sub-ice ablation through the enhanced shortwave flux through open leads, cracks and holes (Maykut and Perovich, 1987). Mechanical and thermodynamic ablation can also be attributed to the freshwater runoff and flushing through the sea ice (Moritz and Perovich, 1996). Dynamic processes play a large role in breakup and can either retard



or delay the timing of a purely 'thermodynamically' driven breakup. Observations have shown that the ponding on the ice surface occurs so long as the brine drainage networks within the ice allow less gravity drainage than is created by new freshwater inputs from the melt of surrounding snow patches. Once the ice warms to an isothermal state and the brine drainage networks are fully coupled, rapid drainage occurs (e.g., within hours). It also appears that melt ponds on sea ice are generally freshwater at the beginning of the melt period. Once the ice has fully drained (i.e., drainage networks are fully dilated) then melt ponds can reform but they are generally saline. The assumption here is that once the ice is sufficiently porous the freeboard of the ocean surface is actually above the level of the original melt pond, thereby creating a saline surface pond.

### **Ablation State 6**

Once ice break-up occurs, pans of sea ice can exist for extended periods of time as decayed ice. This type of ice has fully formed brine drainage channels and is mechanically weak. The melt ponds on the surface are dominated by brine pond types with only isolated occurrences of freshwater ponds. This is due to the fact that the sea ice freeboard is beneath that of the ocean level, thus with brine drainage channels fully dilated, sea water can occur as ponds within the low areas of the sea ice. This ice can last through the summer season and become second year or multiyear forms in the next year.

## Summary Descriptions

In what follows (Table 1.1) we summarize the physical, thermodynamic and visual characteristics of each of the ablation states.

Table 1.1. Geophysical, thermodynamic and visible characteristics of the proposed sea ice ablation states.

Variable	Characteristics
Winter	Large negative temperature gradients occur within the snow and sea ice with little or no diurnal variation within the thermodynamics of the snow and ice volumes. This results in low brine volumes within the sea ice due to the constriction of the brine pockets from the encroaching ice crystals. Visually this ice appears as a dry snow, cold season ice volume.

Ablation 1

Very early melt

Large negative temperature gradients still occur within the snow and sea ice but there is now a significant variation due to the increasing diurnal range in solar irradiance. This atmospheric forcing can now reach the sea ice volume and thereby begin to increase the volume of brine. This begins once the ice volume exceeds temperatures of about  $-7^{\circ}\text{C}$ . Visually this ice still appears as a dry snow cold season ice volume. Microwave RS data are required to identify this point in the ablation state process

## Ablation 2

### Sustained snow melt

In this state, temperatures in the snow and sea ice are dominated by isothermal or positive gradients (in the snow and upper portion of the sea ice). Water in liquid phase occurs throughout most of the diurnal cycle. The surface albedo is reduced considerably at this point. The surplus energy goes into increasing the temperature within the sea ice volume and there is a corresponding increase in the brine volume of the ice making the ice mechanically weaker than winter or Ablation State 1. Visually this ice will appear as a snow covered ice surface with slight variations in the 'greyness' of the snow patches – particularly with thinner snow patches being a darker grey than thicker snow patches. On site examination will reveal a significant decrease in the snow density and the snow will be sticky.

### Ablation 3

#### Saturated snow

In this state, temperatures in the snow and sea ice are dominated by isothermal gradients. Water in liquid phase occurs throughout the diurnal cycle. The surface albedo is reduced considerably at this point. The surplus energy goes into increasing the temperature within the sea ice volume and there is a corresponding increase in the brine volume of the ice making the ice mechanically weaker than preceding ablation states. Visually this ice will appear as a snow covered ice surface with slight variations in the 'greyness' of the snow patches – particularly with snow patches being a darker grey than thick patches. On site examination will reveal large snow grains in the upper layers and a saturated snow/water mixture in the basal layers.

#### Ablation 4

##### Pond formation

In this state, melt ponds form first in areas of low snow thickness with snow patches being retained from the thicker snow drift patterns. The aerially averaged albedo reduces considerably due to the contributions from the melt ponds themselves. The surplus energy goes into increasing the temperature within the sea ice volume and there is a corresponding increase in the brine volume of the ice making for mechanically weak sea ice. Visually this ice will appear as dark patches of saturated snow through to well developed flooded surfaces of the sea ice. The snow patches will be white in colour and the ponds appearing grey through to blue (depending on the bubble density in the ice at the base of the pond). On site examination will show that the ponds are freshwater as are the snow patches (surface salinity has migrated lower into the sea ice through gravity drainage mechanisms).

## Ablation 5

### Pond drainage

In this state, melt ponds will drain from the surface once the sea ice brine drainage mechanisms become fully dilated. This drainage can occur very rapidly (within hours). This is because the temperature will increase in the ice volume thereby increasing the brine volume until the channels become fully formed. Gravity drainage will flush the freshwater from the surface and the ponds may become replaced with saline ocean water. Visually this ice will appear ponded one day and the next it will have a white porous drained surface. Cracks and holes may be evident but the surface is generally dry. On site examination will show that the surface is made up of white porous granular ice which is saline free (taste test).

## Ablation 6

### Rotten ice

Once the ice has broken up it can exist for several months as a form of rotted ice. This form of sea ice has fully opened brine drainage channels thus making the melt ponds mostly saline (except in areas where local melting can create new ponds). The ice appears darker in colour because it is saturated throughout with ocean water. This ice no longer has any appreciable mechanical strength.

---

In the definition of the ablation states we have compartmentalized what is by definition a continuous process. The creation of a thermodynamically weak sea ice volume requires that the brine volume exceed about 5 percent by volume. At this point the brine drainage channels will begin to reform thus significantly reducing the mechanical strength of the sea ice. From field experiments it appears that this point of 5 percent by volume can occur anywhere in Ablation State 3 or 4. The timing of this depends on the thermodynamic controls on the evolution of the snow/ice system and the historical conditions of the original ice formation (salinity and density). Once this point has been reached physical break-up then depends on the magnitude and timing of atmospheric or oceanic forcing on the snow/sea ice system.

In this section we have reviewed the nature of the physical properties of both snow and sea ice within the thermodynamic regimes spanning the freeze-up, winter and proposed six ablation states to compartmentalize the thermodynamic evolution of sea ice. In the next section we will keep the same seasonal structure as a framework for reviewing the electrical properties which are associated with the geophysical and thermodynamic changes described above.



## Electrical Properties of Sea Ice

The relative 'effective complex permittivity'<sup>4</sup> or dielectric constant is the theoretical framework through which we can link the thermodynamic, mechanical and electromagnetic (EM) interactions of sea ice. It is in fact the theoretical cornerstone for this entire report. Although dielectric theory is very well developed it is a rather complex field of study. In what follows we will summarize the salient theoretical issues required within the framework of our 'Electro-Thermophysical' modeling and leave the details for the interested reader to pursue elsewhere<sup>5</sup>.

Dielectric properties are important in microwave remote sensing because they define the electrical conductivity of the material relative to the wavelength and polarization of the incident energy. The dielectric constant is used to express the permittivity ( $\epsilon'$ ) and loss ( $\epsilon''$ ) of the snow and sea ice. Simply put,  $\epsilon'$  is the ability of electromagnetic energy to pass into or through a particular interface or volume and  $\epsilon''$  is a measure of the transfer of energy (by either transmission or absorption) within the material. The dielectric constant is expressed as the complex sum of a real and imaginary part where  $j$  is the square root of negative one [2].

$$\epsilon^* = \epsilon' + j\epsilon'' \quad [2]$$

---

<sup>4</sup>This is also known as the complex dielectric constant with a real (permittivity) and an imaginary (loss) part to the complex number. We use the terms interchangeably in this report.

<sup>5</sup>Numerous references by Barber et al. provide direct support for the theory. Text references include Ulaby et al. 1986 and Matzler (numerous references).

The theory of microwave scattering and emission, and by design, the theory of microwave interaction models, separate the scattering process into an air-snow interface, a snow volume, a snow-ice interface and an ice volume. For computation of  $\sigma^\circ$  (total average relative scattering coefficient), a common approach is to sum the contributions of each scattering medium, weighted by the transmissivity coefficient [7]. This means that the volume scattering term would be weighted by the transmission coefficient across the air-snow interface ( $\Psi_{as}$ ). Note that  $\Psi_{as}$  (or any  $\Psi$  in [7]) is then related to the complex dielectric constant as one minus the Fresnel Reflection Coefficient [3]

$$\Psi_{as} = (1 - |\Gamma_{VV}|) \quad [3]$$

The Fresnel Reflection Coefficient is a measure of the amount of radiation which is reflected at the interface between adjacent mediums. It is computed as a complex ratio of the dielectric properties of the two materials creating the interface (i.e., air-snow or snow-ice). Coefficients are available for either vertically or horizontally polarized energy.

$$\Gamma_{HH} = \frac{\xi_2 \times \cos \theta - \xi_1 \times \cos \theta'}{\xi_2 \times \cos \theta + \xi_1 \times \cos \theta'} \quad [4]$$

Where  $\xi_1$  and  $\xi_2$  are the complex dielectric constants of the air and snow [5 and 6].

$$\xi_1 = \frac{1}{\sqrt[2]{\epsilon' + \epsilon''}}, \text{ for material \#1 (air)} \quad [5]$$

$$\xi_2 = \frac{1}{\sqrt[2]{\epsilon' + \epsilon''}}, \text{ for material \#2 (snow)} \quad [6]$$

The important thing to note here is that the transmissivity term controls the scattering magnitude [7] and allows you to quantify the relative contributions of the various layers in the model and that transmissivity is controlled by the complex dielectric constant as per [4]:

$$\sigma_{\text{total}}^o(\theta) = \sigma_{\text{ss}}^o + \Psi_{\text{as}}^2(\theta) * \sigma_{\text{sv}}^o(\theta') + \Psi_s^2(\theta) * \sigma_s^o(\theta') \quad [7]$$

Typically, dielectric mixture models are used to predict the complex permittivity of a heterogeneous material. A mixture model is required because both snow and sea ice are combinations of water (in liquid, vapour or ice phases), salt (as a solid, or more importantly, as brine) and air inclusions. Each component has a very different complex dielectric constant at microwave frequencies and exists in different characteristic sizes, shapes, volumes and surface distributions. In general the average relative complex dielectric constant of sea ice is a function of these constituent parts relative to the look direction of the electromagnetic field (Ulaby et al., 1986). Thermodynamically the proportions of these constituent parts are controlled by the sea ice phase diagram (Figure 1.1) described previously.

Models of the dielectric constant require that we consider the relative proportions of brine within the mixture and the proportion of salts within the brine. Although there is only a small quantity of brine present in the ice, its large dielectric constant ( $\epsilon^*=70 + j34$ ) has a significant influence on the resulting dielectric properties of the ice-brine mixture. The salinity of the brine ( $S_b$ ) is also a function of the snow/ice temperature. With increasing negative temperatures the proportion of salts within the brine mixture increases (Figure 1.1). Various aspects of these phase relationships can be approximated using polynomial equations. For illustrative purposes we list the equations required to convert between the salinity of the brine ( $S_b$ ) and temperature [8 to 10] and the volume of brine ( $V_b$ ) as a function of salinity ( $s$ ) and temperature [11 to 14]. Similar models are available to convert between temperature and other components of the phase diagram.

$$S_b = 1.725 - 18.756T - 0.3964T^2, -8.2 \leq T \leq -2^\circ C \quad [8]$$

$$S_b = 57.041 - 9.929T - 0.16204T^2 - 0.002396T^3, -22.9 \leq T \leq -8.2^\circ C \quad [9]$$

$$S_b = 242.94 - 1.5299T - 0.0429T^2, -36.8 \leq T \leq -22.9^\circ C \quad [10]$$

$$V_b = 10^{-3} S_i \left( -\frac{52.56}{T} - 2.28 \right), -2.06 \leq T \leq -0.5^\circ C \quad [11]$$

$$V_b = 10^{-3} S_i \left( -\frac{45.917}{T} + 0.930 \right), -8.2 \leq T \leq -2.06^\circ C \quad [12]$$

$$V_b = 10^{-3} S_i \left( -\frac{43.495}{T} + 1.189 \right), -22.9 \leq T \leq -8.2^\circ C \quad [13]$$

$$V_b = 10^{-3} S_i \left( -\frac{49.185}{T} + 0.532 \right), -22.9 \leq T \leq -0.5^\circ C \quad [14]$$

To model the dielectric constant of the snow and/or sea ice we have to separate the material into its host and inclusion components. In the lower portion of the snow pack there is a considerable amount of salinity in the form of brine. This brine is treated as an ‘inclusion dielectric’ within a dry snow ‘host dielectric’, following the approach of Matzler et al. 1984b and Drinkwater and Crocker, 1988. The mixture model is expressed as [15].

$$\Delta \varepsilon_{mix}^* = \chi V_b \left\{ \frac{\varepsilon_b^* - \varepsilon_{ds}^*}{1 + \left[ \frac{\varepsilon_b^*}{\varepsilon_{ds}^*} - 1 \right] A_0} \right\} \quad [15]$$

Where  $\varepsilon_{ds}^*$  and  $\varepsilon_b^*$  are expressed in complex terms and represent the dielectric constants of dry snow and brine,  $\chi$ ,  $A_0$ , and  $V_b$  are: a coupling factor representing the fraction of brine accounted for by  $A_0$ ; the dominant depolarization factor; and the volume of brine contained within the saline snow layer. In this work  $\chi$  is set at 0.66667, a value appropriate for modeling the brine inclusions as isotropically oriented oblate spheroids (Drinkwater and Crocker, 1988). The depolarization factor is set at 0.053, following Denoth, 1980, and the brine volume is computed as per the equations above.

In [15] the host dielectric is considered as a dry snow matrix, consisting of ice grains and air. The parameter  $\varepsilon_{ds}^*$  is computed using an empirical model attributable to Hallikainen et al. (1986). The permittivity of dry snow was computed as [16] and the loss as [17].

$$\varepsilon'_{ds} = 1.0 + 1.9\rho_{ds} \quad [16]$$

$$\varepsilon_{ds}'' = \frac{0.34V_i\varepsilon_i''}{(1 - 0.417V_i)^2} \quad [17]$$

Where  $\rho_{ds}$ ,  $\varepsilon_i''$ , and  $V_i$ , are the density of dry snow, the dielectric loss, and the volume fraction of freshwater ice in the snow matrix.

In [15] the inclusion dielectric is considered to consist of brine pockets held within the interstices of the snow grains. The parameter  $\varepsilon_b^*$  is defined as the complex dielectric constant of brine computed from [18 and 19] based on models of the Debye form, following Ulaby et al. (1986).

$$\varepsilon_b' = \varepsilon_{w\infty} + \left[ \frac{\varepsilon_{b0} - \varepsilon_{w\infty}}{1 + (2\pi f \tau_b)^2} \right] \quad [18]$$

$$\varepsilon_b'' = (2\pi f \tau_b) \cdot \left[ \frac{(\varepsilon_{b0} - \varepsilon_{w\infty})}{1 + (2\pi f \tau_b)^2} \right] + \left[ \frac{\sigma_b}{2\pi f \varepsilon_0} \right] \quad [19]$$

Where  $\varepsilon_{w\infty}$ ;  $\varepsilon_{b0}$ ;  $f$ ;  $\tau_b$ ;  $\sigma_b$ ;  $\varepsilon_0$  are: the high frequency limit of the dielectric constant of pure water; the static dielectric constant of pure water; the frequency of electromagnetic energy (Hz); the relaxation time of the brine; the ionic conductivity of the brine solution (S·m-1); and the permittivity of free space (F·m-1). These parameters are estimated using a series of polynomial models which will not be reproduced here( see Stogryn, 1971; Ulaby et al. 1986; and Hallikainen and Winebrenner, 1992).

When free water becomes available within the snow pack the dielectric properties change considerably. The relationships between  $\varepsilon'$  and  $\varepsilon''$  for wet

and dry snow have been determined empirically. Models for computation of  $\varepsilon'$  and  $\varepsilon''$  of wet snow relative to the values for dry snow, have been developed by Tiuri et al., (1984) and are presented in [20 to 22].

$$\Delta \varepsilon'_{ws} = \varepsilon'_{ws} - \varepsilon'_{dry} \quad [20]$$

$$\Delta \varepsilon'_{ws} = \varepsilon'_w (0.1 W_v + 0.8 W_v^2) \quad [21]$$

$$\varepsilon''_{ws} = \varepsilon''_w (0.1 W_v + 0.8 W_v^2) \quad [22]$$

Where:  $\varepsilon'_{dry}$  is the permittivity of dry snow from [16];  $W_v$  is the volumetric liquid water content measured *in situ*; and  $\varepsilon'_{ws}$  and  $\varepsilon''_{ws}$  are the permittivity and loss of wet snow. The complex dielectric constant of water ( $\varepsilon'_w$  and  $\varepsilon''_w$ ) are computed using the Debye model for liquid water [23] and [24].

$$\varepsilon'_w = \varepsilon_{w\infty} + \left[ \frac{\varepsilon_{w0} - \varepsilon_{w\infty}}{1 + (2\pi f \tau_w)^2} \right] \quad [23]$$

$$\varepsilon''_w = (2\pi f \tau_w) \cdot \left[ \frac{(\varepsilon_{w0} - \varepsilon_{w\infty})}{1 + (2\pi f \tau_w)^2} \right] \quad [24]$$

Where the parameters are the same as in [18] and [19] but for liquid water rather than brine.

In summary, the complex dielectric constant of snow and sea ice is the link between the physical and thermodynamic properties of the icescape. The phase diagram (Figure 1.1) provides the basic constituent proportions as a function of temperature. Polynomial models can be used for specific conversions [e.g., 8 to 14]. These can then be used in models explicitly developed to estimate the effective complex permittivity of the snow and sea ice throughout the annual cycle. By knowing the magnitude and range of both the permittivity and loss, we can link the EM scattering of the surface to its electrical properties. In what follows we utilize the dielectric mixture models described above to investigate the mechanisms responsible for affecting the range and magnitude of the complex dielectric constant within the now familiar surface regimes of 'freeze-up', 'winter', and ablation states 1 through 6.



## Freeze-up

The dielectric permittivity ( $\epsilon'$ ) and loss ( $\epsilon''$ ) of sea ice are found to be highly variable during freeze-up primarily due to spatial and temporal variations in the freezing rate, initial salinity of sea ice and the type of mechanical environment present during formation (calm seas with low winds or waves with strong winds). The amount of brine trapped in sea ice is a function of the sea water salinity and the freezing rate. The faster the freezing rate, the more brine that is entrapped. Modelling of the complex dielectric constant shows that the temperature has a linear effect on both permittivity and loss. Values are considerably higher than the typical winter norms of  $\epsilon^*=3.5 + j0.1$  (Figure 1.13).

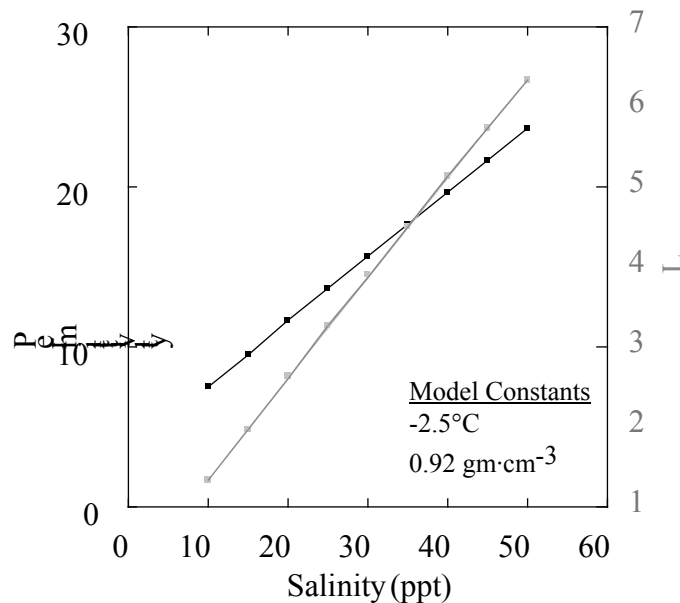


Figure 1.13. Modeled relationships for the dielectric permittivity and loss as a function of bulk ice salinity for newly formed sea ice. Ice temperature and density are held constant.

The effect of temperature on permittivity and loss illustrates that as the ice thickens and the ice temperature decreases there is a rapid drop in the complex dielectric constant of the sea ice (Figure 1.14). In this simplistic model we consider that the salinity and ice density remain constant. In reality, of course, these variables are highly coupled. The curvilinear relationship between the dielectrics and temperature (Figure 1.14) is a direct result of the effect of temperature on brine volume.

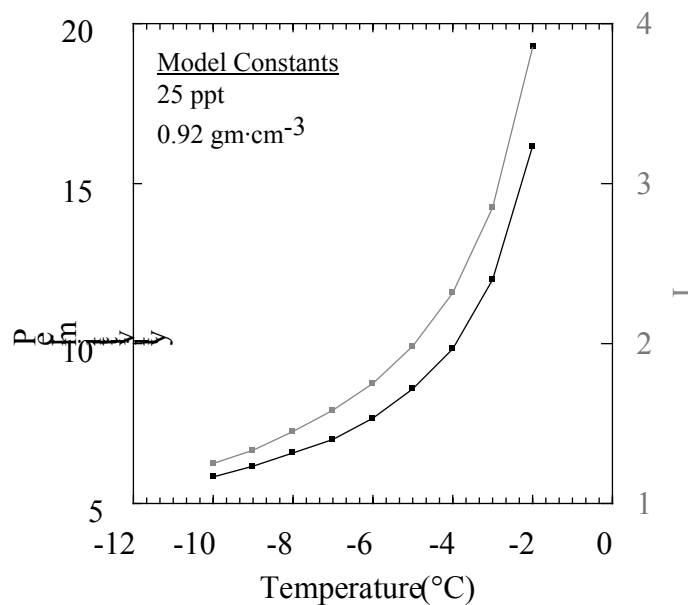


Figure 1.14. Modeled relationships for the dielectric permittivity and loss as a function of ice volume temperature, for newly formed sea ice. Ice salinity and density are held constant.

The brine volume of newly formed ice rapidly decreases as the ice grains enlarge during initial formation of frazil and grease ice layers. The grains grow outward and push the brine concentration towards the surface (as a

hoar layer) and into the water. From initial concentrations of 50 ppt, surface concentrations drop rapidly to about 25 ppt. Nakawo and Sinha (1981) reported a decrease in salinity from 25 ppt on December 2 to 8.5 ppt on December 9 at a depth of 40 cm in Arctic first-year ice. In warmer waters off the Labrador coast, Weeks and Lee (1958) observed the same rapid decline in salinity shortly after ice formation. Typical salinity values for Arctic first-year ice, after initial rapid desalination, appear to be about 10 to 20 ppt near the ice surface, 4 to 6 ppt in the bulk of the ice sheet, and rise to 10 to 30 ppt at the ice-water interface (Haykin et al., 1994). The behavior of the complex dielectric constant under these growth conditions is more realistically a function of a combined decrease in salinity and a decrease in temperature. Modeled illustrations of a freeze-up period show that over a typical temperature and salinity range the dielectric constant decreases in a curvilinear fashion towards winter norms of about  $\epsilon'=3.5$  and  $\epsilon''=0.1$ .

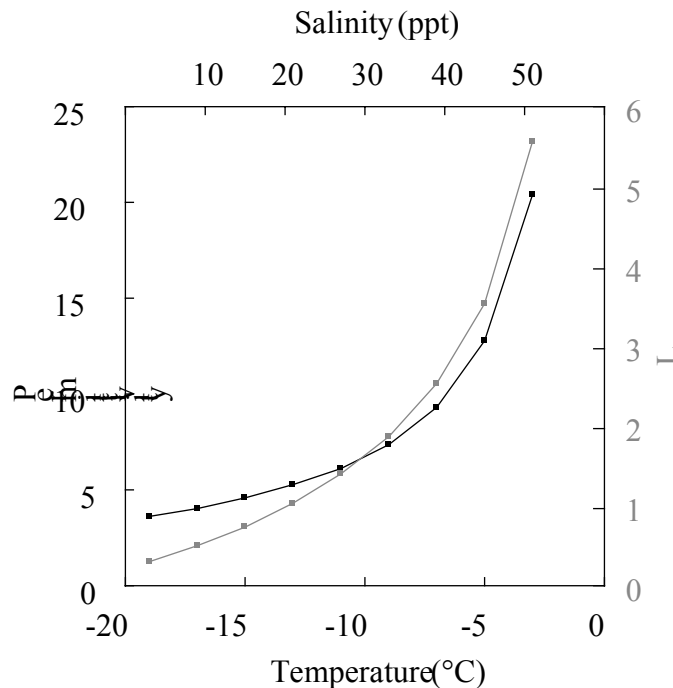


Figure 1.15. Modeled relationships for the dielectric permittivity and loss as a function of typical values of ice salinity and temperature as ice forms and grows to about 30 cm thick. Density is held constant at  $0.92 \text{ gm}\cdot\text{cm}^{-3}$ .

A unique feature of the young ice growth under a strong temperature gradient is the development of a 'frost flower' or 'salt flower' layer on the ice surface. These features have very high bulk salinities and can have a dielectric constant considerably higher than those computed even for the warmest and highest salinity cases in the above model runs. Electromagnetically these features are also strong indicators of new ice formation as will be discussed in a later section.

## **Winter**

To adequately model the dielectric constant within the winter period, we must consider both the snow and sea ice as an integrated environment. Results show that the vertical variability in both the permittivity and loss are a function of the distribution of salinity within the snow layer relative to the vertical structure of the snow density. Typical snow covers on first-year sea ice show a dielectric profile which changes only slightly with changing salinity and density (Figure 1.16) and is sufficiently low relative to that of sea ice to make it essentially transparent at 5.3 GHz frequencies.

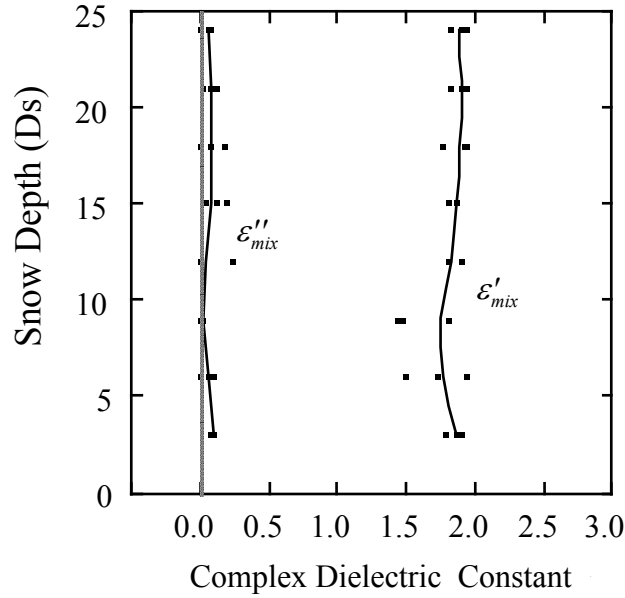


Figure 1.16. Modeled  $\epsilon'_{mix}$  and  $\epsilon''_{mix}$  within the winter conditions based on measured physical parameters of density, salinity and wetness typical of the winter period.

This somewhat surprising result occurs because of the counteracting effects of density and brine on the dielectric constant ( $\epsilon^*$ ). In the basal layer of the snow, density is low (decreases  $\epsilon^*$ ) and salinity is high (increases  $\epsilon^*$ ). In the upper layers of the snow cover, density is high (increases  $\epsilon^*$ ) and salinity is low (decreases  $\epsilon^*$ ). These sum to create a vertical profile with both low permittivity and loss (Figure 1.16), relative to that of the sea ice, making the snow layer transparent to microwave scattering and emission.

The snow cover imparts an indirect effect on the dielectrics of the sea ice by controlling the temperature at the snow/sea ice interface. Models provide a unique insight into the dynamics of the dielectric properties of sea ice which can be attributed directly to the thermodynamic effects of the overlying

snow cover. Results from the application of a physically based thermodynamic model illustrate the effect of increasing snow thickness on the interface temperature between the snow volume and ice surface. The real part of the dielectric constant (Figure 1.17) increases most rapidly, under all atmospheric temperatures, over the 0 to 10 cm snow depth range, illustrating the strong insulating effect of even a thin snow cover. The dielectric loss of the sea ice surface (Figure. 1.18) shows a similar response to the atmospheric forcing at the snow surface under a range of snow thickness conditions. This approach is currently being exploited as a potential mechanism for extracting snow thickness information from EM scattering over snow covered sea ice (Barber and Nghiem, 1998).

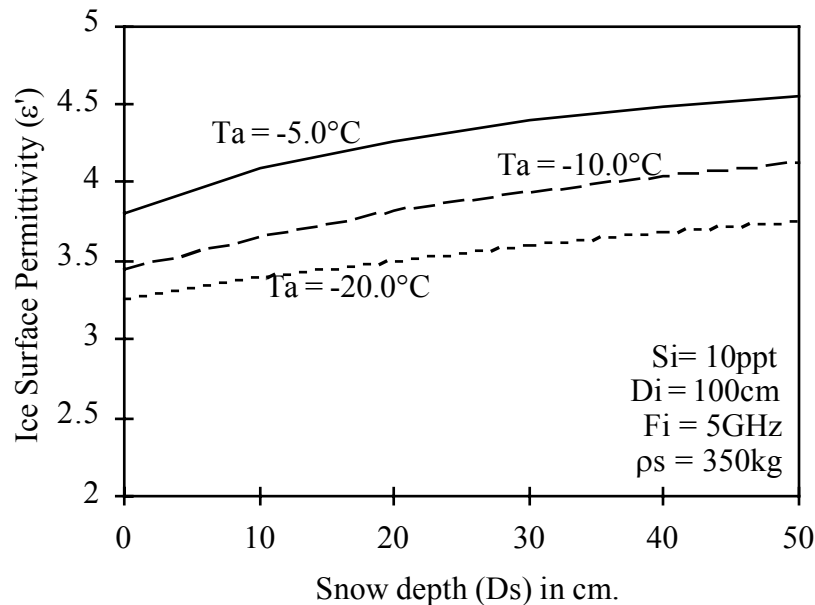


Figure 1.17. Change in permittivity ( $\epsilon'$ ) of the ice surface dielectric constant as a function of snow cover on a 100 cm thick ice sheet.

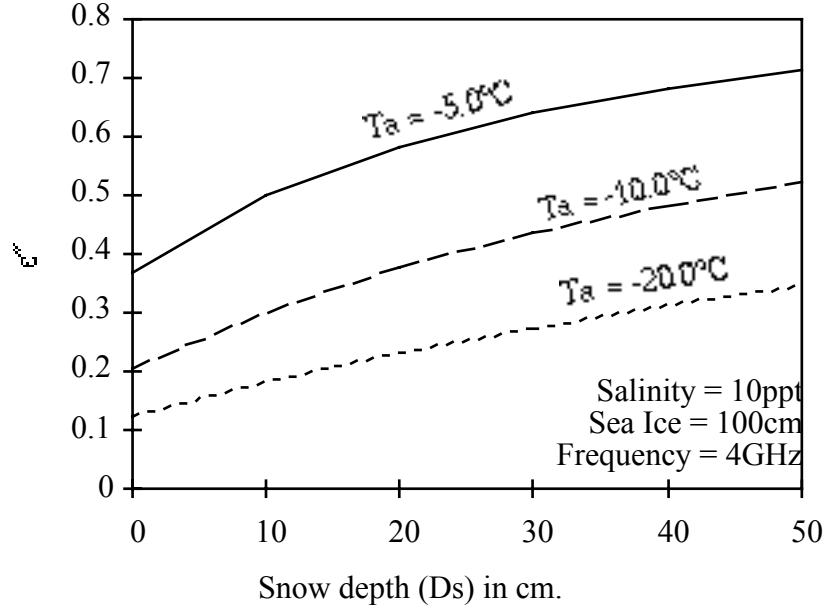


Figure 1.18. Change in dielectric loss ( $\epsilon''$ ) as a function of snow cover on a 100 cm thick ice sheet.

A unique manifestation of this thermodynamic effect occurs over first year sea ice where the basal layer of the snow cover has a significant volume of salinity in the form of liquid brine<sup>6</sup> (Barber et al. 1993). When  $\epsilon^*$  is modeled at a snow salinity (Ss) of 12 ppt and a frequency of 5.3 GHz the resulting relationship illustrates the temperature dependence of the brine volume on the complex dielectric constant of the brine-snow mixture (Figure 1.19). Results for  $\epsilon'_{mix}$  indicate that a quadratic relationship exists at each of the snow densities over the temperature range -3.0 to -21.0 °C (Figure 1.19). The rapid decrease in  $\epsilon'_{mix}$  occurs between -3.0 and -7.0 °C. Between -7.0 and -21.0 °C there is only a small decrease in  $\epsilon'_{mix}$  with temperature. The higher the snow density, the larger the absolute value of  $\epsilon'_{mix}$ .

<sup>6</sup>We note here that this rapid change in both permittivity and loss can occur in the basal layer of the snow even when atmospheric temperatures are <15°C because of the insulating effect of a thick snow cover (i.e., these temperatures are at the snow/ice interface). This concept is exploited later in this report when

Results from modeling  $\epsilon''_{mix}$  (Figure 1.19) under these conditions illustrates a similar relationship; as the temperature decreases from -3.0 to -7.0 °C there is a rapid decrease in  $\epsilon''_{mix}$ . Between -7.0 and -21.0 °C there is a more gradual decrease in  $\epsilon''_{mix}$ . Note that at a higher snow density the slope of the decrease in  $\epsilon''_{mix}$  is greater both between the -3.0 and -7.0 temperature range and the -3.0 and -21.0 °C range. This is due to the fact that at the higher snow densities there are larger brine and ice volumes than there are air volumes. In the mixture model the brine and ice exert a larger control on both the real and imaginary parts of  $\epsilon^*$ .

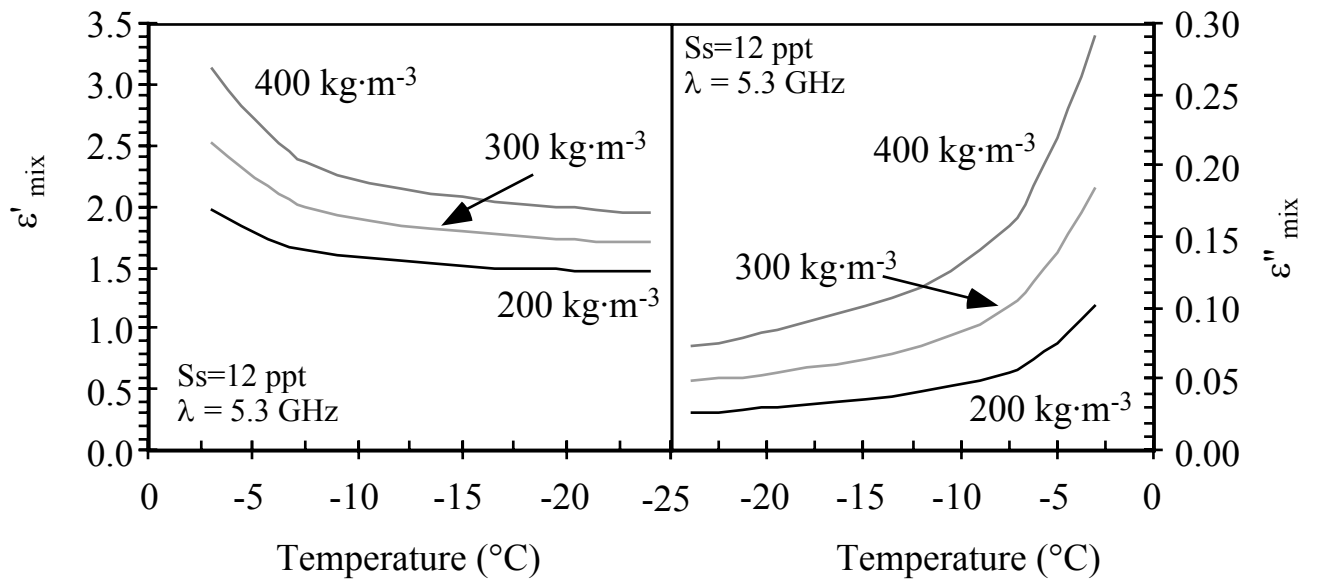


Figure 1.19. Modeled  $\epsilon'_{mix}$  and  $\epsilon''_{mix}$  as a function of snow temperature at snow densities of 200, 300 and 400  $\text{kg}\cdot\text{m}^{-3}$ . Snow salinity was set at 12 ppt and frequency at 5.3 GHz (C-band).



In the winter period the dielectrics are a function of the interface temperature, which is controlled by the thickness of the snow cover. In all modeling cases we consider only the dry snow case.

## **Ablation State 1 and 2**

From a dielectric perspective snow begins to play an important role within Ablation States 1 and 2. We combine these states because they can overlap considerably due to diurnal cycling. In general Ablation State 1 precedes Ablation State 2 but the timing of each state is a function of the strength of the atmospheric forcing upon the surface. The snow contributes to the dielectrics of the volume both through the thermodynamic effects on the ice surface (as described above) and through direct changes in the dielectric constant either as a result of temperature changes in the snow volume or more importantly through the presence of water in liquid phase. In what follows we will use both dielectric and thermodynamic models to provide a variety of insights into the salient mechanisms controlling the dielectric constant within the temperature and geophysical characteristics typical of this early melt period.

At a frequency of 5.3 GHz and a snow density of  $300 \text{ kg}\cdot\text{m}^{-3}$  the behavior of both the real and imaginary parts of  $\epsilon^*$  are shown to be a function of snow salinity and temperature (Figure 1.20). The  $\epsilon'_{mix}$  increases with increasing salinity over the temperature ranges of  $-20$  to  $-4^\circ\text{C}$ . The slope of the increase is largest for the higher temperature due to the role which brine volume plays in specifying  $\epsilon'_{mix}$ . Results from the imaginary part of the mixture model ( $\epsilon''_{mix}$ ) shows that there is a similar increase in the loss of a

brine wetted snow cover. The increase is largest at a temperature of  $-4^{\circ}\text{C}$  for the same reason as  $\epsilon'_{mix}$ . Note that  $\epsilon''_{mix}$  ranges over several orders of magnitude while  $\epsilon'_{mix}$  ranges only over factors. Also note that the magnitude of the dielectric constant of the snow approach that of sea ice ( $\epsilon'=3.5$ ) at temperatures above  $-4^{\circ}\text{C}$  and salinities above 15 ppt.

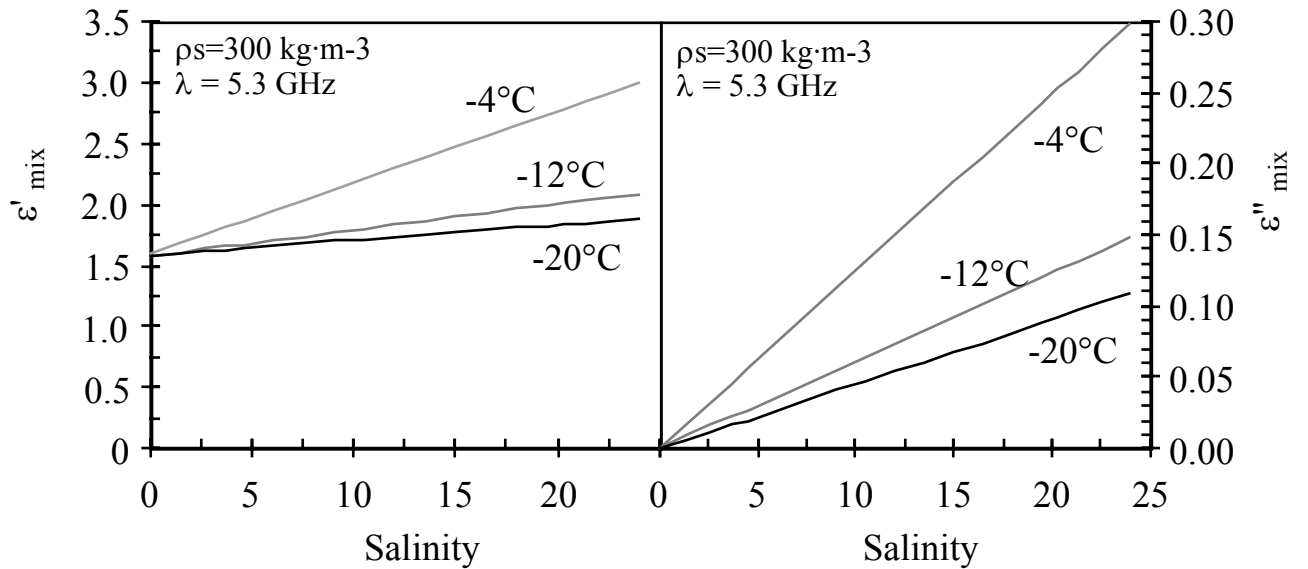


Figure 1.20. Modeled  $\epsilon'_{mix}$  and  $\epsilon''_{mix}$  as a function of snow salinity and snow temperatures of  $-4$ ,  $-12$  and  $-20^{\circ}\text{C}$ . Snow density was set at  $300 \text{ kg}\cdot\text{m}^{-3}$  and frequency at  $5.3 \text{ GHz}$  (C-band).

When water occurs in liquid phase there is a dramatic increase in both the real and imaginary parts of the dielectric constant. This is because the water has a very high dielectric constant ( $\epsilon^*=65.81 + j36.52$ ). This combines in the mixture model to dramatically increase the bulk dielectrics of the snow cover. Model results are again utilized to illustrate the pertinent relationships.

The effect of water volumes between 0.1 and 10 percent are shown to be density and frequency dependent. Permittivity of wet snow increases both with increasing water content and with increasing snow density (Figure 1.21). The dielectric loss of a wet snow cover is density independent and water volume dependent (Figure 1.22). As water volume increases between 0.1 and 10 percent,  $\epsilon''$  increases from 0.004 to 0.667. Note that the  $\epsilon''$  of dry snow is approximately 0.0008 (Tiuri et al., 1984).

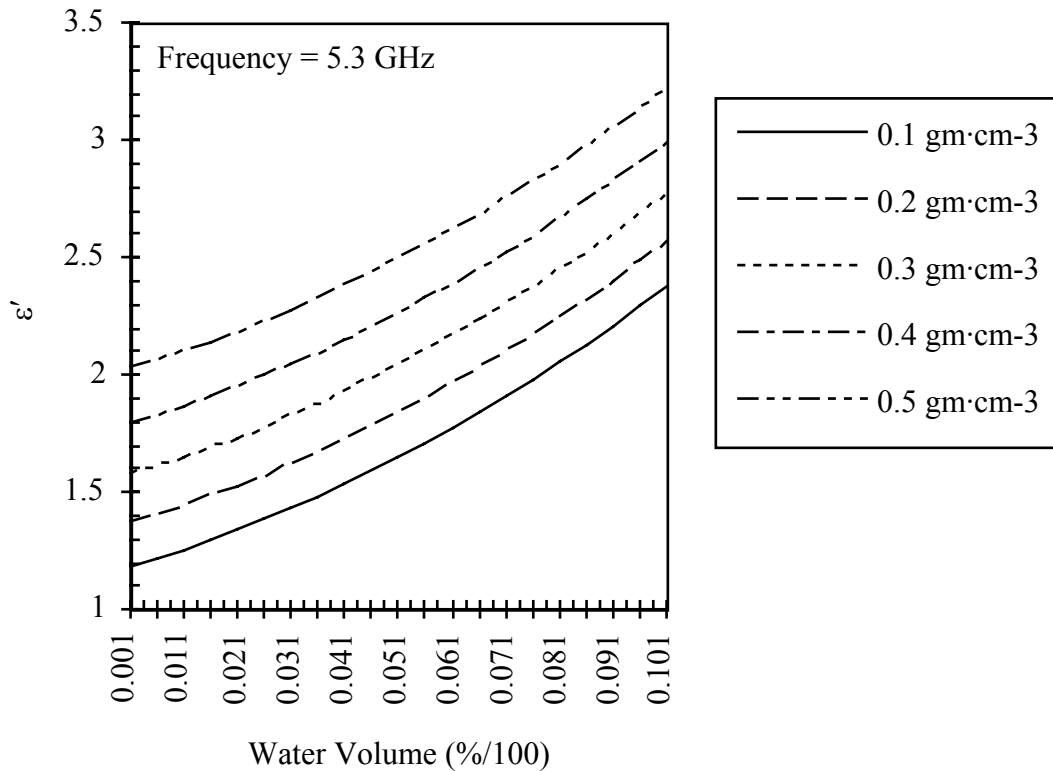


Figure 1.21. Dielectric permittivity ( $\epsilon'$ ) as a function of water volume and snow density.

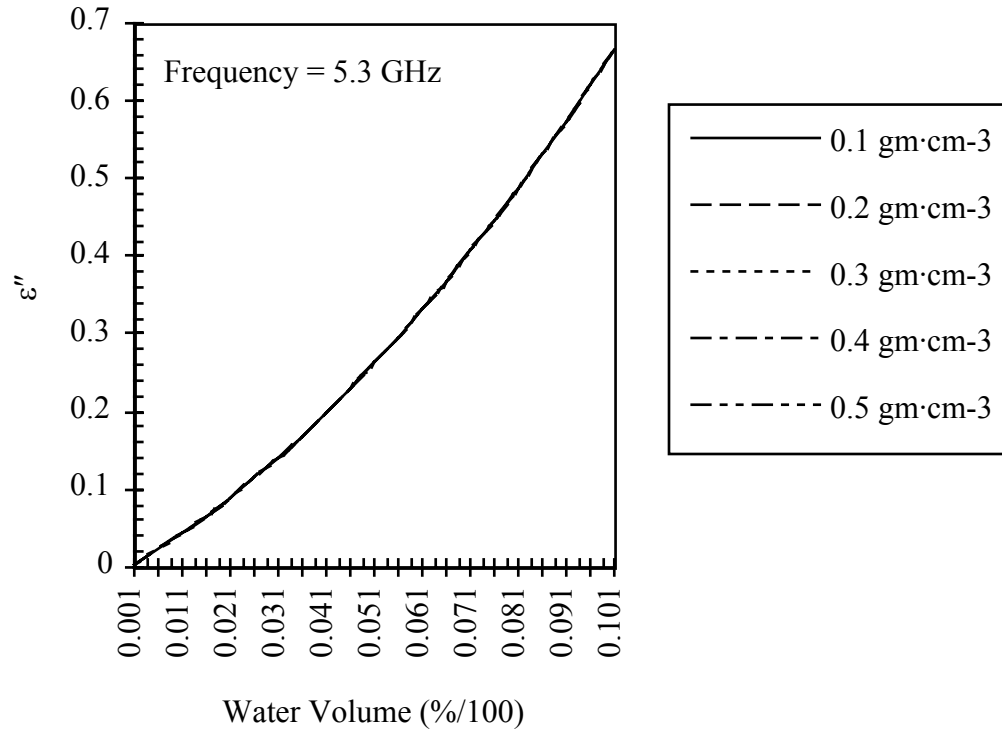


Figure 1.22. Dielectric loss ( $\epsilon''$ ) as a function of water volume and snow density.

### Ablation State 3

Within this period the complex dielectric constant is highly variable in both space and time. Vertically the distribution of water in liquid phase dominates the pattern of both the permittivity and loss. Within the pendular regime the water will affect the dielectrics according to the temperature and density within any particular layer. Once drainage begins (funicular regime) we can expect high water concentrations in the basal layer of the snow volume and much lower ones near the top (because of gravity drainage). This can create a large vertical difference in both permittivity and loss and is

the primary mechanism responsible for our ability to detect this particular surface phenomena using microwave remote sensing data (as described in section 2). Temporally the pattern of cool nights and relatively warm days also creates a highly variable dielectric volume. By extracting typical values for a single diurnal cycle we can visualize the pattern of permittivity for the snow volume as a bulk dielectric (Figure 1.23). Note that the peak in the dielectric constant may not coincide with the maximum air temperature due to the effect of latent heating on the phase changes from ice to water.

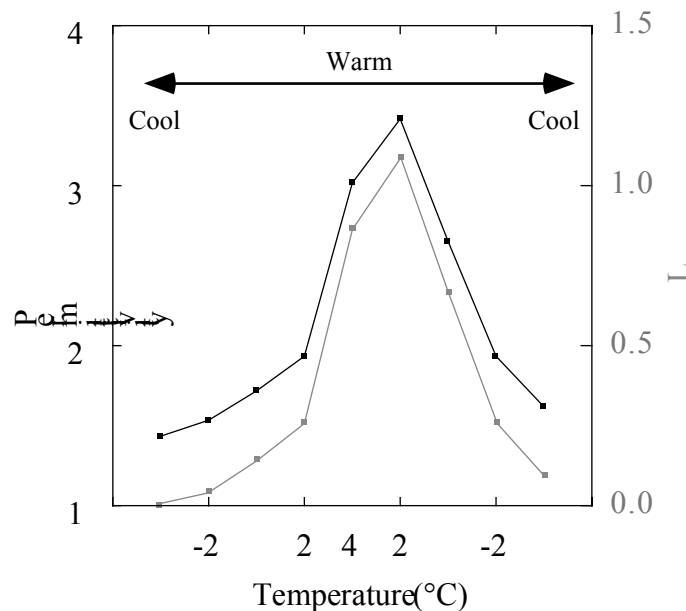


Figure 1.23. Modeled permittivity and loss for a typical diurnal period with cool nights and warm days. Values for temperature and wetness are approximated from field observations, salinity is held constant at 0, density at  $250 \text{ kg}\cdot\text{m}^{-3}$ , and using a bulk dielectric for the snow volume.

## **Ablation State 4**

Once the snow basal layer becomes saturated it takes a tremendous removal of energy from the system to return it to earlier thermodynamic regimes. This period denotes what we consider as the 'point of no return' from an energy balance perspective. The dielectrics of the surface are driven by the spatial pattern of the melt ponds to surface snow patch fractions. In the simplest sense the ponded surfaces have very high permittivity and loss and the remnant snow patches have values at or near saturated snow dielectrics, as described above. We note here that the effective complex permittivity of ocean water is nearly equal to melt pond water since the later is near its freezing point throughout much of the summer period. This means that microwave scattering will not be able to detect the difference between saline surface ponds and freshwater surface ponds.

The dielectric properties of Ablation States 5 and 6 are poorly understood and result from the dynamics of pond re-formation and drainage over the summer period. The complex permittivity during this period is dominated by the presence of water in liquid phase either within the interstices of the freely draining snow or within the melt ponds themselves.

In this section we have introduced the theory required to understand the nature of the complex dielectric constant of both snow and sea ice. We have introduced the physical and thermodynamic variables which are required to drive the dielectric mixture models and have shown that the primary variables of interest are the morphology of the inhomogeneities (e.g., size and shape of brine, ice and air inclusions), bulk values of the brine volume, and the temperature of the material. We reviewed the processes creating the

range and magnitude of the dielectric constant within each of the thermodynamic regimes (Figure 1.2). We also showed that the processes operating within each of the regimes results in highly variable vertical, spatial and temporal variation in the complex dielectric constant of both the snow and sea ice. In the next section we continue our investigation of the development of a 'Electro-Thermophysical' model by examining how the physical and thermodynamic properties, as reviewed to this point, can be linked to the mechanical properties of snow covered sea ice.

## **Mechanical Properties of Sea Ice**

As is evidenced by the preceding description, sea ice is a complicated material in terms of its physical and electrical properties. Not surprising then, is the fact that these complexities carry over to sea ice mechanical properties. Its elasticity parameters are functions of temperature, salinity, brine volume, crystal size, and crystal orientation. Brine inclusions are critically important in determining mechanical properties such as ice strength. Planes of failure in first-year ice crystals coincide with planes of brine and salt concentration, which in turn coincide with structures of ice grains (e.g., frazil versus columnar alignments). Brine and salt inclusions reduce the area of bonding between ice plates causing inter-plate boundaries to be zones of weakness (Schwarz and Weeks, 1977). Coincident with the brine drainage process in first-year ice are changes in entrapped air volume. Brine expulsion and drainage results in vacant pores and cavities in the ice sheet. As the ice sheet ages and thickens the number of air filled pores increase substantially, thereby influencing ice density and strength.

The thickness of sea ice is extremely variable on a multitude of spatial and temporal scales and is a major factor in determining the overall strength of first-year sea ice. Compressive strength, growth rate, surface temperature and salinity are all dependent on ice thickness (Thorndike et al, 1975). Parameters such as temperature, salinity and density have important roles in ice strength, but the thickness of sea ice ultimately determines the efficiency or feasibility of an icebreaking or navigational operation.

There are two primary processes affecting the thickness of sea ice: i) thermodynamic and ii) mechanical. Thermodynamic processes are



responsible for determining mean regional ice thickness. Sea ice thickness can be thought of as an indicator of thermodynamic equilibrium between ice accretion and ice ablation. Regional climatic conditions determine this equilibrium and therefore determine mean ice thickness. Mechanical processes determine the extremes of ice thickness, creating features such as leads, pressure ridges and rubble fields. Pressure ridging affects sea ice thickness and is most prevalent wherever atmospheric or oceanic forcing drive sea ice up against land masses or landfast ice regimes. The Canadian Archipelago is a prime example of such a region. In the Eurasian Seas, the Arctic Drift Stream moves ice away from coastlines into the central Arctic Basin. Consequently, pressure ridging is minimal (LeSchack, 1980). The thickness distribution of an ice pack strongly determines ice strength. If open water and thin ice are present in an area of thick ice, the compressive strength will be much lower than if all the ice is uniformly thick.

The strength of sea ice may be defined as the stress at which fracture occurs, or it may imply the condition at which the material is no longer able to sustain the applied stress, but is in a state of yield (Gold, 1968). Therefore the terms 'strength' or 'stress' are used interchangeably in this report. The properties of the ice and the nature of the stress conditions determine the type of failure. In some circumstances ice may undergo plastic deformation, in others it may experience brittle failure. Ice strength has numerous aspects based both on sea ice properties (ice type, temperature, salinity, brine volume, porosity, grain structure and thickness) and the dominant strength type (compressive, tensile, flexural or shear).

We note here that temperature has a linear effect on ice strength (sea ice strength increases as temperature decreases) while salinity has a non-linear

effect. The influence of temperature and salinity can be converted into a single function - brine volume. Cox and Weeks (1988) found that although temperature and salinity profiles are strong functions of the initial freezing date, small changes in the brine volume profiles can be caused by small variations in the thermodynamics of the volume. This is more fully explained in the preceding section where we showed the relationship of snow thermodynamics on the snow/sea ice interface dielectrics. In addition, factors such as strain rate and load direction also determine ice strength. Assur (1958) developed a theoretical model [25] for sea ice structure and related it to sea ice strength. His model assumed that the reduction in the strength of sea ice is proportional to the reduction in ice volume due to the existence of rows of brine cylinders in the ice. The strength for ice with this structure is:

$$s = s_0 \left( 1 - 2 \sqrt{\frac{\zeta}{\pi \frac{b_0}{a_0}}} \sqrt{V_b} \right) \quad [25]$$

Where,  $s$  and  $s_0$  = the ultimate tensile strengths with and without brine, respectively;  $\zeta = g/g_0$  with  $g$  being the average length and  $g_0$  the average separation of brine pockets along the growth axis, respectively;  $V_{br}$  = the brine volume;  $a_0$  = the average platelet thickness; and  $b_0$  = the average brine cylinder separation. As revealed by the above equations, the strength of sea ice decreases as the brine content increases.

The strength of sea ice can be classified according to a variety of applied stresses. Applied stress to sea ice can be either compressive (horizontal or vertical), tensile (horizontal or vertical), shear, or flexural stress.

For any kind of deformation one can decompose the stresses applied to the ice into pure tensile stress (Figure 1.24a) by an ice cylinder, pure shear stress (Figure 1.24b) by an ice block, and pure compression or dilatation (Figure 1.24c) by a piece of ice immersed in a fluid.

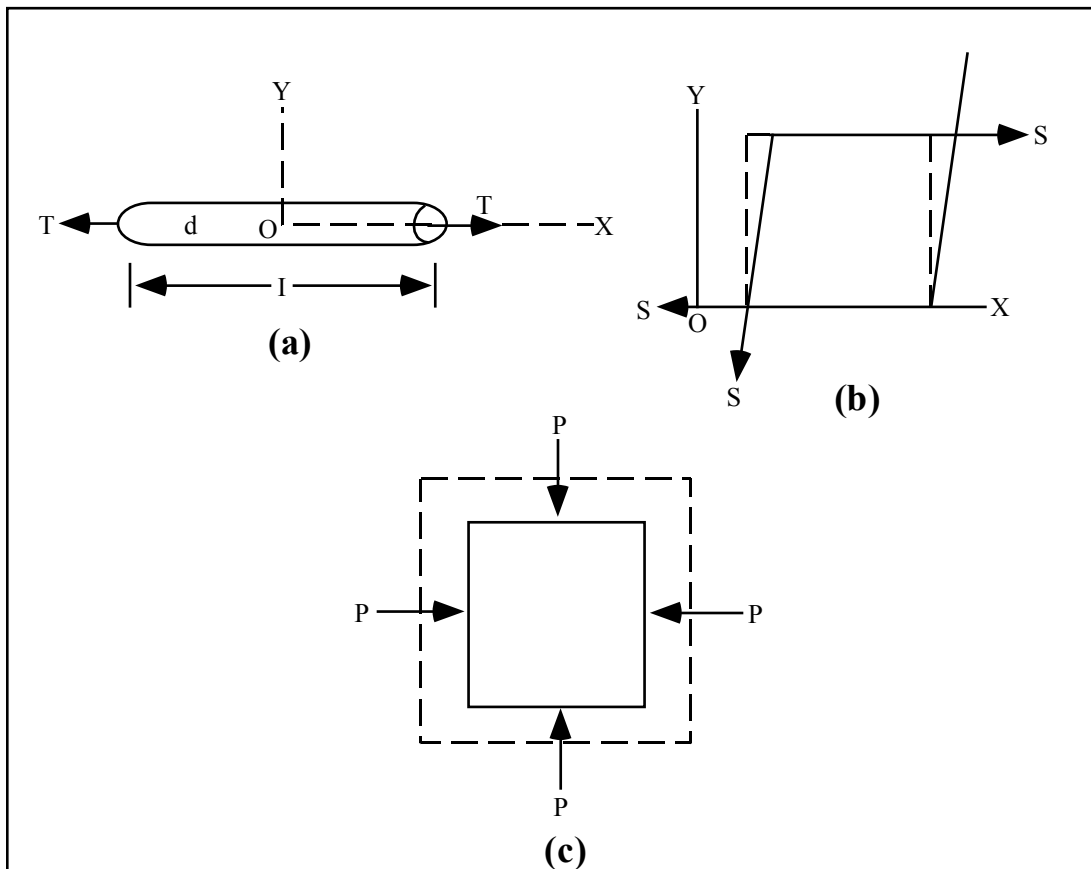


Figure 1.24. Conceptual schematic of pure tensile stress by an ice cylinder (a), pure shear stress by an ice block (b), and pure compression or dilatation by a piece of ice immersed in a fluid (c).(after Pounder, 1965)

The relationships between strain,  $e_{ij}$ , and stress,  $s_{ij}$ , for the three cases are numerically related as [26 to 29 ]:

$$s_{xx} = E_y e_{xx} \quad [26]$$

$$s_{xy} = \mu e_{xy} \quad [27]$$

$$p = k \frac{\Delta v}{v} \quad [28]$$

and,

$$\sigma_p = -\frac{e_{yy}}{e_{xx}} \quad [29]$$

Where,  $E_y$  = Young's modulus of ice

$\mu$  = the shear modulus or rigidity of ice

$k$  = the bulk modulus of ice

$\Delta v/v$  = the fractional decrease in volume

$p$  = hydrostatic pressure

$\sigma_p$  = Poisson's ratio

The fundamental theoretical framework for this report is the fact that the strength of sea ice (measured by any and all stress tests) is inversely proportional to brine volume of the ice. Cox and Weeks (1988) derived empirical formulae [30 to 33] for the various stresses in terms of its brine volume,  $V_{br}$ , based on field data obtained from sites scattered throughout the Arctic (Haykin et al., 1994).

For horizontal tensile stress tests:  $TS = 0.816 - 0.0689\sqrt{V_{br}}$  [30]

$$\text{For vertical tensile stress tests:} \quad TS = 1.54 - 0.0872\sqrt{V_{br}} \quad [31]$$

$$\text{For shear stress tests:} \quad SS = 1.68 - 0.118\sqrt{V_{br}} \quad [32]$$

$$\text{For flexural stress tests:} \quad FS = 0.959 - 0.0608\sqrt{V_{br}} \quad [33]$$

Where, strength is in megapascals (Mpa) and brine volume,  $V_{br}$  is in parts per thousand (ppt).

In what follows we review our current understanding of the primary mechanical properties of sea ice, namely: Compressive Strength; Tensile Strength; Flexural Strength; and Shear Strength as they relate to the objective of this report.

Compressive strength is important when dealing with areas of thick first-year sea ice. In this case, flexural breakup is unlikely to be the dominant failure mechanism. Early compression tests on cylinders of sea ice resulted in vertical strengths of  $76 \times 10^5$  to  $120 \times 10^5 \text{ N}\cdot\text{m}^{-2}$  from  $-5$  to  $-16^\circ\text{C}$  respectively. Horizontal strengths across the same temperature range ran from  $21 \times 10^5$  to  $42 \times 10^5 \text{ N}\cdot\text{m}^{-2}$  (Butkovich, 1956, 1959). Tests by Schwarz (1971) on sea ice from the Baltic Sea produced conflicting results. He reported compressive strengths to be 20% higher than vertical compressive strength. It is argued that ice structure, deformation direction and strain conditions need to be further examined in order to address this discrepancy.

Observations by Poplin and Wang (1994) on both rafted and landfast ice also revealed a discrepancy between horizontal and vertical loading and strength. With vertical loading, shorefast ice had a strength of 8.32MPa compared to 3.28MPa for rafted ice. Horizontally loaded samples of rafted

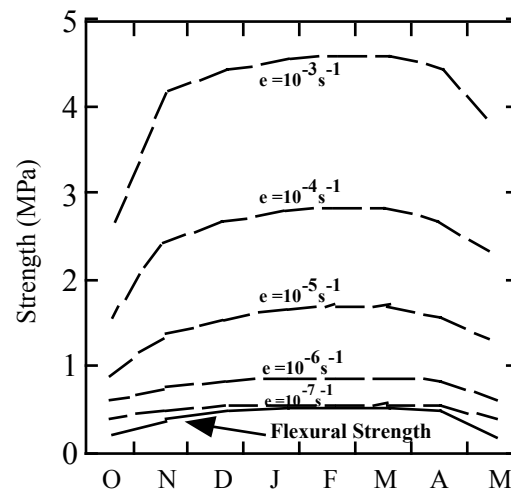
and shorefast ice had mean strengths of 1.3 and 0.7 MPa respectively. The large difference in vertical mean strengths between these two ice types is attributed to their different crystal structures. Landfast samples were characterized by a strong fabric of columnar ice crystals with their long axes oriented parallel to the loading direction. Conversely, half of the rafted ice samples had a weaker fabric which contained granular and mixed grain orientations.

Models which simulate compression of an ice sample with random crystal orientation often result in a rearrangement of crystal C-axes around the compression axis (Azuma and Higashi, 1985). Conversely tension has been found to rotate C-axes away from the tensile axis (Fujita et al, 1987). In model simulations, this crystal reorientation can have the effect of hardening and stiffening ice in direct proportion to the corresponding stress. In reality this non-deforming stage is never reached. Recrystallization occurs whereby a recrystallization fabric is developed after which the rate of deformation is higher than strain hardened or randomly oriented ice. Internal rotation is commonly used as the term to describe the rotation of C-axes due to strain. External rotation refers to the rotation of C-axes associated with bulk deformation. In each case, the bulk strain and the type of deformation can be used to calculate the amount of crystal rotation (Van der Veen and Whillans, 1994).

Modelling experiments on deformation of polycrystalline ice by Van der Veen and Whillans (1994) show that the rate of deformation of polycrystalline ice decreases with time after stress is applied. It is proposed that the formation of a crystal orientation fabric is the primary mechanism

for this behavior. Hardening of the ice sheet results from the creation of this fabric in which ice crystal C-axes are rotated toward unfavorable orientations. At this point ice becomes brittle and the rate of deformation increases rapidly.

The compressive strength is very dependent on the rate of loading (Figure 1.25). At low strain rates, creep properties of ice dominate its response while there is a rapid increase in ice strength with increasing strain rate (Poplin and Wang, 1994; Timco and O'Brien, 1994; and Timco and Frederking, 1990). At higher rates however, ice behaves as a brittle material rather than a ductile material.



(Adapted from Timco and O'Brien, 1994)

Figure 1.25. Comparison of the compressive strength (dotted lines) and flexural strength (solid line) during an average winter in the Beaufort Sea. Note that the compressive strength is highly strain rate ( $\epsilon$ ) dependent.

The air volume of sea ice also has an important influence on compressive strength. This is especially true of multiyear ice where brine volumes are low and where gas volumes can account for a major portion of the total ice porosity. The gas volume of sea ice can be calculated when the temperature, density and salinity of the ice are known (Cox and Weeks, 1983). The compressive strength of sea ice is also a function of brine volume. Since brine volume is closely related to ice temperature through phase equilibrium and thermal expansion contraction and brine expulsion, compressive strength can also be related to ice temperature. Timco and Frederking (1990) extended their flexural strength model to predict the uniaxial compressive strength of an ice sheet. They used air temperature and ice thickness measurements to derive relationships for ice temperature, salinity and density. From ice density they attempted to determine total porosity (brine porosity plus air porosity) and then relate it to compressive strength.

Tensile strength of sea ice shows large differences depending on the load direction. Based on laboratory study, Dykins (1969) concluded that neither the crystal grain size nor the spacing of platelets (smallest elements of ice crystals) have much influence on the tensile strength. He also found the orientation of the crystal grain structure, in relation to the stress field, has a significant influence. That is, the vertical tensile strength is two to three times greater than the horizontal one.

Tensile strength is also found to increase rapidly with the loading rate to a maximum and then decreases to a relatively constant value (Richter-Menge and Jones, 1993). This is similar to compressive strength, except that the maximum occurs at higher initial rates of loading. Limited studies on the



effect of stress rate on tensile strength suggest that tensile strength is not affected by stress rates up to  $1.8 \times 10^5 \text{ N} \cdot \text{m}^{-2}$  (Hawkes and Mellor, 1972). At stress rates above this level, tensile strength rapidly declines by about 50% of the initial value (Dykins, 1970). Richter-Menge and Jones (1993) found the failure strain decreased when the loading rate increased from  $10^{-5}$  to  $10^{-3} \cdot \text{s}^{-1}$ . It is suggested that the stress concentrators such as brine pockets and air bubbles become much more effective failure points at higher stress levels.

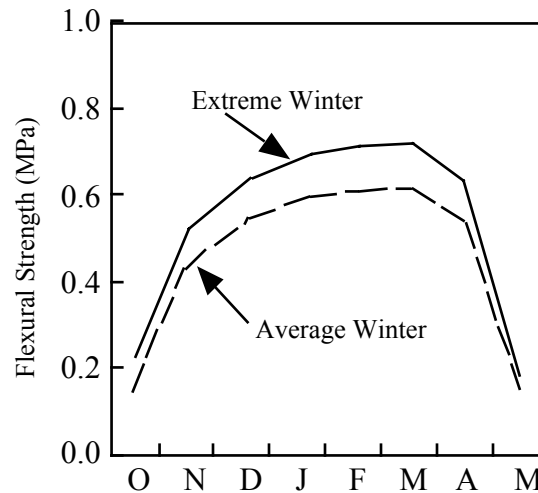
Flexural strength of sea ice is undoubtedly the most important strength property from a ship navigation perspective. Ice failure through flexure is the most likely outcome of ship-ice interaction in thin first-year ice. Flexural strength of sea ice depends on a large number of parameters including ice temperature, grain structure, salinity, load direction, type of test and beam size. Investigations into the flexural strength of sea ice have resulted in a range of estimates from 0.1 MPa to 1.5 MPa. This reflects the variability of sea ice physical properties on which flexural strength depends.

The flexural strength of ice is not a basic material property. The test for flexural strength creates non-uniform stress fields in the ice and assumptions are required about the material behavior in order to interpret the test results (Timco and O'Brien, 1994). Weeks and Anderson (1958) found that first-year sea ice does not indicate large differences in strength between pull-up and push-down tests. Unlike compressive strength which is highly strain rate dependent, strength tests do not indicate a significant variation of flexural strength with strain rate. Timco and O'Brien (1994) gathered

empirically determined strength test results from several studies to develop a flexural relation based on temperature induced brine changes as in [34]:

$$\sigma_f = 1.76 \bullet e^{-5.88 \sqrt{V_b}} \quad [34]$$

Where,  $\sigma_f$  = the flexural strength in MPa and  $V_b$  the brine volume fraction. Their value of 1.76 MPa for zero brine volume is in excellent agreement with the average value (1.73 MPa) measured for freshwater ice. Figure 1.26 shows the variation of the flexural strength of sea ice throughout the winter in the Beaufort Sea.



(adapted from Timco and O'Brien, 1994)

Figure 1.26. Flexural strength versus time of year (October to May) for Beaufort Sea ice sheets for both an average and an extreme winter.

It can be seen that the flexural strength is quite low in the early winter when the ice is thin (and highly saline) and the temperatures are still relatively

warm. As the winter progresses, the ice gets thicker and colder and the strength increases. Peak strength values are, on average, 0.6 to 0.7 MPa. In the spring, the air temperature rises and the strength decreases.

Few *shear strength* tests have been carried out on sea ice. It is a difficult parameter to measure accurately, but tests conclude that shear strength of sea ice is in a similar range to flexural and tensile strengths and that it responds to brine volume in a similar manner (Cox and Weeks, 1988). In addition shear strength has been found not to be significantly affected by different crystal orientations.

From the preceding it should now be clear that the variables of importance in modeling ice strength are the microscale physical properties (e.g., grains size, shape, and inclusion fractions) and the thermodynamics of the volume. Since the former is also dependent on the latter we can utilize a thermodynamic model, in combination with the empirical relationships between brine volume and ice strength to illustrate the average annual strength (tensile, shear and flexure) of landfast first-year sea ice. The following steps are required:

1) Models developed by Cox and Weeks (1974), and confirmed by Timco and Frederking (1990) [35 and 36] can be used to relate the average salinity of an ice sheet to its thickness:

$$S = 13.4 - 17.4h \quad \text{for } h \leq 0.34 \text{ meters [35]}$$

$$S = 8.0 - 1.62h \quad \text{for } h > 0.34 \text{ meters [36]}$$

2) A one dimensional thermodynamic sea ice model (Nakawo and Sinha (1981)) which approximates the temperature profiles of both the snow and sea ice volume as linear functions of their respective thermal conductivities [37] provides a means of determining the snow/sea ice interface temperature. If we assume an average snow thickness of 15 cm on first-year landfast sea ice we can model the average snow/ice interface temperature [37]:

$$T_{s/i} = \frac{(k_i h_s T_m + k_s h_i T_a)}{k_s h_i + k_i h_s} \quad [37]$$

Where,  $k_s$  and  $k_i$  are the thermal conductivities of snow and sea ice;  $T_m$ ,  $T_a$  and  $T_{s/i}$  are the temperatures of the melting point of sea ice ( $-1.8^\circ\text{C}$ ), air temperature and the snow/ice interface temperature, respectively; and  $h_i$  and  $h_s$  are the thickness of the sea ice and snow.

3) We then relate the interface temperature to the brine volume of the ice surface using the empirical models which fit polynomials to the sea ice phase diagram (described above) and restated here as [38 to 41]:

$$V_b = S_i(-\frac{52.56}{T} - 2.28), -2.06 \geq T \leq -0.5^\circ\text{C} \quad [38]$$

$$V_b = S_i(-\frac{45.917}{T} + 0.930), -8.2 \leq T \leq -2.06^\circ\text{C} \quad [39]$$

$$V_b = S_i(-\frac{43.495}{T} + 1.189), -22.9 \leq T \leq -8.2^\circ\text{C} \quad [40]$$

$$V_b = S_i(-\frac{43.495}{T} + 1.189), -22.9 \leq T \leq -8.2^\circ\text{C} \quad [41]$$

4) Finally the various mechanical strength measures are modeled using [30 to 33]. Modeling these over the annual cycle for landfast first-year sea ice

(Figure 1.27) illustrates the seasonal nature and relative magnitude of each of the ice strength parameters of interest<sup>7</sup>.

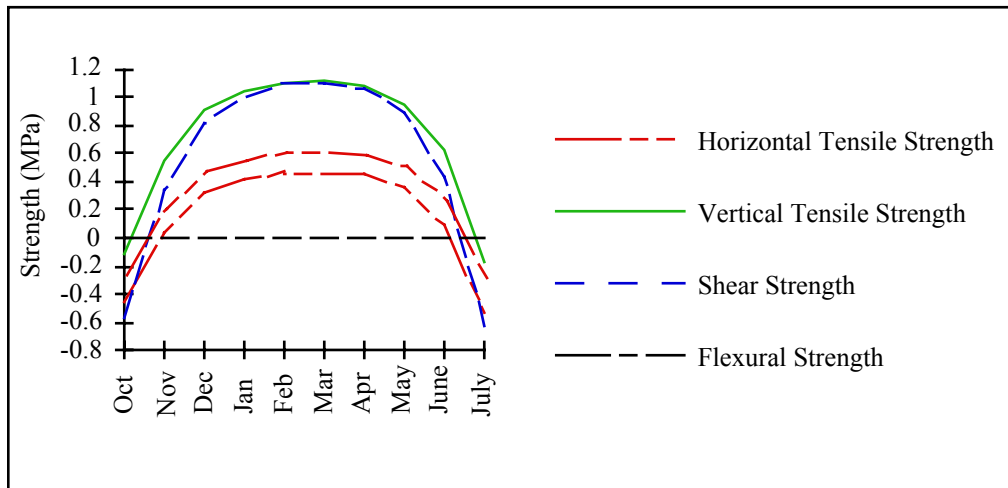


Figure 1.27. Schematic of the seasonal evolution and relative magnitude of various mechanical strengths of first-year Arctic sea ice.

In this section we have introduced the basic theoretical framework required to understand the salient characteristics of sea ice strength. We have defined the basic ice strength parameters as Compressive Strength; Tensile Strength; Flexural Strength; and Shear Strength and have shown that each of these parameters is directly controlled by the volume of brine and the intercrystalline arrangements of the ice grain microstructure. We have also shown that models which relate the brine volume to temperature can also be used to create estimates of each of the ice strength parameters defined here.

In conclusion it should now be clear that the physical, electrical, and mechanical properties of sea ice are highly interrelated. Thermodynamic

<sup>7</sup>Although not depicted here, the compressive strength has been measured to be between 6 to 8 times greater than the flexural strength. A minimum in the compressive to flexural ratio occurs between

processes operating across the ocean-sea ice-atmosphere interface drive the evolution of the physical, electrical and mechanical properties as a direct result of the role which temperature has on defining the brine volume of the surface. This theory represents a significant advancement in our understanding of the icescape and is used here as the building blocks for the development of an 'Electro-Thermophysical' model of snow covered sea ice. In the next section we will review our current understanding of how various forms of electromagnetic energy interact with snow covered sea ice as a background to exploring the 'Electro-' part of our 'Electro-Thermophysical' model.

## **Section 2**

### **Sea Ice Information Products from Remote Sensing**

## Background

Remote sensing of snow covered sea ice has evolved diversified approaches to using electromagnetic (EM) interactions to study sea ice processes and their spatial and temporal evolution. Considerable attention is being paid to linking reflectance, scattering and emission of EM radiation to physical variables, which in turn are coupled through ocean-surface and surface-atmosphere processes to the linkages which control sea ice evolution. Remote sensing technologies are particularly appropriate for studies which focus on the temporal and spatial aspects of processes. Remote sensing measurements can also provide us with a broad area of fine spatial resolution observations which cannot otherwise be obtained with sparse surface instrumentation.

The portion of the electromagnetic spectrum that is most useful for remote sensing of sea ice ranges from visible (VIS) wavelengths (0.3 - 0.7  $\mu\text{m}$ ) through to the infrared (IR) wavelengths (0.7  $\mu\text{m}$  - 12  $\mu\text{m}$ ) and most of the microwave region (1 mm - 23 cm). The IR spectrum is usually subdivided into bands called near IR (NIR) (0.74 - 1.13  $\mu\text{m}$ ), mid-IR (MIR) (1.3 - 2.5  $\mu\text{m}$ ) and thermal IR (TIR) (3 - 15  $\mu\text{m}$ ). The MIR bands are not normally used for the purposes of sea ice remote sensing. In the case of microwave remote sensing, active (system measures returned signal of its own energy source) and passive techniques (system measures returned signal from the target's emitted energy) are commonly used in sea ice information retrieval.

In the VIS portion of the spectrum, vibrational and electronic energy transitions play a key role in the interactions with the surface. Increased molecular kinetic (vibrational) energy and increased molecular electronic



energy levels can result within the surface from its interaction with the incident EM field. These interactions are the key mechanisms for remote sensing in the VIS portion of the spectrum. The VIS band also makes up the majority of the energy received by the earth from the sun and it is for this reason that this spectral band is commonly used to infer the physical characteristics of the snow/ice surface through its reflectivity. Imagers, spectrometers and radiometers are commonly used for sea ice information retrieval in the VIS band. Cloud cover severely constrains the use of VIS wavelengths over snow covered sea ice since a large part of the year has no solar illumination and cloud cover affects the seasonal transitional periods (both fall and winter).

In the TIR band, the main interaction mechanisms include thermal emission, vibrational and molecular rotational (kinetic energy). The TIR emissions from the snow/ice surface are strongly dependent on surface temperature and the emissive properties of the surface according to Planck's law. Thus, remote sensing in the TIR spectrum provides information about the temperature and heat constant of the snow/ice surface. Clouds emit energy in the TIR portion of the spectrum, thereby limiting surface temperature estimation to periods which are cloud free.

In the microwave region, both active and passive techniques are widely used for remote sensing of sea ice due to their all weather, day/night sensing capabilities. Particular attention will be paid to microwave techniques due to its increasing usefulness for sea ice applications. Scattering, thermal emission, and to a lesser extent, rotational processes are all important in the microwave interaction mechanisms with the surface. Scattering plays the most important role in microwave remote sensing which is a complex

function of the dielectric properties, surface roughness and volume inhomogeneities. The average relative scattering coefficient ( $\sigma^0$ ) can change over time and space. The spatial variability is primarily a function of the geophysical properties that contribute to the volume dielectrics or the surface roughness of the snow/ice system. The temporal changes are controlled by the dielectric mismatch across the air-snow and snow-ice interfaces. The key variables involved are the relative phases of water (ice, liquid and vapor), crystal size, brine volume and the vertical and horizontal roughness point estimates of the surface autocorrelation function. In addition, scattering can be dissected into two key components; surface scattering and volume scattering. If there is a strong dielectric mismatch at a particular interface then the surface scattering will dominate.

Snow cover plays an important role in the microwave backscatter characteristics. Snow is essentially transparent in the winter season but as the water content in the snow pack increases (due to increased spring air temperatures), the penetration depth of the microwaves into the snow decreases (Drinkwater, 1989). As the penetration depth decreases, the average scattering from a snow covered ice surface contains an increasing contribution from the snow volume and snow surface geometry (as per equation [7]). The relative contribution of snow surface roughness to the backscatter of microwave energy increases as the free water content of the snow increases (Barber et al., 1991).

There are many satellite based sensors that can be used for snow/sea ice applications. In the VIS bands, AVHRR (Advanced Very High Resolution Radiometer) is typically used on board the NOAA (National Oceanic and Atmospheric Administration) series of polar orbiting satellites. These

satellites have circular, near polar, sun synchronous orbits. However, due to satellite orbital drift, precise return periods are not possible.

In the TIR bands, sensors include the HVIS (High Resolution VIS) on board the DMSP (Defense Meteorological Satellite Program), AVHRR and TOVS (TIROS-N (advanced Television Infrared Observation Satellite-N) Operational Vertical Sounder). The DMSP satellite's orbit is near polar and sun synchronous with a return period twice daily. The TOVS sensor is aboard the TIROS-N series satellites which have similar orbits to the NOAA-N series of satellites.

Passive microwave sensors include the ESMR (Electrically Scanning Microwave Radiometer) on the Nimbus-5 satellite, SMMR (Scanning Multi-channel Microwave Radiometer) on Nimbus-7 and SSM/I (Special Sensor Microwave/Imager) on the DMSP satellite. Both the Nimbus-5&7 satellites had polar orbits with a return period twice daily.

In the active microwave regime, sensors on ERS-1/2 (Earth Remote Sensing Satellite), JERS-1 (Japanese Earth Remote Sensing Satellite) and RADARSAT have proven to be valuable resources for snow/sea ice applications. Both the ERS-1/2 satellites have sun synchronous, near circular, polar orbits with return periods of 35 days. ERS-2 is similar to ERS-1 except ERS-2 is equipped with more instrumentation (mostly for atmospheric chemical analysis) and lags behind the ERS-1 orbit by about one day. The JERS-1 satellite has a sun synchronous sub recurrent orbit with a return period of 44 days. RADARSAT has a return period of 24 days under a circular, sun synchronous, polar orbit.

## **Remote Sensing of Sea Ice through the Annual Cycle**

Remote sensing of sea ice has been available since the early to mid seventies over which time significant advances have been made in our ability to extract ice information. Note however that techniques for information extraction are specific to particular conditions and that what works in one region or time may not be transferable to another region or time. In this section we describe the current set of geophysical variables which can be extracted using a variety of frequencies, polarizations or combinations thereof. Emphasis will be on active microwave techniques then passive microwave, thermal techniques and finally optical methods. Many techniques that apply to a particular stage of sea ice growth/decay can be applied to other growth/decay stages. Cases in which this occurs will be covered in subsequent sections.

Table 2.1 summarizes the types of geophysical variables currently obtainable from remote sensing of sea ice along with the types of sensors, frequencies/wavelengths, spatial resolution and temporal coverage of the remote measurements. Sample references of each technique are also included in the table. Some of the variables in Table 2.1 are not directly related to sea ice (such as cloud fraction) but are key variables/processes that affect sea ice evolution. Each subsection will provide a discussion of the remote sensing techniques used to infer the variables in Table 2.1 as they are related to the different stages of sea ice growth/decay categories typified by the thermodynamic regimes of Figure 1.2.

@insert 3pages for Table 2.doc (landscape format in word)





## Freeze Up

Detection and monitoring of the fall freeze-up using active microwave remote sensing is an active research area. Shuchman et al. (1994) used ERS-1 SAR data to show that the relative scattering coefficient ( $\sigma^\circ$ ) decreases ( $< -15$  dB) within thin ice regions compared to higher  $\sigma^\circ$  values ( $> -7$  dB) in open water along Arctic leads. This trend may also be applicable to the fall freeze up period (in general) since similar physical processes would be occurring. Shuchman et al. (1994) pointed out that the higher radar returns may also be caused by frost flowers on a thin ice surface as opposed to open water, however, their scatterometer results showed that the radar backscatter of thin ice with frost flowers would not be as high ( $-9$  to  $-13$  dB) as those values presumed to be representative of open water. Winebrenner (1996) indicated that thin ice ( $< 70$  cm) thickness may be extracted from L-band (23 cm) SAR imagery using co-polar ratios and phases in backscatter, however, extensive testing and validation of the technique is required due to the limited number of surface observations in the study. Recent work by Holt and Winebrenner shows that SAR can be used to estimate the point of freeze-up by monitoring the seasonal evolution of the microwave scattering coefficient over the summer period and across the transition into freeze-up.

A study by Burns (1990) showed that SAR (23 cm wavelengths) may be useful in the marginal ice zone for inferring the atmospheric drag coefficient. SAR data in the 23 cm wavelength bands can reveal large scale topography (ridges, floes edges) in which high backscatter returns occur from small, broken and heavily deformed floes and rubble areas (Burns, 1990). In addition, the atmospheric drag coefficient increases with increased ice concentration and ice floe deformation in neutrally stratified atmospheric



conditions. Atmospheric drag decreases in more atmospherically stable regimes in which surface roughness has a smaller influence. For example, with the same ice concentration and neutral stability, drag was less in areas of smooth medium-sized ice floes ( $r > 50$  m) than areas of rough ice made up of pancake ice and small floes ( $5 \text{ m} < r < 50 \text{ m}$ ) and was greatest in areas of very rough ice consisting of cakes, small floes and brash ( $r < 5 \text{ m}$ ) (Burns, 1990). With the help of SAR data to determine the ice characteristics and a simple atmospheric boundary layer model, estimates of the atmospheric drag coefficient could be obtained in the marginal ice zone under neutral atmospheric stability.

Passive microwave sensors have been shown to distinguish between open water, thin ice (0 - 9 cm) and thicker first-year ice. Microwave surface observations indicate that a sharp rise in surface temperature during the first 1-2 cm of growth coincide with a decrease in brightness temperature at higher frequencies (37 GHz) (Wensnahan et al., 1993a). They attributed this increase in surface temperature to the upward transport of warm brine from the interior of the ice and resulted in the formation of a salinity enhanced surface layer. Wensnahan et al. (1993b) later applied a principle component analysis technique to decipher between very thin (0 - 4 cm) and thin ice (4 - 9 cm) on microwave surface observations of sea ice. They pointed out that these thin ice ranges would be very difficult to detect by satellites due to spatial resolution and the sometimes enhanced speeds at which the ice can grow at these thicknesses. However, satellite-based microwave sensors have been shown to be good proxy indicators to thin ice regions as outlined below.

Satellite passive microwave techniques at 85 GHz and 37 GHz using the SSM/I sensor can distinguish between open water, thin ice and first-year ice regions (Markus and Cavalieri, 1996; Grenfell, 1996). Two techniques (NASA team ice concentration algorithm (Cavalieri, 1994) and the Polynya Signature Simulation Method (PSSM) (Markus and Burns, 1995) to distinguish thin ice from open water were tested against aircraft measurements in which good agreement was found (Markus and Cavalieri, 1996). Both techniques provided accurate open water/thin ice discrimination, however, the NASA team algorithm was better suited for larger scale analysis (25 km or greater) whereas, the PSSM was appropriate for spatial scales near 6 km. It was also pointed out that both techniques are only valid for seasonal ice zones and not, as of yet, applicable to the entire Arctic.

A recent study by St. Germain and Cavalieri (1996) have linked SSM/I passive microwave radiances with surface temperatures in the Arctic seasonal ice zone. A major advantage of using passive microwave data as opposed to the TIR bands is cloud contamination is minimal at microwave frequencies. The algorithm includes SSM/I techniques to infer ice types/concentrations, atmospheric effects and surface emissivities (from the thin ice algorithm (NASA team algorithm)). Comparisons with AVHRR TIR brightness temperatures were good for several case studies in the seasonal ice zone, however, further research is required to refine the technique (St. Germain and Cavalieri, 1996).

Markus and Cavalieri (1996) also correlated SSM/I ice type/thickness (open water, thin ice and first-year) recognition (using the PSSM and NASA algorithms) with AVHRR brightness temperatures. They showed that as ice

thickness increased, the brightness temperatures decreased with maximum temperature differences between the two techniques (PSSM and NASA) near 2 °K. They also pointed out that the large temperature difference between the open water (275 °K) and thin ice (268 °K) magnifies the importance of the first few centimeters of ice growth on the latent and sensible heat fluxes in that region.

A widely used technique for surface temperature estimation utilizes TIR frequencies on platforms such as the NOAA AVHRR (see for example, Groves and Stringer, 1991; Key et al., 1994; Meier et al., 1996; and the studies outlined above to name a few). The technique is called the split-window approach (Key and Haefflinger, 1992) which uses AVHRR channels 4 (11 m) and 5 (12 m) and cannot be used under cloudy conditions. It involves adjustments for atmospheric effects, ice type, and satellite view angle and errors are typically due to the spatial and temporal variability in the surface temperatures, undetected clouds, assumed atmospheric conditions and sensor error (Key et al., 1994). An in depth discussion of the technique can be found in Key and Haefflinger (1992) and Key et al. (1994a).

Several studies have investigated the use of AVHRR TIR in combination with VIS bands to infer thin sea ice and lead locations, lengths and widths (see for example, Stone and Key, 1993; Lindsay and Rothrock, 1995; Eppler and Full, 1992). Determination of the thin ice and lead characteristics involve the calculation of surface temperature (as above) using the TIR bands and surface albedo (see Winter section, below) using the VIS bands. Several steps are involved in calculating these quantities for each pixel in the images as indicated above in the TIR bands and VIS bands (see Winter section, below). Thin ice and lead discrimination is then accomplished

through observed thermal and brightness level differences between background thick ice and open water signatures (Stone and Key, 1993; Lindsay and Rothrock, 1995). Through this criterion, it is then possible to determine lead lengths and, to a certain degree, lead width (Lindsay and Rothrock, 1995).

## **Winter**

Active microwave remote sensing of sea ice in winter varies according to ice type (thin first-year, first-year and multiyear) (Figure 2.1). Within multiyear ice, microwave scattering is very stable. The primary scattering mechanism is the bubble structure within the surface hummock layer (Onstott, 1992). Older forms of ice appear to have higher scattering characteristics due to the larger and deeper hummock layers that contain larger bubble sizes which are spaced further apart within the hummocks. The snow cover on the multiyear ice is brine free with a low density and small grain sizes which makes it transparent at 5.3 GHz.

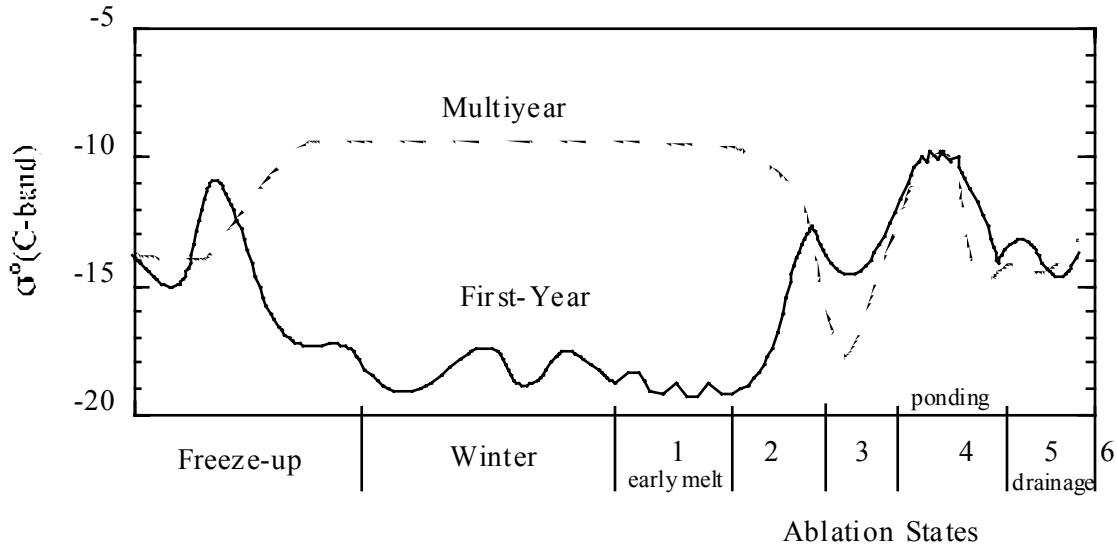


Figure 2.1. Seasonal evolution in scattering at 5.3Ghz, as an average return for both VV and HH polarization.

Within first-year ice, microwave scattering appears to oscillate according to changes in the oceanic and atmospheric heat fluxes but still provides a stable surface in which remote sensing can be useful (Barber et al., 1994). The relationship appears to be related to the effect of heat fluxes on the dielectrics of the first-year ice surface in the very early part of the winter season, followed by the atmospheric heat flux effects on the basal snow layer during the warmer part of the winter season (Barber et al., 1996). Further work is required regarding thin first-year ice due to a more complex seasonal evolution of  $\sigma^o$  because of the dielectric properties and role of the snow cover as the ice matures.

Because of the stable nature of microwave scattering in winter over multiyear and first-year ice, several geophysical variables can be extracted from active and passive remote sensing during this period (see Table 2.1). In

the active regime, the shortwave (0.3 - 3.0  $\mu\text{m}$ ) surface albedo and transmitted Photosynthetically Active Radiation (PAR) (0.4 - 0.7  $\mu\text{m}$ ) for a snow cover can be derived from ERS-1 SAR imagery at 5.3 GHz and 9.25 GHz (Barber and LeDrew, 1994). However, measurement of snow thickness may be required to make remote PAR observations a useful quantity. Barber and LeDrew (1994) developed a statistical relationship (quadratic) between  $\sigma^\circ$  and albedo and  $\sigma^\circ$  and transmitted PAR where as  $\sigma^\circ$  increased, albedo decreased and transmitted PAR increased. The primary physical variables causing the relationship between  $\sigma^\circ$  and albedo were the increased water volume of the snow pack and a larger contribution to snow volume scattering from the increase in the snow crystal radius (Barber and LeDrew, 1994). At very low water volumes ( $< 1\%$  water by volume) in the snow pack, transmitted PAR to the snow/ice surface was almost non-existent. Once the water volume increased above  $5\%$ , transmitted PAR increased logarithmically with  $\sigma^\circ$  due to the increase in snow grain size and increased number density of the water inclusions (Barber and LeDrew, 1994).

Barber et al. (1994) showed there is a statistical relationship between the seasonal evolution of  $\sigma^\circ$  with surface temperature ( $T_s$ ) and the net shortwave flux ( $K^*$ ) over first-year snow covered sea ice. This is due to both variables ( $T_s$  and  $K^*$ ) either causing or covarying with the change in the dielectric properties responsible for the change in  $\sigma^\circ$ . An inverse relationship existed between both  $T_s$  and  $K^*$  relative to  $\sigma$ , and the influence of the surface temperature was about twice that of the net shortwave flux in explaining the variation in  $\sigma$ . Furthermore, Barber et al. (1995) determined that  $T_s$  and the longwave flux ( $L^*$ ) could be considered statistically indistinguishable between first-year and multiyear sea ice, for conditions experienced during

SIMMS'93 (Seasonal Sea Ice Monitoring and Modeling Site, 1993). The  $K^*$  and net all-wave flux ( $Q^*$ ) were however statistically distinguishable between the MYI and FYI sites. They attributed this result to the fact that  $T_s$  and  $L^*$  were, to a large degree, determined by characteristics of the atmospheric boundary layer and that  $K^*$  and  $Q^*$  were largely prescribed by the snow metamorphic state. Because the snow is distributed differently over multiyear versus first-year ice types, differences occurred in the seasonal evolution of these fluxes.

Maslanik and Maybee (1994) and Fowler et al. (1994) derived ice motions from interpolated ice displacements from ERS-1 data. The ice motions were also partially derived from AVHRR data, however, SAR data provides coverage in all weather conditions. Georeferenced ERS-1 data was interpolated to a grid with a resolution of 80 km used by a two-dimensional model (Flato and Hibler, 1992) and consecutive images in time were used to create ice motion vectors. The observed ice motion vectors were then used to initialize and validate the two-dimensional model. Further validation of the technique is required. Malinas and Shuchman (1994) developed a transfer function to convert SAR  $\sigma^0$  values to ice thicknesses using aircraft SAR and upward looking sonar data. The general observation was that an increase in ice thickness corresponded to an increase in  $\sigma$  for multiyear and first-year ice types. However, this technique also requires further verification and testing.

Satellite passive microwave remote sensing sensors provide another valuable source for sea ice monitoring and have been widely used in many studies (see for example Preller et al., 1992; Preller and Posey, 1994; Maslanik and Maybee, 1994). Algorithms for multi-channel microwave data can extract

sea ice concentration for any given pixel, from which ice extent, ice area, water area and overall ice concentration can be derived for broader regions (see for example, Johannessen et al., 1996). Individual pixel concentrations can be derived from SSM/I radiances in the frequencies at 19, 22, 37 and 85 GHz in conjunction with an algorithm such as NORSEX (Norwegian Remote Sensing Experiment; Svendsen et al., 1983) or the PSSM or NASA team algorithms (see Freeze Up section). The NORSEX algorithm uses the vertically polarized SSM/I multi-frequency pair radiances at 19 and 37 GHz to produce the pixel concentrations (Svendsen et al., 1983). Time series of ice extent, ice area and overall ice concentration can then be derived from individual-pixel ice concentrations of consecutive SSM/I imagery. The reader is referred to the cited references for further details.

In the TIR bands, the same surface temperature information that was presented in the Freeze Up section also applies to the winter sea ice growth regime. However, the surface temperature information in the winter season may also be used for small-scale studies of ice extent and movement and can be used for a relative assessment of ice thickness (up to about 1m) (see Barber et al., 1991 for references). Thicknesses are derived by correlating empirical emissivities of different ice types (thin, first-year and some multiyear ice) with the satellite derived surface temperatures. Ice movement (velocities) is determined by cross correlations to match feature locations between pairs of co-registered images typically separated by one to three days (Meier et al., 1996). The ice velocity is calculated by dividing the ice displacement in a pair of images by the time between the images.

The TIR bands have also been used to derive cloud information relevant to sea ice. AVHRR TIR bands are used to distinguish cloudy regions from non-



cloudy regions and then used to derive cloud fraction, cloud optical depth, effective radius, cloud phase and cloud top temperature and pressure in conjunction with the Cloud and Surface Parameter Retrieval (CASPR) software for AVHRR analysis (Key, 1995). CASPR combines the AVHRR TIR band data with a variety of parameterizations, model derived look-up tables and radiative transfer code to determine the cloud properties, as well as radiative fluxes (see Maier et al., 1996). A similar technique was used by Key et al. (1996) in which they also derived the downwelling shortwave and longwave fluxes. However, both studies pointed out that further development and validation of the techniques are required to determine their spatial and temporal accuracy.

Optical (VIS) techniques are mainly used to derive surface reflectance or albedo of sea ice surfaces. Many studies have used VIS data from AVHRR on the NOAA-N series and DMSP satellites to derive surface albedo in the past (see for example, Robinson et al., 1986; Ross and Walsh, 1987; De Abreu et al., 1994; De Abreu and LeDrew, 1996; Key et al., 1996; Meier et al., 1996). The top of the atmosphere VIS radiances are used to calculate surface albedo by correcting for atmospheric effects (ozone, water vapor and aerosol attenuation), viewing geometry and sensor spectral response. Typical errors in the derived albedos are due to unaccounted for atmospheric attenuation (undetected clouds and incorrect ozone, water vapor or aerosol profiles) and anisotropic scattering within the surface (De Abreu et al., 1994). The technique for extracting surface albedos from satellite imagery has been applied to many different seasonal conditions in which good accuracy has been cited in the referenced literature.

## **Ablation States 1 and 2**

Within multiyear sea ice, microwave scattering remains fairly stable into the early melt period because hummock volume scattering still dominates (see Figure 2.1). Diurnal differences may be present as small amounts of water in liquid phase become available near the surface of the snow cover at or near solar noon. Because the snow cover is brine free and the grains are fairly small we do not expect any significant scattering (at 5.3 GHz) from the snow volume during this period. Within first-year sea ice, microwave scattering appears to be dominated by a combination of basal layer volume scattering and ice surface scattering (see Figure 2.1). During this period we would expect to find a significant difference in solar noon versus solar midnight observations as small amounts of water in liquid phase would contribute both to grain growth and the elevated temperatures would significantly increase the brine volume of the snow basal layer. The overall magnitude of  $\sigma$  will be dependent on the ice surface microscale roughness and its surface brine volume.

All of the geophysical variables extracted from microwave remote sensing (active and passive) and optical remote sensing in Table 2.1 are transferable to the early melt season. The same can be said about the TIR bands with the possible exception of deriving ice extent, movement and relative estimates of ice thicknesses in some cases. The validity of deriving sea ice characteristics such as these using TIR imagery may be subject to the extent of liquid water within the snow cover (if present). If extensive liquid water exists within the snow pack, the thermal signatures may not represent the ice radiances since a great deal of the observed thermal energy may be emitted from the snow pack. This could result in contamination of sea ice extent, movement and thickness due to the thermal snow cover characteristics. This

problem would be enhanced further during the melt onset and advanced melt stages.

### **Ablation State 3**

In multiyear sea ice, melt onset is denoted by a rapid decrease in  $\sigma^\circ$  (see Figure 2.1). The mechanism responsible is the absorption of microwave energy by the water in liquid phase within the snow cover (Winebrenner et al. 1994) and by the presence of water in liquid phase within the hummock structures free of a snow cover. An increase in permittivity and in particular an increase in the dielectric loss effectively mask the volume scattering from the hummocks thereby decreasing  $\sigma^\circ$ . The decrease in  $\sigma^\circ$  proceeds over both the pendular and funicular regimes of snow ablation. In first-year sea ice, melt onset is denoted by a rapid increase in  $\sigma^\circ$  (see Figure 2.1). There are two mechanisms which are likely candidates for the observed increase. At relatively low water volumes (1 to 3 percent) the large wet snow grains in the basal layer may contribute a significant volume scattering term to  $\sigma^\circ$ . As the water in liquid phase continues to increase (but is maintained within the pendular regime) it is likely that the snow surface may also contribute a surface scattering term to  $\sigma^\circ$  (Drinkwater, 1989; Livingstone and Drinkwater, 1991; Barber and LeDrew, 1994). In a case study done by Barber et al. (1995) it was found that the snow volume scattering term was the dominant mechanism since the maximum  $\sigma^\circ$  reached at the first-year ice (FYI) site was larger than the corresponding one at the multi year ice (MYI) site (Figures 2.2 and 2.3), even though the snow surface roughness was approximately equivalent

between the two sites. A distinct dip in  $\sigma^\circ$  at the FYI site corresponded with the transition from the pendular and funicular regimes. This transition marks the reduction of brine within the basal layer to near zero, an increase in the water in liquid phase at the base of the snow cover and a reduction of water in liquid phase in the top parts of the snow volume (as the surface begins to drain). These processes could lead to a reduction of both the volume scattering and snow surface scattering hypothesized to dominate the pendular regime conditions.

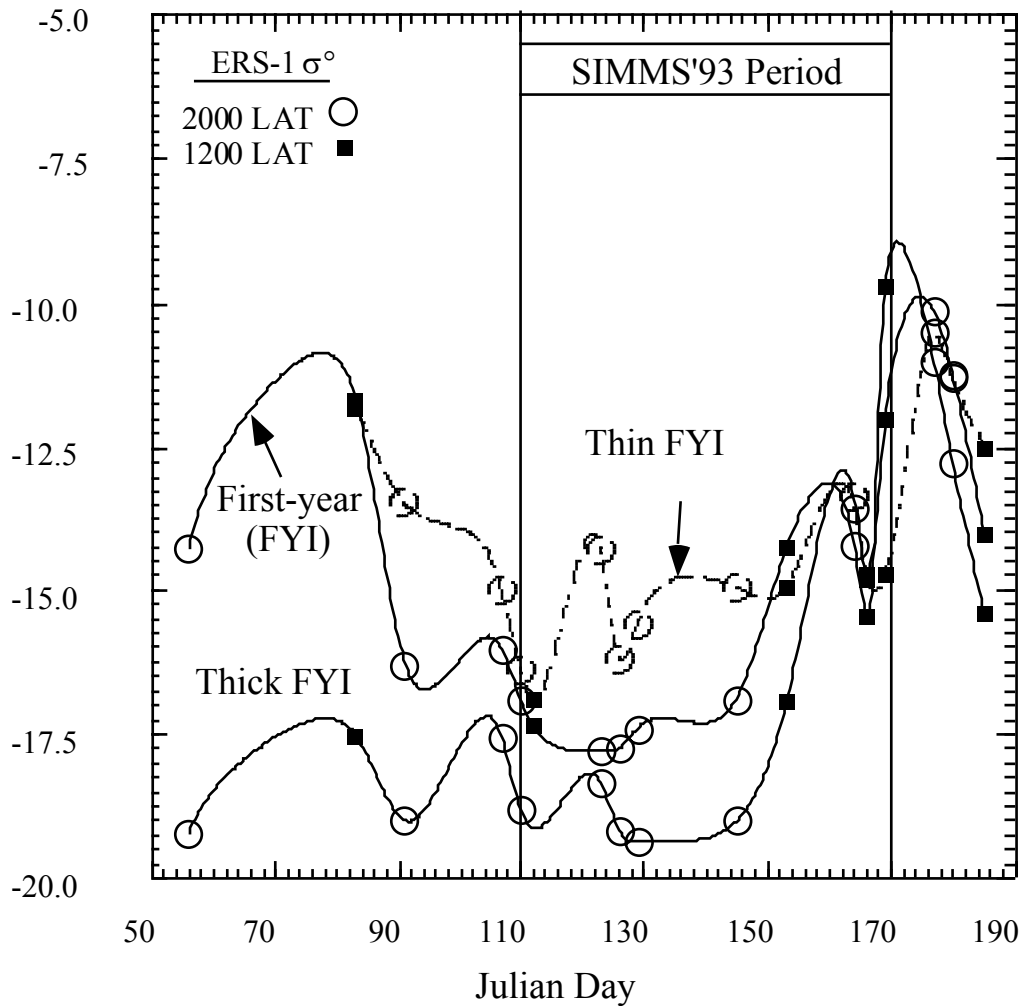


Figure 2.2. ERS-1 SAR total average backscatter coefficient (dB) versus Julian Day for Thick Ice, First-year Ice and Thin Ice during SIMMS'93 (adapted from Barber et al. 1995).

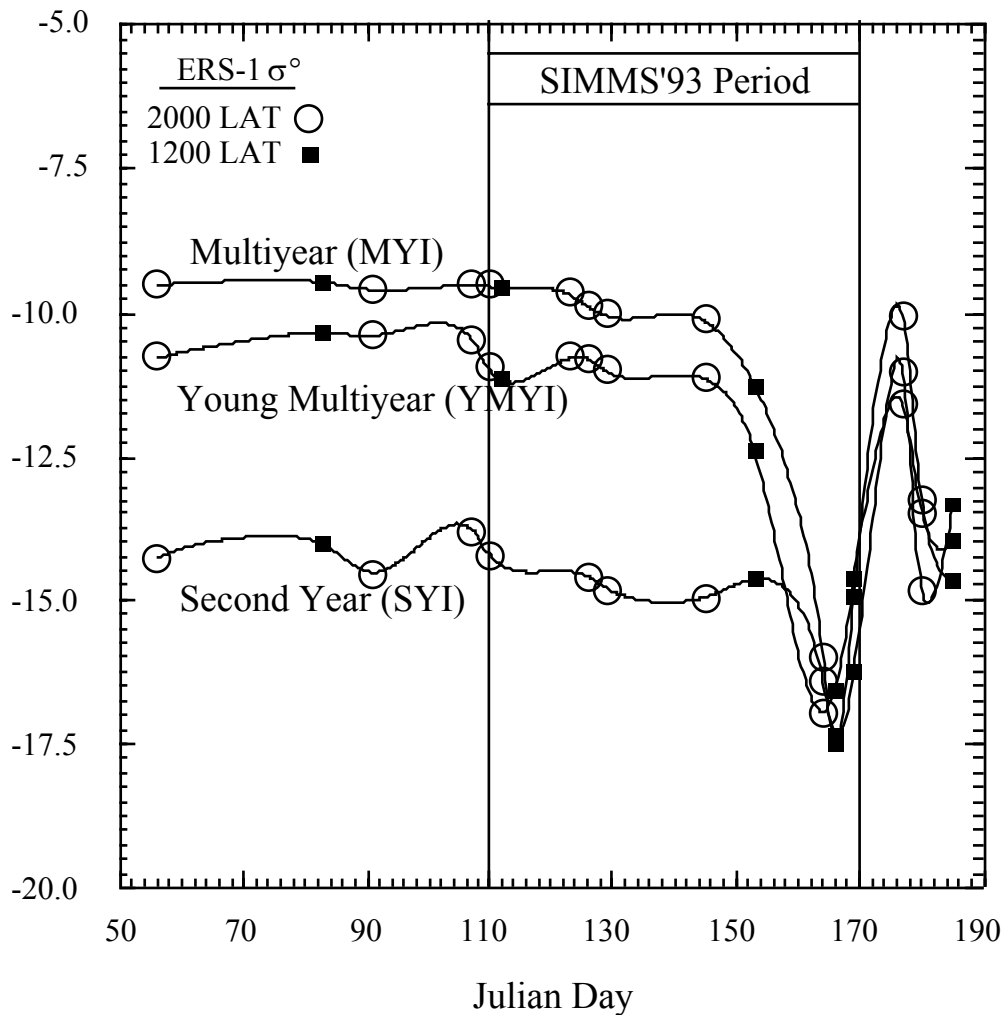


Figure 2.3. ERS-1 SAR total average backscatter coefficient (dB) versus Julian Day for Second Year Ice, Young Multiyear Ice and Multiyear Ice during SIMMS'93 (adapted from Barber et al. 1995).

All of the geophysical variables extracted from microwave remote sensing (active and passive) and optical remote sensing in Table 2.1 may be transferable to the melt onset season. However, the high variability in the spatial patterns of most geophysical parameters within the icescape may produce large differences between pixels within the satellite imagery depending on the spatial resolution of the remote sensor. The same can be said about the TIR bands, once again especially in deriving ice extent, movement and relative estimates of ice thicknesses in some cases due to abundant liquid water within the snow pack or on the sea ice surface. It is unknown whether the variation in the icescape would affect the TOVS and AVHRR retrievals of cloud and other atmospheric parameters.

#### **Ablation State 4**

In multiyear sea ice, advanced melt is denoted by a rapid increase in  $\sigma^\circ$  (see Figure 2.1). As surface water forms in the previous years melt ponds there is an increase in the discontinuity at the air/water interface. The dielectric permittivity and loss of this freshwater (which has a surface temperature of about +0.5°C) is sufficiently large that we can expect a penetration depth on the order of 1 cm into the snow pack (Ulaby et al. 1986). The penetration depth is computed as [42] following Drinkwater (1989) and is based on the complex permittivity of air versus that of the volume.

$$\delta_p = \frac{\lambda}{4\pi} \left\{ \left[ \left( 1 + \left( \frac{\epsilon''}{\epsilon'} \right)^2 \right)^{\frac{1}{2}} - 1 \right] \frac{\epsilon'}{2} \right\}^{\frac{1}{2}} \quad [42]$$

Where  $\lambda$  is the SAR wavelength in meters,  $\epsilon'$  and  $\epsilon''$  are the dielectric permittivity and loss given a particular material of interest (snow or water). We note here that the penetration depth model will provide a maximum depth of penetration since it does not account for forward scattering processes.

We can expect an increase in scattering if the melt pond surfaces are wind roughened. A reduction of water in liquid phase within the hummocks may also cause an increase in  $\sigma^\circ$  by increasing the volume scattering component of  $\sigma^\circ$ . Once the ice surface begins to drain there is a pronounced decrease in the multiyear  $\sigma^\circ$ . This period coincides with a reduction in the areal extent of the melt ponds and cyclical changes of water in liquid phase within the hummocks. The exact mechanisms for scattering over multiyear sea ice in the advanced melt season remain largely unexplored and are identified here as a priority for future research. In first-year sea ice  $\sigma^\circ$  increases over the ponding period and decreases as the ice begins to drain analogous to that described for the multiyear ice surface (see Figure 2.1). The mechanisms for first-year ice scattering during the advanced melt period are also largely unknown.

Due to the high variability in the icescape during the advanced melt period, it is not known whether most of the geophysical variables that are extracted from remote sensing (appearing in Table 2.1) are valid. Most studies do not include this stage of sea ice evolution within the temporal scales of the techniques. This is mostly due to the limited number of surface observations for validation during this period in which dangerous ice conditions exist. However, Barber and Yackel (1997) showed that SAR scattering may be

able to infer surface albedo using ERS-1 or RADARSAT during advanced melt but only applied to first-year landfast sea ice in windy ( $2\text{--}3\text{ m s}^{-1}$ ) conditions. They also indicated that the microwave scattering could be used to obtain an unambiguous measure of the onset of melt, both by a decrease in scattering over multiyear ice and by an increase in scattering over first-year ice. Furthermore, the transition between pendular and funicular regimes may be detectable in first-year scattering but not necessarily over multiyear ice types (Barber and Yackel, 1997).

Table 2.2. Microwave scattering characteristics of the proposed sea ice ablation states.

Variable	Characteristics
Winter	Microwave remote sensing can distinguish first-year smooth from multiyear ice forms. Confusion can occur between rubble first-year and multiyear sea ice. Ridges are usually detectable.
Ablation 1 Very early melt	The temporal evolution of scattering (relative to the winter magnitudes for the same ice type) will show a distinct oscillation in scattering over a diurnal period. This oscillation is due to changes in temperature at the interface of the snow and sea ice. Multiyear signatures will be stable (relative to winter scattering) during this period.



## Ablation 2

### Sustained snow melt

The temporal evolution during this period is most effectively seen in the change in multiyear sea ice scattering. Once sufficient water is available in the snow pack ( $> \sim 2$  percent) there is a rapid reduction in the multiyear sea ice scattering (Figure 11??). There is also a corresponding increase in scattering for smooth first-year sea ice due to an increase scattering coming from the enlarged, wet snow grains in the basal layer of the snow cover.

## Ablation 3

### Saturated snow

The temporal evolution of scattering during this period often shows a dip in scattering over first-year sea ice forms (Figure 11??) and an increase in multiyear sea ice scattering. The first-year dip is not always apparent and may be due to differences in scattering from the snow surface. This feature may not always be resolved due to the fact that it occurs quickly in some snowpacks. The multiyear scattering increase is most likely due to the removal of snow from the old hummocks and water drainage from these structures thereby returning a large volume scattering term to the total measured scattering.

Ablation 4	Once ponds form on the sea ice there is an oscillation of the scattering which is both spatially and temporally variable. The scattering is dominated by specular return for smooth pond surfaces and volume scattering from the snow patches. For surfaces roughened by wind the scattering will increase dramatically due to the rough surface scattering from the pond surfaces. The larger the pond fraction the more variable the scattering will be due to the fact that the water surfaces (rough versus smooth) will dominate the scattering.
Pond formation	
Ablation 5	Microwave scattering during this period remains a research topic area.
Pond drainage	
Ablation 6	Microwave scattering during this period remains a research topic area.
Rotten ice	

---

### **Role of Radarsat in the detection and monitoring of sea ice ablation.**

Much of the theory developed here (and elsewhere) has made use of the European SAR satellites (ERS-1 and 2). Although the polarization is different between ERS and RADARSAT the operating frequency is about the same (C-band). Work at CEOS has focused lately on the utility of

RADARSAT in the thermodynamic-scattering relationships described here. In general the theoretical relationships, developed for ERS, hold true for RADARSAT. For example the seasonal evolution of the microwave scattering coefficient followed the same seasonal evolution as ERS when we used RADARSAT digital numbers (rather than scattering coefficients). Surprisingly this relationship also holds true to ScanSAR data products (Figure 2.4) which opens the door to using these data operationally for estimating the thermodynamic state of snow covered sea ice.

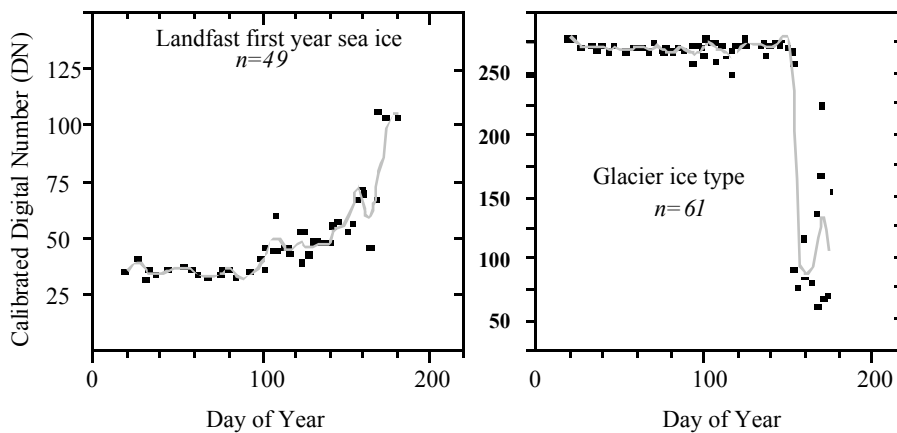


Figure 2.4. Examples of a ScanSAR wide temporal evolution in scattering for landfast first-year sea ice and a glacier ice type from the North Water Polynya study (Yackel et al. 1999).

We have also found that the physical mechanisms which give rise to this observed scattering is controlled by the distribution and percent fraction of water in liquid phase within the snow covered sea ice. This relationship is important to sea ice decay since the thermodynamics of the sea ice volume are controlled by the role which water plays in moderating the conductive and radiative fluxes over the evolving sea ice surface. Results using RADARSAT data show that there is also a relationship between standard

beam calibrated digital numbers and the percent coverage of melt ponds on sea ice and that this relationship is controlled by the wind roughening on the pond surfaces (Figure 2.5).

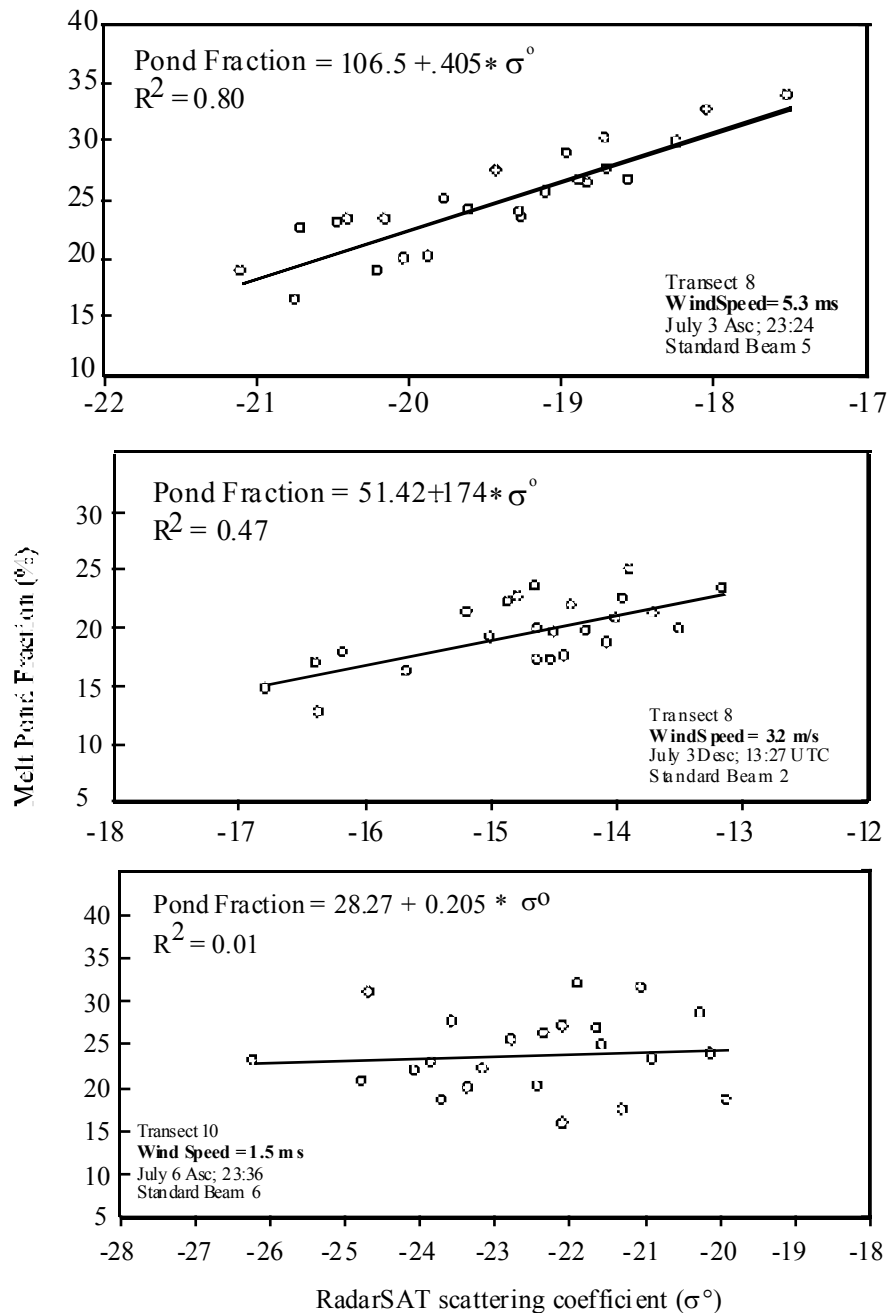


Figure 2.5. Relationship between RADARSAT scattering the melt pond percent cover over landfast first-year sea ice relative to wind speed. Results

show the role which wind roughening plays in estimating pond fraction from microwave scattering.

The operationalization of the theory presented in this report is being address by Mr. John Yackel. His thesis work and related publications more fully specify the relationship between microwave scattering with RADARSAT-1, thermodynamic evolution of the sea ice system and approaches we can use to estimate thermodynamic information for AIRSS related ice products (see upcoming PhD thesis by J. Yackel, 2000).

In this section we have provided a brief review of the current status of sea ice information retrieval from remote sensing. We have summarized the pertinent literature within a tabular structure and identified the approaches as being either research or operational in nature<sup>8</sup>. We then described the nature of the ice related information within the thermodynamic regimes of freeze-up, winter, and ablation states 1-6. In the next section we will specifically focus on the requirements of the Arctic Ice Regime Shipping System (AIRSS) structure using the theoretical base developed here and in Section 1.

---

<sup>8</sup> Note that the literature reviewed is considered illustrative rather than exhaustive

## **Section 3**

### **Ship Navigation, Sea Ice Ablation, and Remote Sensing**

## Introduction

Synthetic Aperture Radar (SAR) is ideally suited for operational sea ice information extraction. Over the past 20 years we have seen a continual evolution in our understanding of the physical mechanisms controlling microwave scattering over sea ice. More recently we have developed a sophisticated set of tools whereby we can quantify the microwave interaction physics mathematically. We now have operationally tested forward scattering models<sup>9</sup> and various research groups are actively pursuing the development of inverse scattering models<sup>10</sup>. This development in EM interaction modeling has been paralleled with an increased understanding of the physical, thermodynamical and electrical properties of snow and sea ice (as described in Section 1). Numerical models now exist which can capture the principal processes occurring across the ocean-sea ice-atmosphere interface (see for example Flato and Brown, 1996 and Curry and Ebert, 1993). Through the links with brine volume there is an entire field of research which will look towards the development of an 'Electro-Thermophysical' model of snow covered sea ice. This model will use a combined forward and inverse scattering model, coupled to a 1-dimensional thermodynamic sea ice model to predict various physical, thermodynamical and mechanical properties of snow covered sea ice. A recent example of developments towards this goal was the Electromagnetics of Sea ice - Accelerated Research Initiative (ARI) funded by the U.S. Navy (ONR) to the level of \$5M over the period 1993 to 1998 (see the ONR-ARI special

---

<sup>9</sup>Forward scattering models using physical and electrical properties of the snow/ice volume and predict the EM interaction magnitude.

<sup>10</sup>Inverse scattering models measure the EM response from the surface and then determine what mix of physical and electrical properties are most likely to have caused the observed scattering.

issue of IEEE Transactions on Geoscience and Remote Sensing. 65(5), 1998). Similar efforts are underway in both Europe and Australia. The timeline for operational implementation of a fully functioning 'Electro-Thermophysical' model is however, somewhat distant. The theoretical framework being developed to drive the model does however, have relevance to both the immediate and near future needs of the Canadian Ice Service.

In this section we step back from the theory presented to this point in the paper and develop a more practical focus by addressing the issues of sea ice ablation as they pertain to the Arctic Ice Regime Shipping System (AIRSS) of the Arctic Shipping Pollution Prevention Regulations (ASPPR). We begin with a brief overview of the AIRSS system and the concepts of ice multipliers, particularly as they pertain to our ability to measure proxies of these ice multipliers using SAR. We then define the geophysical characteristics of sea ice ablation with specific reference to the development of a definition for 'decayed' or 'decaying' ice. We conclude this section with a summary review of the role which the temporal evolution of the microwave scattering coefficient ( $\sigma^\circ$ ) can play in the specification of two requirements of the AIRSS regulations:

- 1) Extraction of ice type information from SAR.
- 2) Measurement of sea ice ablation from SAR.

### **The AIRSS system**



The Arctic Waters Pollution Prevention Act (AWPPA) of 1970 sets out the responsibilities of the Federal Government in the area of marine vessel navigation as it pertains to Arctic waters. Historically the Zone/Date shipping Safety Control scheme was used as a guide to determine both the timing and routing of Arctic voyages. An evolution of this system occurred with the development of the Arctic Ice Regime Shipping System (AIRSS). The AIRSS framework provides for a more flexible approach to Arctic navigation; it relies more heavily on expert Ice Navigators, and a more full utilization of available ice information.

The AIRSS system creates an Ice Numeral (IN) based on a weighted sum of the components of a particular 'ice regime'. An Ice Regime is defined as a relatively consistent distribution of any mix of ice types, including open water. The concept is that a table of Ice Multipliers (IM) provides an index of the hazard potential of a particular type of ice relative to the class of vessel under consideration. The table specifies Ice Multipliers for both CAC (3 and 4) and Type (A-E) vessels. The computation of the IN is done by multiplying the percent cover of a particular ice type (obtained from the egg code of a CIS Ice Chart) by the IM for the particular vessel being considered. The products are then summed for the mix of ice types within the 'Ice Regime' to obtain the IN. For a ship to enter an ice regime the IN must be zero or higher. Ice Multipliers may be increased for decayed ice and must be decreased for ridging.

## **Evolution of $\sigma^\circ$**

The CIS has what is arguably one of the most sophisticated ice information systems currently operational. The approach to generating ice information relies heavily on the visual analysis of SAR images from RADARSAT. A significant source of information now available from RADARSAT is the temporal evolution of the scattering. Although we have touched upon the salient theory in Sections 1 and 2 we summarize the seasonal evolution here as a preamble to proposing methods of utilizing tone/texture; incidence angle and the temporal evolution of  $\sigma^\circ$  directly within the AIRSS structure.

Recent research results (Barber et al. 1994; Barber et al. 1995, Drinkwater, 1989; Onstott, 1992; Winebrenner et al. 1994; Kwok and Cunningham, 1994; and others) have shown that a distinct pattern exists for the seasonal evolution of the microwave scattering coefficient ( $\sigma^\circ$ ) over various ice types. Although these patterns are undoubtedly frequency and polarization dependent it would appear that the C-VV manifestation for snow covered thick first-year and multiyear sea ice follows a form approximated in Figure 3.1<sup>11</sup>. Following the same seasonal nomenclature used in the preceding section (Livingstone et al., 1987) we can summarize the seasonal evolution of  $\sigma^\circ$  as follows:

---

<sup>11</sup>We note here that this schematic represents the most recent conceptualization we have of the temporal evolution of  $\sigma^\circ$ . Spatial and temporal variability in this signature does occur.

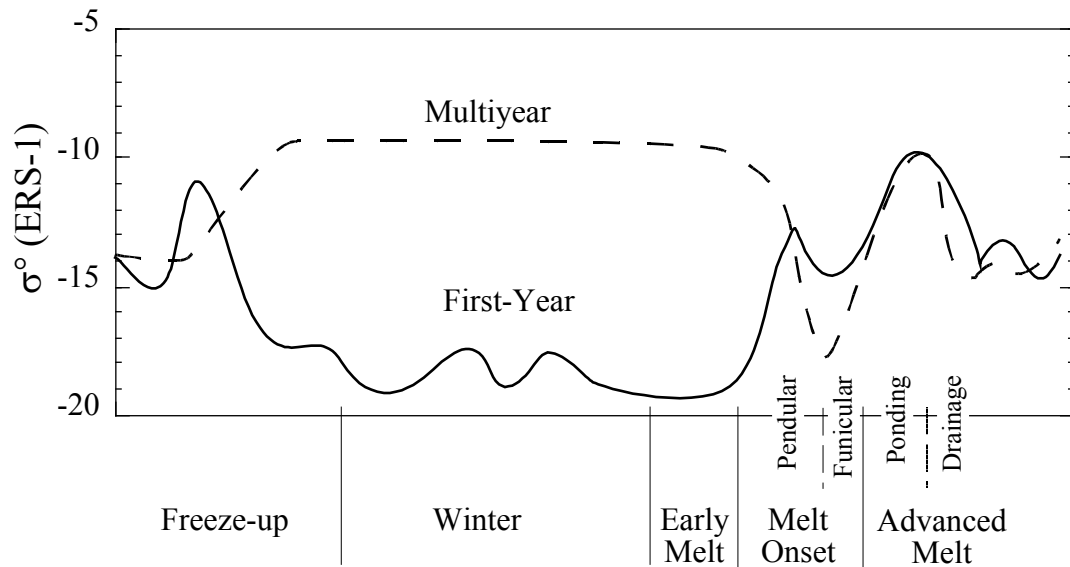


Figure 3.1. Phenomenological summary of the seasonal evolution of  $\sigma^0$  from the ERS-1 SAR for thick first-year and multiyear sea ice over the seasonal periods spanning the annual sea ice cycle.

*Freeze-up* - The high dielectric constant of the ocean surface causes variable scattering over water as a function of wind speed. Young ice types can have high  $\sigma^0$  (presence of frost flowers) or low  $\sigma^0$  (grease ice reduces wind roughening). As ice thickens there is a decrease in the scattering. Snow deposition further reduces scattering. Remnant water in liquid phase causes low scattering from MYI forms. As the water changes phase from liquid to solid the hummock volume scattering increases - returning  $\sigma^0$  values to winter norms.

*Winter:* Within multiyear sea ice, microwave scattering is very stable during the Winter period. Older forms of ice appear to have a higher magnitude of scattering due to the larger and deeper hummock layers which contain larger bubble sizes spaced further apart within the

hummocks. The variability in image texture of multiyear sea ice is due to the spatial pattern of hummock and frozen melt pond surfaces within the multiyear sea ice. The snow cover on the multiyear sea ice is brine free and of a sufficiently low density and small grain size as to be transparent to 5.3 GHz energy.

Within first-year sea ice, microwave scattering appears to oscillate according to changes in the oceanic and atmospheric heat fluxes. Thin first-year ice types produce a much more complicated seasonal evolution of  $\sigma^\circ$  because of the dynamics of the near surface dielectric properties and the role of the snow cover in altering the scattering volume as the ice matures.

*Early Melt* (Ablation State 1) - Within multiyear sea ice, microwave scattering remains stable into the Early Melt period because hummock volume scattering still dominates. Diurnal differences may be present as small amounts of water in liquid phase become available near the surface of the snow cover at or near solar noon. Because the snow cover is brine free and the grains are fairly small we do not expect any significant scattering (at 5.3 GHz) from the snow volume during this period.

Within first-year sea ice, microwave scattering is dominated by a combination of basal layer volume scattering and ice surface scattering. During this period we would expect to find a significant difference in solar noon versus solar midnight observations as small amounts of water in liquid phase would contribute both to grain growth and the elevated temperatures would significantly increase the brine volume of the snow basal layer. The overall magnitude of  $\sigma^\circ$  will be dependent on the ice surface microscale roughness and its surface brine volume.

*Melt Onset* (Ablation State 2 and 3) In multiyear sea ice, Melt Onset is denoted by a rapid decrease in  $\sigma^\circ$ . The mechanism responsible is the absorption of microwave energy by the water in liquid phase within the snow cover and by the presence of water in liquid phase within the hummock structures free of a snow cover. An increase in permittivity and in particular an increase in the dielectric loss, effectively mask the volume scattering from the hummocks thereby decreasing  $\sigma^\circ$ . The decrease in  $\sigma^\circ$  proceeds over both the pendular and funicular regimes of snow ablation.

In first-year sea ice, Melt Onset is denoted by a rapid increase in  $\sigma^\circ$ . There are two mechanisms which are likely candidates for the observed increase. At relatively low water volumes (1 to 3 percent) the large brine wetted snow grains in the basal layer contribute a significant volume scattering term to  $\sigma^\circ$ . As the water in liquid phase continues to increase (but is maintained within the pendular regime) it is likely that the snow surface contributes a surface scattering term to  $\sigma^\circ$  (Drinkwater, 1989; Livingstone and Drinkwater, 1991; Barber and LeDrew, 1994). A distinct dip in  $\sigma^\circ$  at the first-year ice site corresponds with the transition from the pendular and funicular regimes. This transition marks the reduction of brine within the basal layer to near zero, an increase in the water in liquid phase at the base of the snow cover and a reduction of water in liquid phase in the top parts of the snow volume (as the surface begins to drain). These processes lead to a reduction of both the volume scattering and snow surface scattering hypothesized to dominate the pendular regime conditions.

*Advanced Melt* (Ablation States 4 and 5) - In multiyear sea ice, Advanced Melt is denoted by a rapid increase in  $\sigma^\circ$ . As surface water forms in the previous years melt ponds there is an increase in the discontinuity at the

air/water interface. The dielectric permittivity and loss ( $\epsilon'$  and  $\epsilon''$ ) of this freshwater (which has a surface temperature of about  $+1^{\circ}\text{C}$ ) is sufficiently large that we can expect a penetration depth on the order of 1 cm (Ulaby et al. 1986). We can expect an increase in scattering if the melt pond surfaces are wind roughened. A reduction in the water in liquid phase within the hummocks may also cause an increase in  $\sigma^{\circ}$  by increasing the volume scattering component of  $\sigma^{\circ}$ . Once the ice surface begins to drain there is a pronounced decrease in the multiyear  $\sigma^{\circ}$ . This period coincides with a reduction in the spatial extent of the melt ponds and cyclical changes in the water in liquid content within the hummocks. In first-year sea ice  $\sigma^{\circ}$  increases over the ponding period and decreases as the ice begins to drain analogous to that described for the multiyear ice surface. Pond surface scattering increases  $\sigma^{\circ}$  when wind roughened. Snow patches have low volume scattering. Breakup initialization is often directly evident as the ablated ice sheet opens due to oceanic or atmospheric momentum forcing.

## Extracting Sea Ice Information

With the launch of ERS-1 we began to realize that most of the ice information in a SAR dataset is actually contained within the temporal evolution of the microwave scattering coefficient ( $\sigma^\circ$ ). With the launch of RADARSAT we now have three different types of information from which we can develop approaches to separating the icescape into functionally specific components: Tone/Texture; Incidence Angle; and the Temporal Evolution of  $\sigma^\circ$

Tone and texture are the 'image' features that have been traditionally used in both visual segmentation and machine classification of SAR images of sea ice (see Tsatsoulis and Kwok, 1998). An improved understanding in the EM interaction physics means we are now able to understand why we get a certain tone or texture within a particular type of sea ice and this information can then be utilized in automatic or semiautomatic information extraction algorithms.

Incidence angle effects are proving to be a very valuable (although perhaps not initially intended) piece of information which we can utilize in image segmentation and subsequent ice information retrieval. The concept is that under certain conditions two particular surfaces may have very similar  $\sigma^\circ$  values<sup>12</sup>. Microwave scattering theory has shown us that a surface will consist of a range of surface and volume scattering (as per equation [7]). A pure volume scatterer will display only a small decrease with incident angle range whereas pure surface scattering will drop rapidly with incidence angles (Figure 3.2). If we view a surface from two different incidence

angles we can compare the difference in magnitude of the scattering and determine whether the feature is more a volume or surface scatterer. This approach could, for instance, be used to calculate the fraction of ponding on first-year sea ice (surface scatterer) or separate ice from open water.

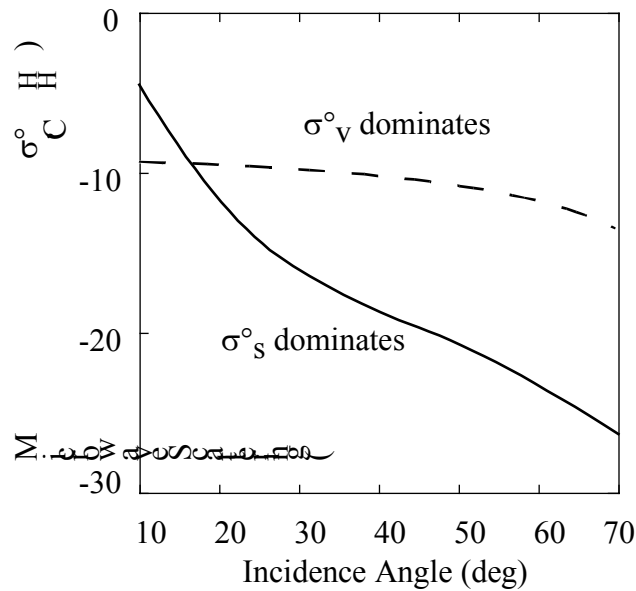


Figure 3.2. Modeled relationship between a predominantly volume ( $\sigma^0_v$ ) and surface ( $\sigma^0_s$ ) scattering phenomena for snow covered sea ice.

The temporal evolution of  $\sigma^0$  is also a significant source of information in SAR when it comes to estimating characteristics of the seasonally evolving surface. By exploiting temporal information we have shown that rubble ice can be separated from thin rafted ice, thick first-year and multiyear (Thomas, 1996). We can also separate second year from various forms of multiyear sea ice. The temporal information also provides a link to the mechanical properties of the sea ice, through the brine and temperature relationships

---

<sup>12</sup>In this section  $\sigma^0$  and grey level or image tone can be used interchangeably






described in Section 1. This has the potential for application in the identification of various ablation states as the surface of landfast first-year sea ice progresses from cold/strong ice in the winter through until breakup.





From a physical and mechanical perspective we proposed a series of discrete ablation states: Freeze-up; Winter; Ablation 1 (very early melt); Ablation 2 (sustained snow melt); Ablation 3 (saturated snow); Ablation 4 (melt pond formation); Ablation 5 (drainage of ponds) and Ablation 6 (rotten ice). We consider breakup can occur at some point within or beyond Ablation 3.




The AIRSS structure calls for both information on ice type (which is used within its definition of an 'Ice Regime') and on the thermodynamic decay of sea ice (decayed or decaying ice). In what follows we summarize our current understanding of how SAR data may be used in meeting requirements of ice type (Table 3.1) and ice decay (Table 3.2). The status column indicates the current status of the approach over the research-to-operational continuum ('R' for research and 'O' for operational over each status bar).

Table 3.1. Summary of the capabilities of SAR for extraction of ice type information required by the AIRSS<sup>13</sup>.

Variable	Approach	Status
Open Water	Change in surface roughness between image dates (i.e., wind speed changes scattering of water but not ice); compare same area from different angles (surface scattering dominates over water).	R  O
Grey Ice (0-0.15m)	Rapid drop in scattering as ice dampens ocean scattering. Dynamic variation in surface due to frost flowers. Microwave scattering coupled to thermodynamic model holds potential as an approach.	R  O
Grey White (0.15-0.30m)	Scattering drops but remains higher than thick FYI with same surface autocorrelation function. Diurnal variation in scattering is smaller than for thicker FYI types. Microwave scattering coupled to thermodynamic model holds potential as an approach.	R  O



<sup>13</sup>All of the SIMMS research and most of the literature review is based on landfast or pack ice conditions. Marginal Ice zones present unique problems. In general if the floes are large enough the scattering physics describe above will transfer. Tracking ice becomes NB if radiometry changes are to be used as an information source.

Thin FYI (0.30-0.70m)	Scattering continues to drop as the surface brine volume drops. Diurnal variation in scattering is smaller than for thicker FYI types. Microwave scattering coupled to thermodynamic model holds potential as an approach.	
Medium FYI (0.70-0.1.2m)	Scattering reaches a minimum defined by the surface autocorrelation function. Diurnal variability may occur but magnitudes are small.	
Thick FYI (>1.2m)	Dark surface scattering from smooth ice types. Large diurnal variations can be expected as snow/air interface brine volumes change.	
Second Year (>2.0m)	Scattering magnitudes smaller than true multiyear forms and absence of the MYI texture pattern evident on older floes. Scattering is stable over the winter period until water becomes available in the snow cover.	

Multiyear (>3.0m)	Scattering increases rapidly with onset of freeze-up (as compared with decreasing $\sigma^\circ$ over FYI types). Textural information appears to be related to relative age of MYI. Small change in scattering at different incidence angles hold potential for separating MYI from rubble ice (since MYI is dominated by volume scattering).	R 
Ridged FY Ice	Development of ridge severity index may be possible for particular scales. Seasonal evolution of surface shows MYI and FYI types change but ridged and rubble areas do not. This has application in segmentation of ridge severity.	R 
Rubble Ice	Rubble ice in combination with MYI types in rubble fields can be defined visually. Diurnal variation can separate rubble from smooth FYI but not MYI. Seasonal signature changes can separate rubble from pure MYI floes.	R 

---

Table 3.2. Summary of the capabilities of SAR for extraction of thermodynamic state information required by the AIRSS.

Variable	Approach	Status
Freeze-up	Best signal is the return of MYI signatures to winter norms. Oscillation of FYI type signatures over a period of days may also be useful. Tracking FDD from onset of freeze-up would help drive thermodynamic model of particular areas using regional forcing variables of temperature and wind.	R 
Ablation 1	Onset of Melt can be mapped over regional scales. This is the point where sufficient water occurs within liquid phase to reduce the scattering over MYI types. Change in MYI signatures is best identified using a threshold to avoid 'false starts'.	R 
Melt Onset		

Ablation 2 and 3

Brine Channel  
Formation

There exists a point within the sea ice where the brine reaches a critical level of 5 percent by volume. This point coincides with a dramatic reduction in all mechanical properties of the sea ice because of the control which brine volume exerts on mechanical properties. Research suggests that the increase in FYI signatures may have application in defining this point.

R  O

Ablation 4 and 5

Surface Ponding

Development of ponded surfaces over both FYI and MYI can be determined from the temporal evolution of  $\sigma^{\circ}$ . Computation of percent cover appears to be possible by exploiting the fact that pond surfaces are dominated by surface scattering and snow patch surfaces are strong volume scatterers.

R  O

## Breakup Prediction

By targeting ponded surfaces it follows that breakup prediction may be possible by measuring the rate of decay of the surface using changes in the evolution of  $\sigma^\circ$ . This rate information could then be used in a climatologically based ice breakup model.

---

## **Section 4**

### **Summary and Conclusions**



## **Summary of Section 1**

In Section 1 we reviewed details of the physical, electrical and mechanical properties within the framework of the thermodynamic regimes of freeze-up, winter, and ablation states 1 through 6. We showed that brine volume controls both the dielectric constant and the mechanical properties of sea ice, and that brine volume was in turn controlled by the thermodynamic conditions through the snow/sea ice interface. We have identified the principal processes creating this linkage within each of the thermodynamic seasons in light of the development of an 'Electro-Thermophysical' model for snow covered sea ice.

Ice formation resulted in mechanically weak forms of sea ice with high brine volumes and temperatures. The evolution of the surface towards winter averages resulted in increased mechanical strength, decreasing brine volumes and development of brine pockets in the frazil and columnar layers. Desalination occurred quickly after freeze-up and grain structure was shown to be related to the historical conditions experienced during freeze-up.

Ice accretion rates and total ice thickness during the winter and early melt periods is driven by atmospheric temperatures and snow thickness. Ice thickness was found to be the dominant factor in determining the overall strength of sea ice. The total brine volume was also found to significantly influence mechanical strength. Brine volumes in the ice are found to decrease over time in first-year ice primarily through gravity drainage. As a result, total mechanical strengths increase and the dielectric permittivity and loss decrease during the 'winter' period.

With the return of shortwave radiation as a significant contributor to the surface energy balance the process of sea ice ablation begins. Increasing temperatures towards the later winter period increase the brine volume of the ice. Metamorphism in the snow advances and eventually water becomes available in liquid form. Small amounts of water influence the amount of shortwave energy being absorbed within the snow cover, thereby enhancing the ablation process. Once gravity drainage begins the ice mass is warmed through both radiative and conductive mechanisms. Brine volumes increase to a point where brine drainage channels are reconnected. This appears to occur at about 5 percent brine by volume. Surface ponding occurs over both first-year and multiyear forms of ice. Ice thickness is retained throughout this process and the ablation is really defined by a reduction in brine volume and creation of surface ponding (rather than reduction in thickness). Rapid drainage of ponds appears to be related to the complete opening a percolation structures between the ocean and ice surface.

Our review of the physical, electrical, and mechanical properties of sea ice has reinforced the fact that we still do not completely understand many of the processes which give rise to the spatial and temporal variability we see within naturally occurring sea ice. The following questions serve to illuminate some of these challenges:

#### *Freeze-up*

- 1) What role does snow cover play during Freeze-up in defining the rate and or equilibrium thickness of sea ice?
- 2) What are the rates of snow metamorphosis on young ice and how are they affected by high ice surface brine volumes?

- 3) Of the energy deficit required for ice growth, how much is generated locally, regionally, or synoptically?
- 4) What are the rates of brine expulsion both to the surface and subsurface and how does this process affect thermohaline circulation within the ocean mixed layer?

### *Winter*

- 1) What are the statistical properties of snow distribution on winter forms of sea ice?
- 2) How does the presence of varying snow thicknesses affect the electrical and mechanical properties of winter ice forms?
- 3) What are the rates of snow metamorphosis during the winter period and can we relate observed metamorphism to ice type, snow thickness and the temperature profile through the snow and ice?
- 4) What are the physical, electrical and mechanical differences in ice that forms under strong atmosphere/ocean temperature gradients versus that which forms under weaker (fall like) regimes?
- 5) Can the age of multiyear sea ice be defined by the topography and bubble inclusion size distribution within hummocks.
- 6) At what point do we develop 'depth hoar' on both first-year and multiyear sea ice?

### *Ablation I*

- 1) At what depth in the snow cover does the maximum absorption of shortwave energy occur?
- 2) How variable are the processes of snow metamorphism spatially, temporally and as a result of varying ice type and snow depth?
- 3) Where does water first occur in liquid phase within the vertical profile of the snow cover?
- 4) How is liquid phase water distributed over the vertical profile of the snow cover?
- 5) At what point does sea ice growth stop and ablation begin?
- 6) What is the role of clouds in moderating the metamorphism of snow volume and thereby the ablation of the sea ice?
- 7) What are the statistical properties of the brine inclusions in the sea ice over the vertical dimension?
- 8) How variable is the brine structure spatially?

#### *Ablation 2 and 3*

- 1) Can we model the change in shortwave energy absorbed due to grain growth and phase changes in the snow?
- 2) How variable is the onset of melt spatially and temporally?
- 3) How is liquid phase water distributed over the vertical profile of the snow cover?

- 4) When does subice ablation begin and what are the principal mechanisms creating this ablation?
- 5) What is the role of clouds in moderating the metamorphism of snow volume and thereby the ablation of the sea ice?
- 6) How do the brine inclusions and ice grain structure in the ice respond to the warmer core temperature during this period?
- 7) How variable is the response of brine interconnectivity over a diurnal scale and within various ice types?

#### *Ablation 4 and 5*

- 1) How is differential snow metamorphism related to pond formation?
- 2) How is the statistical pattern of snow distribution from the winter period related to the melt pond pattern?
- 3) How is the statistical pattern of melt ponds related to the type of ice upon which they occur?
- 4) What are the physical processes which allow ponds to occur over ice for extended periods of time and then - abruptly drain?
- 5) How is the presence of melt ponds related to the mechanical strength of sea ice?
- 6) Why do thaw holes occur within floes of sea ice over the summer period?
- 7) What is the relationship between floe size and the rate of ice ablation?

- 8) Can we predict the timing of breakup by monitoring the process of ice ablation from winter to the melt pond formation period?

## **Summary of Section 2**

Several physical parameters and processes of sea ice can be extracted from satellite based remote sensing as outlined in Section 2 and 3. Many of the techniques involve the use of active and passive microwave, thermal infrared and optical wavelengths or combinations of each. Some techniques also require the use of physical models in combination with remotely sensed information to derive some parameters (e.g., cloud properties, atmospheric drag and young ice thickness). However, not all of the parameters and processes can be extracted over an entire sea ice seasonal cycle. Furthermore, some techniques have been used and refined over a longer period of time than others that are fairly new techniques that require further research and/or refinement.

The parameters and processes that have been refined over a period of time and can be extracted from satellite based remote sensing with a fair degree of accuracy include: 1) ice extent using optical, thermal infrared and passive microwave, 2) ice type and concentration using optical, thermal infrared and passive microwave, 3) surface melt using active microwave, 4) young ice thickness (during fall freeze up or within leads) using passive microwave, 5) multiyear ice concentrations (except during advanced melt) using passive microwave, 6) ice motion/velocity using optical, thermal infrared and active microwave, 7) surface albedo (at all ice stages but requires strong enough winds during advanced melt) using active microwave, and 8) surface temperature using thermal infrared.

Our review of the remote sensing of sea ice shows that we have made considerable progress in extracting ice related information from a variety of EM frequencies. In particular the microwave approaches, both passive and active, are progressing well. There are a number of developments, particularly in the area of SAR information extraction which show considerable promise as a means of determining both the type of ice and its thermodynamic state. The following questions serve to illuminate some of questions we now face:

*Freeze-up*

- 1) Can we develop an approach to estimating the thickness of young ice forms using active microwave ( $A_{\mu w}$ ) interactions?
- 2) Can the integration of active microwave and thermal IR provide useful information in estimating the critical end of young ice growth (i.e., 0-30cm)?
- 3) Can we develop an approach to identifying frost flower development using SAR?
- 4) Can we extract information (from SAR) on ridging and rubbing when these processes are actively occurring in young ice?
- 5) Can we obtain information on the rate of ice growth using time series information from SAR or Passive Microwave ( $P_{\mu w}$ )?
- 6) Can we detect the presence of snow on young sea ice?
- 7) Can we develop proxy indicators of the total conduct flux between the ocean and atmosphere during this period?

### *Winter*

- 1) Can we segment winter SAR data into ridged, rubbled, FYI and MYI classes using variations in scattering due to temporal and incidence angle effects?
- 2) Can we estimate snow thickness distributions on sea ice using the diurnal effects on the surface brine layer of thick FY ice?
- 3) Can we identify new ice growth in this period which is associated with leads, polynyas, etc.?
- 4) Can we determine ice production and export rates in leads and polynyas?
- 5) Can we determine the age of multiyear sea ice by exploiting the differences in its surface topography and bubble inclusion properties?
- 6) Can we measure the grain size of snow on sea ice using active or passive  $\mu$ w interactions?

### *Ablation states 1-3*

- 1) Can we estimate the shortwave flux at the surface during this period using  $A_{\mu w}$  or  $P_{\mu w}$  interactions?
- 2) Can we estimate the subsnow PAR at the surface during this period using  $A_{\mu w}$  or  $P_{\mu w}$  interactions?



- 3) Can we link the temporal evolution of the microwave scattering or emission to the bulk brine volume of the sea ice?
- 4) Can we estimate the conductive flux at the surface using a combination of TIR and microwave remote sensing data during this period?

#### *Ablation States 4 and 5*

- 1) Can we unambiguously identify the formation date of surface ponding using active or passive  $\mu\text{w}$ ?
- 2) Can we estimate the percent cover of ponding using active or passive  $\mu\text{w}$ ?
- 3) Can we unambiguously identify the drainage of melt ponds on sea ice?
- 4) Can we relate diurnal and temporal variation in  $\sigma^\circ$  to the shortwave and/or longwave fluxes across this surface?
- 5) Can we directly identify evidence of sea ice breakup (e.g., thaw holes, leads, etc.)?

### **Summary of Section 3**

In section 3 we examined the applied aspects of sea ice remote sensing throughout the annual cycle and the requirements of the AIRSS system for sea ice multipliers. We identified two separate characteristics of sea ice which are now available from the time series SAR scattering: 1) ice type and 2) thermodynamic state. The former is important as a means of improving ice information within AIRSS and the latter is a prerequisite for determining

the thermodynamic state of the snow/sea ice system. The process of decay, as described in sections 1 and 2 is pivotal in the formation of ablation states from synthetic aperture radar (SAR).

## **Conclusions**

The research presented in this report should be considered as a voyage rather than a destination. Our work reinforces the requirement for an 'Electro-Thermophysical' model for snow covered sea ice. We are making good progress towards this goal and can see operational spin offs available immediately with more sophisticated applications evolving in the next 3 to 5 years. The theory that is required for the model demands that we treat the ocean-sea ice-atmosphere interface as an integrated environment. In a practical sense this creates two different types of ice information: i) Ice types and ii) the thermodynamic state of sea ice. Significant advances have been made on both of these fronts and we are now operationalizing the first of these research results at the Canadian Ice Service (CIS) and their requirements within the AIRSS structure. The dissertation of Mr. John Yackel should be available by the spring of 2000. Research results in this thesis will complete certain aspects of the RADARSAT measurements of sea ice ablation and will also extend the research results into other aspects of the operational requirements of the CIS.

## **Literature Cited**

Aargaard, K., L.K. Coachman and E. Carmack., 1981. On the Halocline of the Arctic Ocean. *Deep-Sea Research*, 28A, 529-545.

Anderson, D.L. 1960. The physical constants of sea ice. *Research applications in Industry*, 13, pp. 310-318.

Arcone, S. A., A.G. Gow. and S. McGrew., 1986. Structure and dielectric properties at 4.8 and 9.5 GHz of saline ice, *J. Geophys. Res.*, 91(C12), 14,281-14,303.

Assur, A. 1958. Composition of sea ice and its tensile strength. *Arctic Sea Ice*. U.S. National Academy of Sciences-National Research Council, Pub. 598, 106-138.

Assur, A. 1960. Composition of sea ice and its tensile strength. *Research Report 44*, U.S. Army Snow and Ice and Permafrost Research Establishment, Wilmette, Illinois.

Azuma, N and A. Higashi, 1985. Formation processes of ice fabric patterns in ice sheets. *Ann. Glaciol.*, 6, 130-134.

Barber, D.G., D.D. Johnson and E.F. LeDrew, 1991: Measuring climatic state variables from SAR images of sea ice: The SIMS SAR validation site in Lancaster Sound. *Arctic*, 44, 108-121.

Barber, D.G., D.G. Flett, R.A. De Abreu, and E.F. LeDrew, 1992, Spatial and Temporal Variations in Sea Ice Geophysical Properties and Microwave Remote Sensing Observations: The SIMS'90 experiment. *Arctic*, 45(3), 233-251.

Barber, D.G. 1993: Assessment of the Interaction of Solar Radiation (0.3 to 3.0  $\mu\text{m}$ ) with a Seasonally Dynamic Snow Covered Sea Ice Volume, from Microwave (2.0 to 5.0 cm) Scattering. Ph.D. dissertation, Faculty of Environmental Studies, Earth Observations Laboratory Technical Report Series ISTS-EOL-TR93-002. Department of Geography, University of Waterloo, Ontario.

Barber, D.G., T.N. Papakyriakou and E.F. LeDrew, 1994: On the relationship between energy fluxes, dielectric properties and microwave scattering over snow covered first-year sea ice during the spring transition period. *J. Geophys. Res.*, 99(C11), 22,401-22,411.

Barber, D.G. and E.F. LeDrew, 1994: On the links between microwave and solar wavelength interactions with snow-covered first-year ice. *Arctic*, 47, 298-309.

Barber, D.G., T.N. Papakyriakou, E.F. LeDrew and M.E. Shokr, 1995: An examination of the relation between the spring period evolution of the scattering coefficient and radiative fluxes over landfast sea ice. *Intl. J. Remote Sensing*, 16(17), 3343-3363.

Barber, D.G., S.P. Reddan and E.F. LeDrew, 1995: Statistical characterization of the geophysical and electrical properties of snow on landfast first-year sea ice. *J. Geophys. Res.* 100(C2), 2673-2686.

Barber, D.G., A. Thomas and T. Papakyriakou. 1998 The role of synthetic aperture radar (SAR) in surface energy flux measurements over sea ice. Invited Chapter #3 in Tsatsoulis, C. and R. Kwok. *Synthetic Aperture Radar Remote Sensing of Sea ice*. John Wiley and Sons. pp 35-67.

Barber, D.G. and Yackel, J.J. 1999. The physical, radiative and microwave scattering characteristics of melt ponds on sea ice. *International Journal of Remote Sensing* 20(10):2069-2090.

Barber, D.G., and S.V. Nghiem. 1999. On the Estimation of Snow Thickness Distributions over Sea Ice using Active Microwave Scattering. *Journal of Geophysical Research (Oceans)*. In Press (July'98).

Burns, B.A., 1990: SAR image statistics related to atmospheric drag over sea ice. *IEEE Transactions on Geoscience and Remote Sensing*, 28(2), 158-165.

Butkovich, T.R., 1956. Strength studies of sea ice. SIPRE Report RR20, Wilmette, Illinois.

Butkovich, T.R., 1959. On the mechanical properties of sea ice. Thule, Greenland, SIPRE Report RR54, Wilmette, Illinois.

Comiso, J.C., 1986: Characteristics of Arctic winter sea ice from satellite multispectral microwave observations. *J. Geophys. Res.*, 91(C1), 975-994.

Campbell, K.J., R.O. Ramseier, W.F. Weeks and P. Gloersen., 1975. An intergrated approach to the remote sensing of floating ice. In: *Proceedings of the 3rd Canadian Symposium on Remote Sensing*, 39-72.

Campbell, K.J., J. Wayenberg, J. Ramseyer and R.O. Ramseier., 1978. Microwave remote sensing of sea ice in the Aidxex main experiment., *Boundary Layer Meteorology*, 13, 309-337.

Cavalieri, D.J., 1994: A microwave technique for mapping thin sea ice. *J. Geophys. Res.*, 99, 12,561-12,572.

Chedin, A., N.A. Scott, C. Wahiche and P. Moulinier, 1985: The improved initialization inversion method: A high resolution physical method for temperature retrievals from satellites of the TIROS-N series. *J. Clim. Appl. Meteorol.*, 24, 128-143.

Colbeck, S.C., 1981. The geometry and permittivity of snow at high frequencies. *Journal of Applied Physics* , 53(6), 45-61.

Colbeck, S.C., 1982. An overview of seasonal snow metamorphism. *Rev. Geophys. Space Phys.*, 20(1), 45-61.

Cole, D.M., L.H. Shapiro, W.F. Weeks, C. Byers, J. P. Dempsey, R.M. Adamson, V.F. Petrenko and O.V. Gluschenkov, 1995. Overview of recent program on mechanical properties of sea ice.

Cox, G.F. and W.F. Weeks., 1974. Salinity variations in sea ice. *Journal of Glaciology*, 13(67), 109-120.

Cox, G.F. and W.F. Weeks., 1983. Equations for determining the gas and brine volumes in sea ice samples. *Journal of Glaciology* , 29(102), 306-316.

Cox, G.F. and W.F. Weeks., 1988. Numerical simulations of the profile properties of underformed first-year sea ice during the growth season. *J Geophys. Res.*, 93(C10), 12449-12460.

Cox, S.K., D.S. McDougal, D.A. Randall and R.A. Schiffer, 1987: FIRE - the First ISCCP Regional Experiment. *Bull. Amer. Meteorol. Soc.*, 68, 114-118.

Crocker, G.B. 1984. The physical properties of snowcover on sea ice in the Central High Arctic. Department of Geography., McGill University., M.Sc. Thesis. 180 p.

DeAbreu, R.A., J. Key, J.A. Maslanik, M.C. Serreze and E.F. LeDrew, 1994: Comparison of insitu and AVHRR broadband albedo over Arctic sea ice. *Arctic*, 47, 288-297.

DeAbreu, R.A. and E.F. LeDrew, 1996: Multispectral analysis of fast sea ice albedo using AVHRR data. Proc. IGARSS'96, 651-653.

Drinkwater, M.R. and G.B. Crocker, 1988: Modeling changes in the dielectric and scattering properties of young snow covered sea ice at GHz frequencies. J. Glaciol., 34(118), 274-282.

Drinkwater, M.R., 1989, LIMEX'87 Ice surface characteristics: implications for C-Band SAR backscatter signatures. IEEE transactions on Geoscience and Remote Sensing, 27(5), 501-513.

Dykins, J.E. 1969. Tensile and flexural properties of saline ice. N. Riehl, B. Bullemer and H. Engelhardt (Eds.), Proc. Int. Symp. Phys. of Ice, Plenum, New York, 251-270.

Eppler, D.T. and W.E. Full, 1992: Polynomial trend surface analysis applied to AVHRR images to improve definition of Arctic leads. Rem Sens. Env., 40, 197-218.

Fily, M. and D.A. Rothrock, 1986: Extracting sea ice data from satellite SAR imagery. IEEE Trans. Geosci. Remote Sensing, GE-24, 849-854.

Flato, G.M. and W.D. Hibler, 1992: On modeling pack ice as a cavitating fluid. J. Phys. Oceanogr., 22, 626-651.

Fowler, C., J.A. Maslanik and W. Emery, 1994: Observed and simulated ice motion for an annual cycle in the Beaufort Sea. Proc. IGARSS'94.



Francis, J.A., 1994: Improvements to TOVS retrievals over sea ice and applications to estimating Arctic energy fluxes. *J. Geophys. Res.*, 99(D5), 10,395-10,408.

Frankenstein, G. and R. Garner. 1967., Equations for Determining the Brine Volume of Sea Ice From -0.5 to -22.9 degrees C., *Journal of Glaciology*, 6(48):943-944.

Fujita, S., M. Nakawo and S. Mae., 1987. Orientation of the 700-m Mizuho core and its strain history. In: *Proceedings NIPR Symposium on Polar Meteorology and Glaciology*, 1, 122-131.

Gold, L.W. 1968. The ice pressure problem. In: *Ice Seminar*, Petroleum Society of C.I.M, Calgary, Alberta, 27-30.

Grenfell, T.A., 1996: Microwave and thermal infrared emission from young sea ice and pancake ice. *Proc. IGARSS'96*, 959-961.

Groves, J.E. and W.J. Stringer, 1991: The use of AVHRR thermal infrared imagery to determine sea ice thickness within the Chukchi polynya. *Arctic*, 44, 130-139.

Gudmandsen, P. 1985. Application of SAR and other remote sensing data in studies of Atmosphere-Ocean-Ice interaction. *Proceedings of a Conference on the Use of Satellite Data in Climate Models*, Alpbach, Austria, June 10-12.

Hawkes, I. and M. Mellor., 1972. Deformation and fracture of ice under uniaxial stress. *Journal of Glaciology*, 11(61), 103-131.

Haykin, S., E.O. Lewis, R.K. Raney and J.R. Rossiter., 1994. Remote sensing of sea ice and icebergs. John Wiley and Sons, Inc., Toronto.

Hoekstra, P. and P. Cappillino. 1971., Dielectric Properties of Sea and Sodium Chloride Ice at UHF and Microwave Frequencies. *Journal of Geophysical Research*, (76):4922-4931.

Hollinger, J.P., B.E. Troy, R.O. Ramseier, K.W. Asmus, M.F. Harman and C.A. Luther, 1984: Microwave emission from high Arctic sea ice during freeze up. *J. Geophys. Res.*, 89(C5), 8104-8122.

Holt, B. and S.A. Digby, 1985: Processes and imagery of first-year sea ice during the melt season. *J. Geophys. Res.*, 90(C3), 5045-5062.

Johannessen, O.M., M.W. Miles and E Bjorgo, 1996: Global sea ice monitoring from microwave satellites. *Proc. IGARSS'96*, 932-934.

Key, J. and M. Haeflinger, 1992: Arctic ice surface temperature retrieval from AVHRR thermal channels. *J. Geophys. Res.*, 97(D7), 5885-5893.

Key, J., J.A. Maslanik, T.N. Papakyriakou, M.C. Serreze and A.J. Schweiger, 1994: On the validation of satellite derived sea ice surface temperatures. *Arctic*, 47, 280-287.

Key, J., 1995: The Cloud and Surface Parameter Retrieval (CASPR) system for polar AVHRR: Users guide, version 1.0A, Cooperative Institute for Research in Environmental Sciences, University of Colorado, pp.71.

Key, J., R.S. Stone and A.J. Schweiger, 1996: Expected errors in satellite-derived estimates of the high latitude surface radiation budget. Proc. IGARSS'96, 639-641.

Lindsay, R.W. and D.A. Rothrock, 1995: Arctic sea ice leads from advanced very high resolution radiometer images. J. Geophys. Res., 100(C3), 4533-4544.

Livingstone, C.E. and M.R. Drinkwater, 1991: Springtime C-band SAR backscatter signatures of Labrador Sea marginal ice: measurements versus modeling predictions. IEEE Trans. Geosci. Remote Sensing, 29, 29-41.

LeDrew, 1995. The role of remote sensing in understanding the effects of sea ice on global changes. In: The Canadian Remote Sensing Contribution to Understanding Global Change. Edited by E. LeDrew, M. Strome and F. Hegyi. Department of Geography Publication Series. No. 38, University of Waterloo.

LeDrew. E.F. and D.G. Barber 1994. The SIMMS Program: A Study of Change and Variability within the Marine Cryosphere. *Arctic*. 47(3):256-264.

LeSchack, L.A. 1980. Arctic ocean sea ice statistics derived from the upward-looking sonar data recorded during five nuclear submarine cruises. LeSchack Associated, Ltd., Silver Spring, Md.

Malinas, N.P. and R.A Shuchman, 1994: SAR derived sea ice thickness during ICEX'92. IEEE transactions on Geoscience and Remote Sensing, 1756-1758.

Markus, T. and B.A. Burns, 1995: A method to estimate subpixel-scale coastal polynyas with satellite passive microwave data. J. Geophys Res., 100, 4473-4487.

Markus, T. and D.J. Cavalieri, 1996: Comparison of open water and thin ice areas derived from satellite passive microwave data with aircraft measurements and satellite infrared data in the Bering Sea. Proc. IGARSS'96, 1523-1525.

Martin, S., 1979: A field study of brine drainage and oil entrainment in first-year sea ice. J. Glaciol., 22(88), 473-502.

Maslanik, J.A. and H. Maybee, 1994: Assimilating remotely-sensed data into a dynamic-thermodynamic sea ice model. IGARSS'94, 1306-1308.

Mätzler, C. 1987. Applications of the interaction of microwaves with natural snow cover. Remote Sensing Review., 2, 259-387.

Maykut, G.A., 1978: Energy exchange over young sea ice in the central Arctic. *J. Geophys. Res.*, 83(C7), 3646-3658.

Maykut, G.A. and D.K. Perovich., 1987. The role of shortwave radiation in the summer decay of a sea ice cover. *J. Geophys. Res.*, 92(C7), 7032-7044.

Meier, W., J. Maslanik, J. Key and C. Fowler, 1996: Retrieval of Arctic surface conditions and cloud properties from AVHRR data: A time series for the Beaufort Sea. *Proc. IGARSS'96*, 148-150

Miller, D.H., 1981: Energy at the surface of the earth: An introduction to the energetics of ecosystems. Academic Press. New York. 516 pp.

Moritz R.E. and D.K. Perovich (eds). 1996. Surface Heat Budget of the Arctic Ocean Science Plan, ARCSS/OAII Report Number 5, University of Washington, Seattle, 64 pp.

Nakawo, M. and N.K. Sinha. 1981., Growth Rate and Salinity Profile of First-Year Sea Ice in the High Arctic., *Journal of Glaciology*, 27(96), 315-330.

Onstott, R.G., 1992, SAR and scatterometer Signature of Sea Ice. Chapter 5. In; Carsey F. (Editor) *Microwave Remote Sensing of Sea Ice*. (American Geophysical Union. 1992. Geophysical Monograph 68.

Parkinson, C. D. Cavalieri, P. Gloersen, H. Zwally and J. Comiso. Arctic sea ice extents, areas, and trends, 1978-1996. *Journal of Geophysical Research (Oceans)*. C9:20,837-20,856.

Poplin, J.T. and A.T. Wang., 1994. Mechanical properties of rafted annual sea ice. *Cold Regions Science and Technology*, 23, 41-67.

Preller, R.H. and P.G. Posey, 1989: The polar ice prediction system (PIPS)-A sea ice forecasting system, NORDA report 212, Naval Oceanographic and Atmospheric Research Laboratory, 45 pp.

Preller, R.H., J.E. Walsh and J.A. Maslanik, 1992: The use of satellite observations in ice cover simulations. *Microwave Remote Sensing of Sea Ice*, American Geophysical Union, 385-404.

Richter-Menge, J.A. and K.F. Jones, 1993. The tensile strength of first-year sea ice. *Journal of Glaciology*, 39(133), 609-618

Robinson, D.A., G. Scharfen, M.C. Serreze, G. Kulka and R.G. Barry, 1986: Snow melt surface albedo in the Arctic basin. *Geophys. Res. Letters*, 13, 945-948.

Ross, B., and J.E. Walsh, 1987: A comparison of simulated and observed fluctuations in summertime Arctic surface albedo.

Schiffer, R.A. and W.B. Rossow, 1985: ISCCP global radiance data set: a new resource for climate research. *Bull. Amer. Meteorol. Soc.*, 66, 1498-1505.

Schwarz, J. 1971. The pressure of floating ice-fields on piles. In: *International Association of Hydraulic Research Symposium: ice and its action on hydraulic structures*, Reykjavik, Iceland.

Schwarz, J and W.F. Weeks, 1977. Engineering properties of sea ice. *Journal of Glaciology*, 19(81), 499-531.

Shuchman, R.A., R.G. Onstott, R.W. Flett and C.C. Wackerman, 1994: Satellite remote sensing of the Beaufort Sea during LEADDEX'92. *IEEE transactions on Geoscience and Remote Sensing*, 1015-1017.

St. Germain, K.M and D.J. Cavalieri, 1996: A microwave technique for mapping ice temperatures in the Arctic seasonal ice zone. *Proc. IGARSS'96*, 1208-1210.

Stone, R.S. and J.R. Key, 1993: The detectability of Arctic leads using thermal imagery under varying atmospheric conditions. *J. Geophys. Res.*, 98(C7), 12,469-12,482.

Svendsen, E., et al., 1983: Norwegian Remote Sensing Experiment: Evaluation of the Nimbus 7 Scanning Multichannel Microwave Radiometer for sea ice research. *J. Geophys. Res.*, 88, 2781-2791.

Swift, C.T. and D.J. Cavalieri, 1985: Passive microwave remote sensing for sea ice research. EOS (Trans. Amer. Geophys. Union), 66, 1210-1212.

Thorndike, A.S., D.A. Rothrock, G.A. Maykut and R. Colony., 1975. The thickness distribution of sea ice. J. Geophys. Res., 80, 4501-4513.

Timco, G.W. and S.O. O'Brien., 1994. Flexural strength equation for sea ice. Cold Regions Science and Technology, 22, 285-298.

Timco, G.W and R.M.W. Frederking., 1990. Compressive strength of sea ice sheets. Cold Regions Science and Technology, 17, 227-240.

Tiuri, M.E., A.H. Sihvola, E.G. Nyfors and M.T. Hallikainen. 1984., The Complex Dielectric Constant of Snow at Microwave Frequencies., IEEE Journal of Oceanic Engineering OE-9 (5):377-382.

Ulaby, F.T., R.K. Moore and A.K. Fung, 1986: Microwave Remote Sensing: Active and Passive. Vol 3, Norwood, MA: Addison-Wesley Publishing Company.

Van der Veen, C.J. and I.M. Whillans., 1994. Development of fabric in ice. Cold Regions Science and Technology, 22, 171-195.

Vant, M.R., R.O. Ramseier and V. Makios, 1974. Dielectric properties of fresh and sea ice at 10 and 36 GHz. Journal of Applied Physics, 45, 4712-4717.



Vant, M.R. 1976. A combined empirical and theoretical study of the dielectric properties of sea ice over the frequency range 100 MHz to 40 GHz. Technical Report, Carleton University, Ottawa, Ontario.

Vant, M.R., R.O. Ramseier and V. Makios, 1978: The complex dielectric constant of sea ice at frequencies in the range 0.1 to 40 GHz. J. Appl. Phys., 49(3), 1264-1280.

Wakatsuchi, M. and T. Kawamura, 1987: Formation processes of brine drainage channels in sea ice. J. Geophys. Res., 92(C7), 7195-7197.

Weaver, R.L., C. Morris, R.G. Barry, 1987: Passive microwave data for snow and ice research: planned products from the DMSP SSM/I system. EOS (Trans. Amer. Geophys. Union), 68, 769, 776-777.

Weaver, R.L. and V.J. Troisi, 1996: Remote sensing data availability from the Earth Observation System (EOS) via the Distributed Active Archive Center (DAAC) at NSIDC. Proc. IGARSS'96, 73-77.

Weeks, W.F. and D. Anderson., 1958. An experimental study of strength of young sea ice. Am. Geophys. Union, 4, 641-647.

Weeks, W.F and O.S. Lee., 1958. Observation on the physical properties of sea ice at Hopedale, Labrador. Arctic, 11, 135-155.

Wenshanan, M.R., T.C. Grenfell, D.P. Winebrenner and G.A. Maykut, 1993a: Observations and theoretical studies of microwave emission from thin saline ice. *J. Geophys. Res.*, 98(C5), 8531-8545.

Wenshanan, M.R., G.A. Maykut, T.C. Grenfell, D.P. Winebrenner, 1993b: Passive microwave remote sensing of thin sea ice using principle component analysis. *J. Geophys. Res.*, 98(C7), 12,453-12,468.

Winebrenner, D.P., E.D. Nelson, R. Colony and R.D. West, 1994: Observations of melt onset on multiyear Arctic sea ice using the ERS-1 SAR. *J. Geophys. Res.*, 99, 22,425-22,442.

Winebrenner, D.P., 1996: Polarimetric backscatter at 23 cm wavelength from Antarctic lead ice and estimation of ice thickness. *Proc. IGARSS'96*, 941-943.

Yackel, J., D. G. Barber. And J.M. Hanesiak. An Examination of the Morphological, Climatological and Microwave Scattering Characteristics of Melt Ponds on Landfast First-Year Sea Ice using RADARSAT-1. *Journal of Geophysical Research-Oceans In Review* (March'99).

Yang, S.K., S.S. Zhou, L.M. McMillan and K.A. Campana, 1996: Characteristic of the NOAA/NESDIS cloud retrieval algorithm using HIRS-MSU radiance measurements. *J. Appl. Meteorol.*, 35, 1980-1990.

Zibordi, G. and M.L. Van Woert, 1993: Antarctic sea ice mapping using the AVHRR. *Rem. Sens. Env.*, 45, 155-163.

